UNIVERSITÀ DEGLI STUDI DI TRIESTE

XXIV CICLO DEL DOTTORATO DI RICERCA IN NANOTECNOLOGIE

Cell biomechanics and metastatic spreading: a study on human breast cancer cells

Settore scientifico-disciplinare: MED/35

Dottoranda:
Federica Tavano

Coordinatore Dottorato di Ricerca:
Prof. Maurizio FERMEGLIA

Supervisore:
Dott. Serena Bonin
Università degli Studi di Trieste

Tutore:
Dott. Dan COJOC
CNR - IOM Laboratorio TASC

ANNO ACCADEMICO 2010/2011

Abstract

Despite the intensive research of the past decades in oncology, cancer invasion and metastasis still represent the most important problem for treatment and the most common cause of death in cancer patients. Metastasis refers to the spread of malignant cells from a primary tumour to distant sites of the body and the adaptation of these cancer cells to a new and different tissue microenvironment. Usually, millions of cells can be released by a tumour into the circulation every day, but only a tiny minority of these cells are able to reach and colonize a distant organs: the utter inefficiency of the metastatic process implies that cells might strongly need biomechanical alterations that allow them to invade and colonize different tissues. The hypothesis that cellular biomechanics may play a significant role in tumour genesis and cancer invasion, gains every day more and more support: therefore characterizing these properties in connection with the membrane and cytoskeleton organization could be very important for understanding better the migration mechanisms and to develop new diagnostics and therapeutics tools.

The goal of our study was the mechanical characterization of cell lines chosen as model of cancer progression using different biophysical techniques and the correlation of the mechanical properties with possible alterations of the cytoskeleton structure and plasma membrane composition.

We used a custom built Optical Tweezers to extract the local viscoelastic properties of the cell plasma membrane, an Atomic Force Microscopy (AFM) to locally measure cell elasticity of cells, and a Microfluidic Optical Stretcher to measure the deformability of cells as whole bodies. We investigated then the actin organization of the cytoskeleton by STimulated Depletion and Emission (STED) and confocal microscopy. The lipid composition of cells was analysed by MALDI-mass spectroscopy in order to correlate the mechanical alterations of cells with alteration at the cytoskeleton and plasma membrane level. The techniques for cell biomechanical experiments are described in 3.1, while the imaging and spectroscopy techniques and described in detail in 3.3 and 3.4.

The cell lines analyzed derive from breast tissue and represent a model of human epithelial cells towards malignancy. In particular, two cell lines -MDA-MB-231 and MCF-7- provided by American Type Culture Collection (ATCC) were originally derived from breast cancers patients with different level of cancer aggressiveness. Cells were chosen according to the nowadays accepted classification of breast cancer

based on gene expression pattern and proteomic expression, which divide breast cancers in subtypes that differ in terms of risk factor, distribution, prognosis, therapeutic treatment responsiveness, clinical outcomes and survival. The third cell line, HBL-100, is an immortalized but non-neoplastic cell line derived from the milk of a nursing mother with no evidence of breast lesions, representing a earlier stage of the cell transformation. Cell lines description is reported in detail in 2.1.

A pulling membrane tether approach by means of Optical Tweezers has been chosen since it allows an accurate quantitative characterization of local viscoelastic properties of plasma membranes. Bovine Serum Albumine (BSA) coated silica beads were used to bind the plasma membrane and grab membrane tethers of several microns measuring the force exerted on the bead. By fitting with the Kelvin body model our force-elongation curves obtained by experimental data we extracted the parameters of interest: tether stiffness, membrane bending rigidity, and tether viscosity. The Optical Tweezers setup and experimental approach are described in 2.2.1.We observed that lower values of tether stiffness and membrane bending rigidity corresponded to cells associated to a higher aggressive behaviour, while viscosity showed an inverse tendency.

We also probed elasticity of the cells using by indentation experiments with AFM. We used a bead probe attached to the cantilever and measured the Young Modulus. The technique is described in 2.2.2. The results obtained could not clearly discriminate the three cell types in terms of elasticity.

Cell deformability was further investigated by means of Microfluidic Optical Stretcher. Cells in suspension were trapped by two counter propagating laser beams of low intensity from two optical fibers. Adjusting the intensity of the laser light, the forces acting on the cell surface increased, leading to a measurable elongation of the cell body along the laser beam axis. With MOS we were able to discriminate between cancer and control cells lines, while differences between the two cancer cell lines were not significant. However a trend could be observed: lower aggressive tumour cells were more resistant to deformation compared to the higher aggressive tumour cells. This technique is described in 2.2.3.

The results of the mechanical analysis are reported in 3.1

We investigated the cells cytoskeleton structure by STED and confocal microscopy confirming that malignancy involves cytoskeleton structure alterations. Differences in

the organization. of the actin filaments and in the presence of actin drifts were observed. We peformed also a preliminary analysis of the cell lipid composition by MALDI MASS spectroscopy. We could observe that highly aggressive cells with softer membranes presented alterations at the level of Phosphatidylethanolamines (PEs) and Phosphatidylinositoles (PIs). STED and confocal images, and MALDI mass spectra are reported in 3.3 and 3.4.

The work of this thesis is partially published in the article “Custom Built Optical Tweezers for locally probing the viscoelastic properties of cancer cells” in the International Journal of Optomechatronics (June 2011). A second article including the comparative results of the biomechanical analysis on the breast cell lines is in preparation.

TABLE OF CONTENTS

1. INTRODUCTION

1.1 Cancer and metastasis

Despite the intensive research in oncology, cancer invasion and metastasis are still unsolved problems, representing the most common cause of death in cancer patients and the main problem for cancer treatment. The spreading of tumors cells from primary site to other tissues is the results of different events. Physiology, therapy, tumor type are some of the variables which compete with this complex phenomenon and represent the reason why patients with the same tumor type and stage present completely different outcome.

Cancers of the lung and bronchus, colon and rectum, prostate and breast respectively for males and females continue to be the most common fatal cancers and account for half of the total deaths in industrialized countries. In the last decades, due to the great advances that have been made in the understanding of the molecular, genetic and environmental factor that influence the onset and the progression of cancer, mortality rates have continued to decrease across all these four major cancer sites in both men and women–except for female lung cancer in which death rates are continuing to increase. However, the incidence trends are mixed (Jemal A., Siegel R. et al. 2008) and some cancer type's incidence rates are increasing due to bad life style, diet and exposure to risk factors, but also for longer life duration and screening programs that lead to more frequent diagnosis.

In figure 1.1 the annual age-adjusted cancer incidence and mortality rates (by sex/ by sex for selected cancers) in United States from 1975 to 2004 are reported.

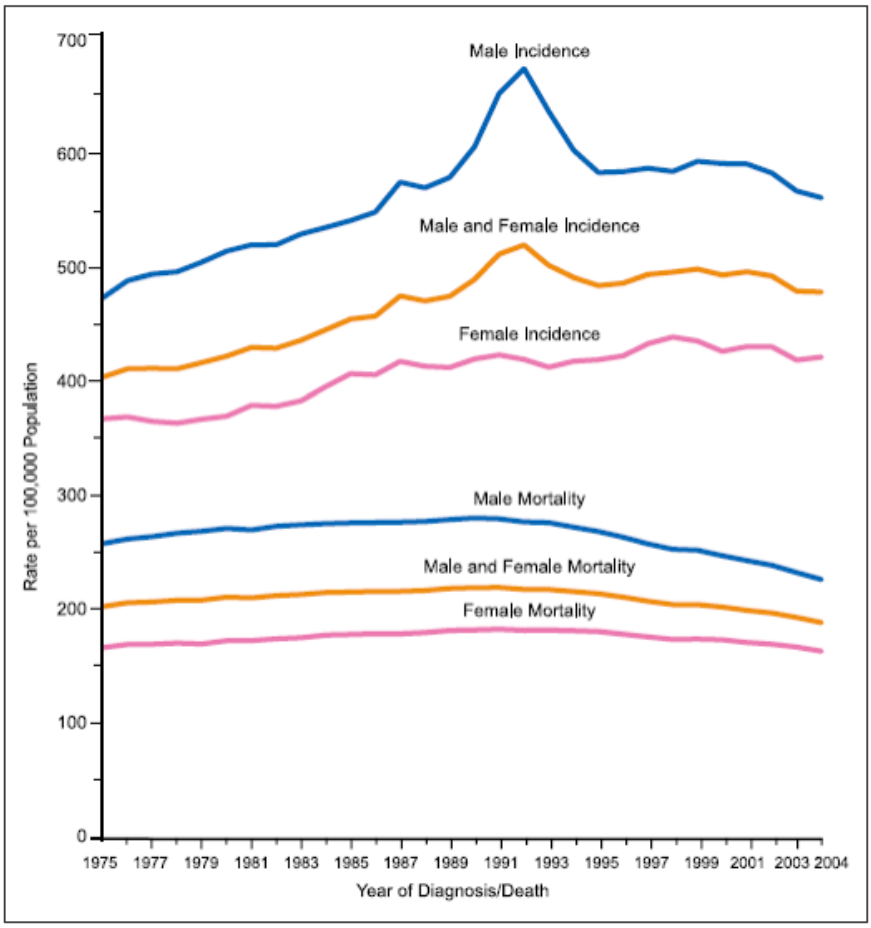

Figura 1.1: Cancer incidence and death rates.
Figure report the annual age-adjusted cancer incidence and death rates for all sites by sex in United States from 1975 to 2004. Rates are age-adjusted to the 2000 US standard population. Incidence rates are adjusted for delays in reporting. Adapted from Jermal A et al.2008.

The most common cause of death in cancer patients with solid tumors is metastasis, accounting for 90% of the deaths but still the mechanism is not completely understood. In physiological conditions tissues are only seemingly static, cell division is controlled by continuous stimulatory and inhibitory signals that maintain tissues homeostasis. When a normal cell switches its phenotype and becomes a neoplastic cell, genetic and epigenetic mutations occur altering this equilibrium: diseased cells proliferate uncontrollably and disrupt the organization of tissue causing cancer formation. Malignant transformation is the process in which a cell changes morphology over time from a benign phenotype into an invasive or metastatic entity undergoing many genetic and epigenetic changes: these oncogenic events, such evasion of growth suppression or DNA-damage checkpoints create the genomic instability that contributes to the evolution of tumours to the metastatic state (Gupta G.P. and Massaguè . 2006).

This transformation leads to a progressive loss of tissue homeostasis and stereotypic alterations in the tissue architecture that ultimately culminates in tumor cell invasion of

the parenchyma and metastasis to distant organ sites. (Kumar and Weaver 2009): it occurs in a series of steps which have been described as a "metastatic cascade" (Geiger T.R. and D.S 2009). The detailed description of the metastatic process in a solid tumor is reported in fig.1.2.

As mentioned above, after neoplastic transformation cells proliferate uncontrollably as benign tumour forming a mass in the epithelial tissue until genetic alterations allow them to break through the basal membrane and reach the extra cellular matrix (ECM), invading capillaries. Once tumour cells enter the bloody or lymphatic system they can travel through the vessels to another site, even distant from the primary tumour.

Circulating Tumoral cells (CTCs) must adhere the vessel walls before they can extravasate: if the microenvironment is established, the tumor cell(s) may proliferate at this distant site and eventually form lethal metastases.

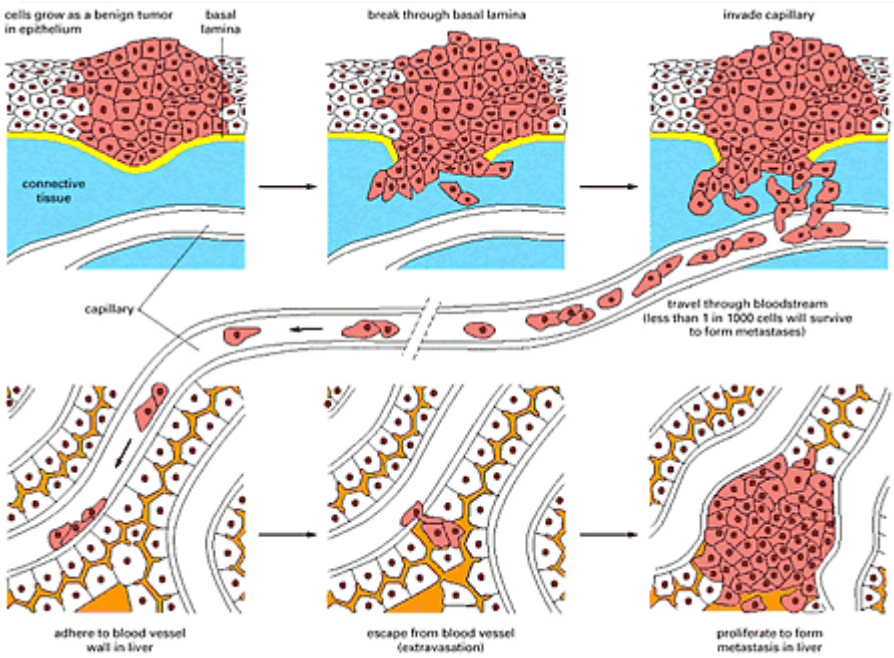

Figure 1.2: Metastatic cascade.
(a) Cells grow as benign tumor (b) Cells break through the basement membrane (c) Invasion and Travel through the blood stream (d) Adhere to capillary wall (e) Escape from blood vessel (Extravasation) (f) cells proliferate to form metastases adapted from Alberts B. et al, Molecular Biology of the Cell 4th ed. New York Garland 2002, p1325

Metastasis is an inefficient process: only few cells survive after the travel through the circulation system and are potentially able to form metastasis: it requires many mechanisms as matrix degradation, cell migration, evasion of host immune response, metastatic colonization and angiogenesis for the survival of cells forming the secondary tumour. It is accompanied by phenomena like the epithelial-mesenchymal transition (EMT) which means the loss of cell polarity, the alterations of the cytoskeleton

structure and membrane modifications that reflect in changes at the level of proliferation rates, cell survival, cell mechanical properties and in the ability to attach move and spread in host healthy tissues.

1.2 Breast cancer

1.2.1 Breast cancer: epidemiology and risk factors

Invasive breast cancer is the most frequent carcinoma in females: it accounts for 22% of all female cancers (Parkin D.M., Bray F. et al. 2001) The areas of higher risk are the affluent populations of North America, Europe, Australia and countries that have acquired the Western lifestyle. In regions which have featured this lifestyle for a long period of time (North America, Northern Europe, Australia) the disease had been increasing until the early 1980s and then reached a plateau of an incidence rate of 70 to 90 new cases per 100,000 population/year while countries that have more recently become industrialized and affluent show a marked increase in incidence and mortality (Tavassoli F. A. and Devilee Peter. 2000).

Despite the increasing incidence of breast cancer in some areas encouraging trends have been observed regarding mortality and survival over the past decades. Since the late 1970s significant improvements in survival have been recorded in western countries since the late 1970s (Adami H.O., Sparen P. et al. 1989; Chu K.C., Tarone R.E. et al. 1996) and the mortality trend declined in several high risk countries (WHO 2000): this reflects a combination of factors such as earlier diagnosis due to population screening programmes, more efficacious adjuvant hormonal treatments and systemic therapy.

Geographical variations and studies of populations migrating from low to high risk areas show that migrant populations approach the risk of the host country in one or two generations (Balzi D., Buiatti E. et al. 1993; Ziegler R.G., Hoover R.N. et al. 1993; Kliewer E.V. and Smith K.R. 1995) suggesting that breast cancer is a multifactorial disease and its aetiology involves mainly environmental factors. These risk factors are: diet and physical activity, reproductive factors, related hormonal imbalances and exposure to ionizing radiation. An overview of the main risks factors is reported in this section and summarized in Fig. 1.3.

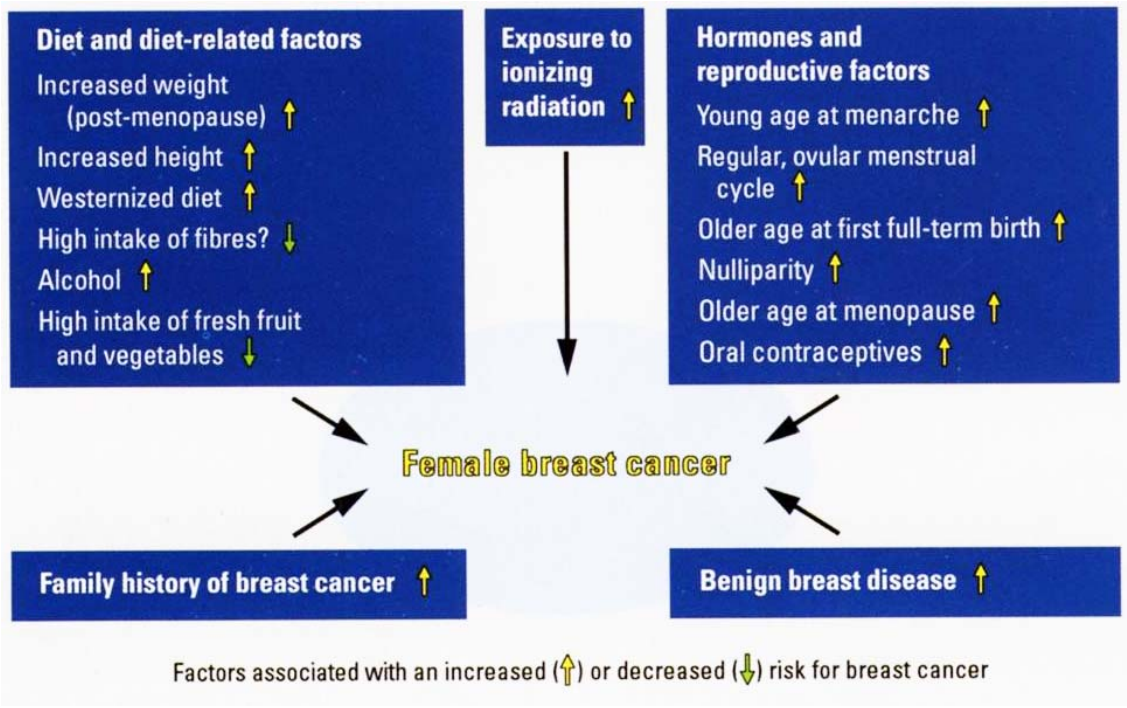

Figure 1.3: Aeziological factor involved in breast cancer incidence
Adapted from Tavassoli F.A. et al. 2000.

1.2.2 Breast cancer classification

Invasive breast carcinoma is a group of malignant epithelial tumours characterized by invasion of adjacent tissues and a marked tendency to metastasize to distant sites.
Breast cancer's heterogeneity arises from many different factors, such as the cell of origin, the molecular alterations causing them and the susceptibility and defences of the patient. All this makes difficult to give the most appropriate treatment and prognosticate the clinical outcome (Bertucci F. and Birnbaum D. 2008)

Thus, several parameters, such as histopathological type, histopatological grade, stage, receptor status and the present or absence of particular genes, are used to classify breast cancer and each of them influences treatment response and prognosis. The next sections provide a brief description of these parameters

Histopathological classification

The basic component of the breast is the mammary gland. Each mammary gland, whose structure is reported in figure 1.4 , is made of multiple lobules connected to ducts and surrounding tissue, which includes blood vessels. Breast malignant lesions may arise from any of these structures giving rise to different types of tumours exhibiting a wide range of morphological phenotypes and specific histopathological types with particular prognostic or clinical characteristics (Tavassoli F. A. and Devilee Peter. 2000).

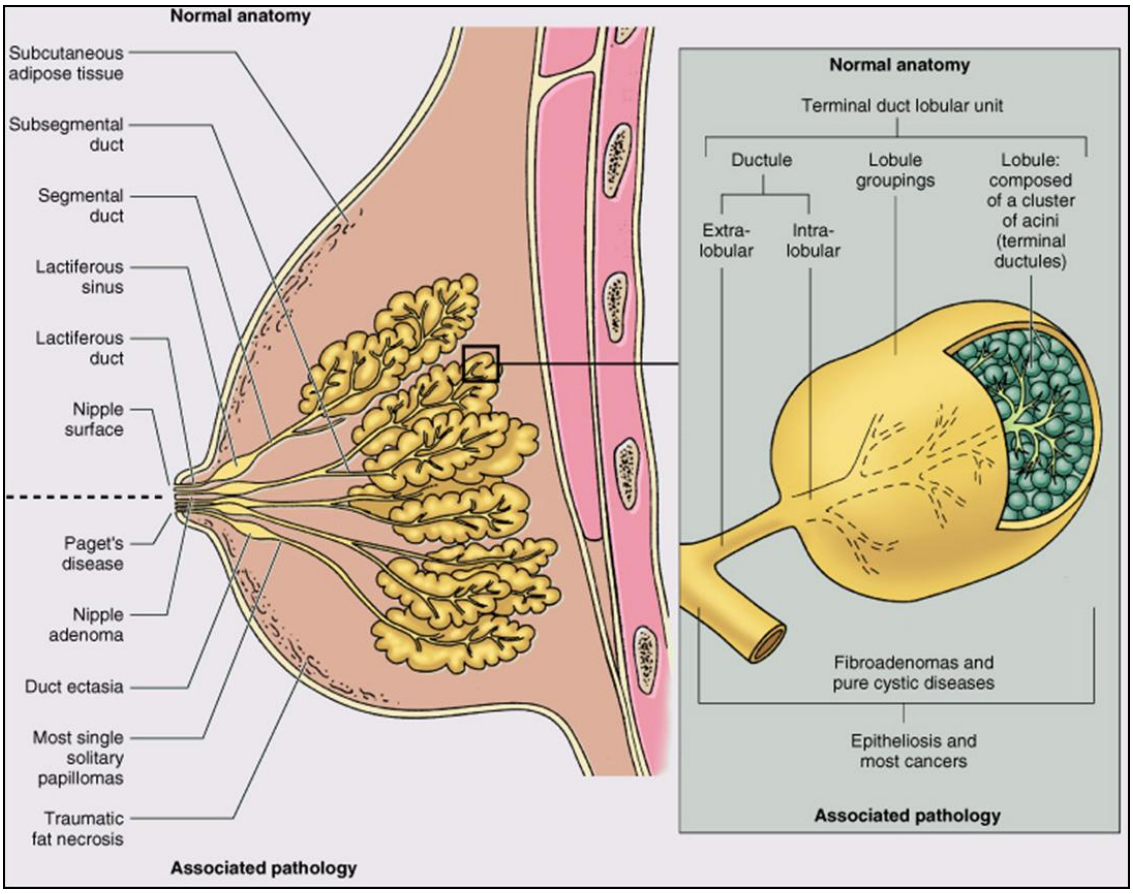

Figure 1.4:Mammary gland normal anatomy and associated pathologies.
The whole mammary gland (left) and the terminal duct lobular unit (right) are represented and associated to their correlated pathologies. (copyright 2004,2000, 1995 by Elsevier Inc.)

The vast majority of breast tumours are adenocarcinomas whose origin is referred to the mammary parenchymal epithelium, particularly cells of the terminal duct lobular unit.

Despite the wide and complex histological classification of breast cancers, here the most common types are reported: ductal carcinoma in situ (DCIS) and lobular carcinoma in situ (LCIS), invasive ductal carcinoma (IDC), and invasive lobular carcinoma (ILC)

Ductal carcinoma in situ (DCIS)

It consist of malignant epithelial cells confined to the mammary ducts without microscopic evidence of invasion through the basement membrane into the surrounding tissue: according to the tumour differentiation DCIS can be further divided into low, intermediate and high grade with prognostic implications.

Lobular carcinoma in situ (LCIS)

By definition, these cancer cells are characterized by a solid proliferation of small cells confined to the mammary lobules without invasion. This type of tumour generally lacks specific clinical or mammographic signs and occurs more frequently in premenopausal women.

Invasive ductal carcinoma (IDC)

Invasive ductal carcinoma comprises the largest group of invasive breast cancers. It is a heterogeneous group of tumours that fail to exhibit sufficient characteristics to achieve classification as a specific histological type, such as lobular or tubular carcinoma. It is the most common 'type' of invasive carcinoma of the breast comprising between 40% and 75% in published series (Tavassoli F. A. 2003; Rakha E.A., Putti T.C. et al. 2006) The morphological macroscopical features vary considerably from case to case: there is a marked variation in size (10-100 mm) with an irregular, stellate outline or nodular configuration. Invasive ductal carcinoma commonly spreads to the regional lymph nodes and carries the poorest prognosis among various ductal types.

Invasive lobular carcinoma (ILC)

Invasive lobular carcinoma (ILC) is composed of non-cohesive cells individually dispersed or arranged in single-file linear pattern in a fibrous stroma. These infiltrating cords frequently present a concentric pattern around normal ducts and the mean diameter has been reported to be slightly larger than that of IDC in some series(Silverstein M.J., Lewinsky B.S. et al. 1994; Sastre-Garau X., Jouve M. et al. 1996; Winchester D.J., Chang H.R. et al. 1998). Invasive lobular carcinoma represents 5-15% of invasive breast tumours (Martinez V., Azzopardi J.G. et al. 1979; du Toit R.S., Locker A.P. et al. 1989; Ellis I.O., Galea M. et al. 1992; Sastre-Garau X., Jouve M. et al. 1996; Toikkanen S., Pylkkanen L. et al. 1997; Winchester D.J., Chang H.R. et al. 1998). ILC can be difficult to define macroscopically because of the the irregular and poor delimited tumours and the diffuse growth pattern of the cell infiltrate (Silverstein M.J., Lewinsky B.S. et al. 1994).

Ductal and lobular carcinomas incidence rates are followed by more rare malignancies arising from other connective tissues such as Tubular carcinoma, Medullary carcinoma and Paget's disease of the nipple. The description of all histological breast cancer subtypes is beyond the scope of this manuscript, for a detailed analysis see (Tavassoli F. A. 2003).

Tumour size and lymphonode involvement status: the TNM classification

The tumour size, the lymphonode involvement and whether the tumor has metastatized or not contribute to predict the patient clinical outcome and can be useful for the therapeutic choice. In particular the status of the axillary lymph nodes is actually one of the most important prognostic factor for patients with breast cancer. Numerous studies have shown that disease - free and overall survival rates decrease as the number of positive nodes increases (Fisher B., Dignam J. et al. 1999). Together with the lymphonode status, also tumour size is an important prognostic factor, however the methods reporting the pathological tumour size varies. Pathologists report varies according to : the macroscopic size of tumor , the microscopic size which includes both the invasive and in situ components and the microscopic size of the invasive component only. There is often poor correlation between the tumour size determined by gross pathological examination and the size of the invasive component as determined by histological measurements (Abner A.L., Collins L. et al. 1998). The size of the invasive component is clinically significant, and so the pathological tumour size for classification is a measurement of the only invasive component (Verlag 2002). Therefore the microscopic size prevales, when there is a discrepancy between the gross and the microscopic size of the invasive component.

Taken together the size of the primary tumour, the presence of metastatic regional lymph nodes and/or of distant metastases are the key elements for the so called TNM categorization (Veronesi U., Viale G. et al. 2005). This staging system classifies cancers based on their T, N, and M stages. Briefly, the letter T followed by a number from 0 to 4 describes the tumor's size and spread to the skin or to the chest wall under the breast. Higher T numbers mean a larger tumor and/or wider spread to tissues near the breast. The letter N followed by a number from 0 to 3 indicates whether the cancer has spread to lymph nodes near the breast and, if so, how many lymph nodes are affected. Finally, the final M followed by a 0 or 1 indicates whether the cancer has spread to distant organs (1) or not (0).

Histological Grade

The histological grade focuses on the appearance of the breast cancer cells compared to the appearance of normal breast tissue. During cell progression towards malignancy, cells that would normally line up in an orderly way to make up the milk ducts become disorganized, lose their differentiation and start to proliferate uncontrollably. Cell

nuclei become less uniform. Pathologists divide cells into 3 categories: highly differentiated (low grade), moderately differentiated (intermediate grade), and poorly differentiated (high grade) as the cells progressively lose the features seen in normal breast cells.

Grading is recommended for all invasive carcinomas of the breast, regardless of morphological type (Pereira H., Pinder S.E. et al. 1995; Commission 1996). Higher rates of distant metastasis and poorer survival are observed in patients with higher grade (poorly differentiated) tumours, independent of lymph node status and tumour size (Contesso G., Mouriesse H et al. 1987; Rosen P.P., Groshen S. et al. 1989; Elston C.W. and I.O. 1991; Fisher E.R., Anderson S. et al. 1993; Nixon A.J., Schnitt S.J. et al. 1996; Goldhirsch A., Glick J.H. et al. 1998). The combination of histological type and grade provide a more accurate assessment of prognosis than does histological type alone(Pereira H., Pinder S.E. et al. 1995).. Histological grade may also provide useful information with regard to response to chemotherapy and, therefore, be a predictive factor as well as a prognostic indicator.

Receptor status

Actually, three important receptors, taken together with other predictive factors, contribute to prognosticate the patient's clinical outcome. These are the steroid hormone receptors for oestrogen (Oestrogen receptor, ER) and progesterone (Progesterone receptor, PR); and the Human Epidermal Growth Factor Receptor 2 (HER2/neu)

Oestrogen receptor (ER) and Progesterone receptor PR

Oestrogen is an important mitogen exerting its activity by binding to its receptor (ER). Approximately 60% of breast carcinomas express the ER protein. Initially, ER-positive tumours were associated with an improved prognosis, but studies with long-term follow-up have suggested that ER-positive tumours, despite having a slower growth rate, do not have a lower metastatic potential. Nonetheless, ER status remains very useful in predicting the response to adjuvant tamoxifen (Anon. 1992; Osborne C.K. 1998; Isaacs C., Stearns V. et al. 2001). PR is a surrogate marker of a functional ER. In oestrogen target tissues, oestrogen treatment induces PR. Both can be detected by ligand binding assay, or more commonly nowadays, by immunohistochemical (IHC) analysis using monoclonal antibodies. ER/PR-positive tumours have a 60-70% response rate compared to less than 10% for ER/PRnegative tumours. ER-positive/PR-negative tumours have an intermediate response of approximately 40%. The impact of

hormone receptor status on prognosis and treatment outcome prediction is complex, nevertheless, measurement of both ER and PR has been clinical practice for more than 20 years.

The Human Epidermal Growth Factor Receptor 2 (HER2/neu)

The ERBB2 gene, which codify HER2 receptor has been shown to play an role in the pathogenesis and progression of certain aggressive types of breast cancer and it is evolving to become an important biomarker and target of therapy. Amplification of the HER-2/neu gene is a significant predictor of both overall survival and time to relapse in patients with breast cancer. (Slamon D.J., Clark G. M. et al. 1987)

Molecular classification

Clinical-pathological information described above, such as the histological type, grade, tumour size, lymph-node involvement represents the current standard to estimate a patient's likelihood for recurrence and assess the right prognosis (Andre F. and L. 2006) nevertheless tumours characterised by similar histopatological features could present significantly different outcome and treatment responsiveness. Despite the great advances that have been made in breast cancer therapy, still the major challenge is to exactly determine which patients are most likely to benefit from which therapies and in identifying subgroups of patients who are at the highest risk for recurrence.

Breast cancers phenotypic diversity could be explained by diversity in gene expression (Perou C.M. 2000). A large number of genetic alterations have been identified in invasive breast carcinomas, many of which are of potential prognostic or predictive value. Some provide treatment–independent information on patient survival, others predict the likelihood that a patient will benefit from a certain therapy. Some alterations may have both prognostic and predictive value (Tavassoli F. A. 2003).

In the last decade, the gene expression profiling improved the classification of breast cancer: several microarray analyses on breast cancers have identified gene expression profiles able to separate tumour classes associated with patient survival with implications for prognosis and drive therapy as specifically as possible.

Perou et al. (Perou C.M. 2000) and Sorlie et al.(Sorlie T., Perou C.M. et al. 2001) showed that the expression profiles primarily distinguished ER+ from ER- tumors. They called them luminal and basal subtypes because of their respective luminal and basal characteristics. In particular, Perou and colleagues characterized the variations in gene expression patterns in a set of 65 surgical specimens of human breast tumours from 42 different individuals, using complementary DNA microarrays representing

8,102 human genes. These patterns provided a distinctive molecular portrait of each tumour and were able to identify four groups of breast cancers that might be related to different molecular features of mammary epithelial biology. These four groups were as follows:

1. normal breast like;.
2. luminal cell like tumours, expressing oestrogen receptor (ER+) and showing similar profiles to those of normal luminal cells of breast gland;
3. basal cell-like (BCL) or 'triple negative' phenotype (ER-, PR- and HER2-) associated with aggressive behaviour, poor clinical outcomes, lack of response to the usual endocrine therapies and shorter;
4. finally Erb-B2 tumors, negative for estrogen receptor as BCL subtype but with overexpresion of the HER2) (Perou C.M. 2000; Sotiriou C. 2003; Liu H. 2008)

Another microarray-based analysis by Sorlie and collagues (Sorlie T., Perou C.M. et al. 2001), confirmed the previous results of Perou et al. and segregated further tumours into distinct subgroups mainly based on their luminal (ER+) and basal (ER-) characteristics. In this case the luminal-like tumours were further segregated into at least two (possibly three) smaller subgroups, which correspond to luminal A, B, and C subtypes.

Although the luminal A subtype showed a favourable clinical outcome when compared with other luminal subtypes, this difference was not statistically significant. However, luminal A tumours were shown to be strongly associated with good prognosis an a less aggressive behaviour also when compared with the BCL or Her2/neu groups (Sotiriou C. 2003).

An important implication of this study is that the clinical designation of `estrogen receptor negative' breast carcinoma encompasses at least two biologically distinct subtypes of tumours (basal-like and ErB-B2 positive), which may need to be treated as distinct diseases. Furthermore it has been found that a metastasis and primary tumour were as similar in their overall pattern of gene expression as were repeated samplings of the same primary tumour, suggesting that the molecular program of a primary tumour may generally be retained in its metastases. A deeper characterization to define the portraits of each tumour and the correct interpretion of their patterns of variation, could undoubtedly lead to a deeper and more complete understanding of breast cancers (Perou C.M. 2000; Sotiriou C. 2003). More precisely, the accurate prognostic

signatures can identify patients with good or poor survival rate and can drive to the more efficient individual therapy.

1.3 Cancer and biomechanical properties

1.3.1 Biomechanical properties alteration in cancer cells

The biophysics of cells in human diseases is emerging as a topic of rapidly expanding scientific interest. In particular in the past decade, the interest on the correlation between the biophysical properties of cells and the onset and progression of cancer has significantly increased (Suresh 2007). The well known genetic and molecular alterations that characterize cells cancer can not completely explain alone the complex process of malignant transformation and invasion; therefore cancer biologists have begun to recognize that a critical component of the neoplastic transformation process involves marked alterations in the mechanical phenotype of the cell and its surrounding microenvironment (Kumar and Weaver 2009).

During progression, cells undergo from a fully mature, post mitotic state to a replicating, motile and immortal cancerous cell and the cytoskeleton devolves from a rather ordered to a rigid structure as well as to a more irregular and compliant state. These changes influence the overall mechanical properties. Therefore, the biomechanical properties (rigidity, elasticity, deformability) of malignant cells (usually marked by high replication and motility) can provide useful information about their state and they can be viewed as a new biological markers, which offer an alternative identification to current proteomic techniques (Guck J. 2005) .

It has been demonstrated that even though tumours are relatively stiff (due to their ECM), the tumour cells themselves are softer in comparison to their normal counterpart (Lincoln B., Erickson H.M. et al. 2004; Guck J. 2005; Suresh 2007) and hence they are able to move and spread through dense ECM suggesting a continuous biomechanical interaction between the cells and their ECM leading to the adaptation of the cell motility (Huang H. 2005).

Following this hypothesis, in the last decades several groups tried to discriminate cancerous and non cancerous cells by mechanical analysis.

Lekka et al. used the atomic force microscope (AFM) to study the elasticity of normal human bladder epithelial cells and cancerous ones by performing AFM indentation experiments (Lekka M., Laidler P. et al. 1999). Normal cells risulted an order of magnitude stiffer than cancer cells and this was attributed to the reorganization of the

cytoskeleton. With the same technique, Park and colleagues (Park S., Koch D. et al. 2005) compared the mechanical properties of normal and transformed mouse fibroblast cells, demonstrating that fibroblast cells were stiffer than their transformed counterparts.

In 2007 Gimzewki and co-workers (Cross S., Jin Y.S. et al. 2007) reported on the stiffness of live metastatic cancer cells taken from the body (pleural) fluids of patients with suspected lung, breast and pancreas cancer. Within the same sample, they found that the cell stiffness of metastatic cancer cells was more than 70% softer than the benign cells, which line the body cavity as indicated by the elastic modulus. The elastic moduli for the benign cells exhibited a wider variation with a log-normal distribution, whereas the malignant cells displayed a much narrower normal distribution of elastic stiffness. Different cancer types were found to display a common stiffness.

On the same trend many other works in the last decades (Thoumine 1997; Lekka M., Laidler P. et al. 1999) confirmed evident differences in the mechanical properties among cancer and non- cancer cells(Ward K.A., Li W.I. et al. 1991; Zhang G., Long M. et al. 2002).

Thus, the hypothesis that cellular biomechanics could help in explaining tumour genesis and cancer invasion (Geiger J. 2005; Makale 2007).

1.3.2 Microrheological approaches for local investigation of cell biomechanics

Rheology is the study of deformation and flow of material in response to forces. Rheological studies on cells and tissues have a long history at the intersection of cell biology, cell physiology and biophysics (Heidemann S.R. and Wirtz D. 2004)

The first publications on cellular rheology were often soundly mathematical, with methodologies unusual to biologists, investigating the cell and its components as nonliving materials.

Viscoelastic properties of materials, their relative stiffness, their resistance to both fluid flow and solid deformation, are dynamically regulated by the cell and also depend sensitively on the details related to the measurement (speed, magnitude and force of the measurement) (Heidemann S.R. and Wirtz D. 2004) This is the reason why new mathematical models are needed to characterize mechanical properties of living materials. In recent years, rheology gave a large contribution to cell biology and the interest in this research area is rapidly expanding among scientific community. Recently, a number of techniques have been developed to probe the material properties of systems ranging from polymer solutions to the interior of living cells on microscopic

scales. These techniques are referred as microrheology, since they can be used to locally measure viscoelastic parameters. The strongest motivations for such developments is the prospect of being able to study inhomogeneity (MacKintosh and Schmidt 1999), which is characteristic of biological samples.

At the moment a wide variety of experimental biophysical techniques are commonly used to extract both local and global mechanical properties of living cells such as microplate stretcher (Hochmuth M. R. 1996; Thoumine 1997; Hochmuth 2000), micropipette aspiration (Hochmuth 2000) or, more recently, the AFM (Radmacher 1996; Rotsch C. and Radmacher M. 2000; Cross 2007). Other researchers have employed magnetic bead rheology, (Wang N., Butler J. P. et al. 1993; Choquet 1997; Shures 2007), microneedle probes (Zahalak G. I., McConnaughey W.B. et al. 1990), acoustic microscopes (Kundu T., Bereiter-Hahn J. et al. 2000), sorting in microfabricated sieves (Carlson R. H. G., Gabel C.V. et al. 1997), the manipulation of beads attached to cells with OT (Sleep, optical et al.) (Choquet 1997; Guck J. 2005; Allioux-Guerin 2009; Remmerbach 2009) and MOS (Guck J., Ananthakrishnan R. et al. 2001). As a general rule, malignant cells responded either less elastic (softer) or less viscous (less resistant to flow) to stresses applied, depending on the measurement technique and the model employed. Metastatic cancer cells have been found to display an even lower resistance to deformation (Raz A. and Geiger B. 1982; Guck J. 2005).

1.3.3 Biomechanics in breast cancer research

The described trend of mechanical alterations in cancer cells in general has been observed also for breast cancer cells, both when using cell lines (Guck J. 2005; Li Q.S., Lee G.Y.H. et al. 2008) or primary cells cultures (Cross 2007). For instance, Lincoln et al. were the first to investigate the deformability of non-malignant and malignant human breast epithelial cells using the MOS and they found that malignant cells can stretch about five times more than their non-malignant counterparts (Lincoln B., Erickson H.M. et al. 2004; Guck J. 2005)

In a study of 2008, malignant (MCF-7) breast cells were found to have an apparent Young's modulus significantly lower (1.4–1.8 times) than their non-malignant (MCF-10A). Both confocal and AFM images showed a significant difference in the organization of their sub-membrane actin structures, which directly contribute to their difference in cell elasticity (Li Q.S., Lee G.Y.H. et al. 2008).

Beyond the mechanical alterations characterizing the single tumoral cells, the whole mammary gland tissue runs into dramatic changes at the macroscopic level during breast cancer progression.

The matrix of normal resting mammary gland is highly compliant but does become progressively stiffer during malignant transformation (Krouskop T.A., Wheeler T.M. et al. 1998; Plewes D.B., Bishop J. et al. 2000) there is a chronic increase in mammary gland tension that is linked to elevated compression force and tensile stress. The tissue homeostasis is not more maintained and the three dimensional architecture of the mammary gland is disrupted.

Transformed malignant epithelial cells residing within the ductal tree or in the expanding fibrotic tumour mass experience a compression stress, furthermore the surrounding tissue, that is a mechanical elastic solid, is not passive and respond to the tumour generated compression force by exerting a reciprocal force on the expanding tumour mass.

This process is described more in detail in fig.1.5: A, B describe the transformation event characterized by the acquisition of genetic alterations and the induction of proliferation in luminal epithelial cells, residing within the mammary ducts. C,D illustrate the proliferating pre-malignant luminal epithelial cells in the ducts exerting compression forces (solid stress) of increasing magnitude on the basement membrane and adjacent myoepithelium. In parallel, the infiltrating immune cells and activated resident fibroblasts induce a desmoplastic response in the surrounding stroma. The desmoplastic stroma is characterized by transdifferentiation of resident fibroblasts and changes in the interstitial matrix that include alterations in extracellular matrix composition, cross-linking and collagen and elastin reorientation. This manifest as an increase in stromal extracellular matrix stiffness. As malignancy progresses, the transformed epithelium continues to proliferate, exerting chronic incremental outward directed compression forces (solid stress) on the basement membrane, the myoepithelium and the surrounding stromal tissue. The outward projecting solid stress is countered by a reciprocal resistance force exerted by the stromal tissue that is proportional to the magnitude of the tumor-derived compression force and the elastic modulus of the stroma. Because the desmoplastic tissue is stiffer than normal tissue the transformed stroma will have a greater elastic modulus and hence exert larger resistance forces against the expanding tumor mass. The combination of these multiple

tensional stresses act upon the genetically aberrant malignant cells by stimulating signalling cascades to induce their growth and invasion into the interstitial tissue.

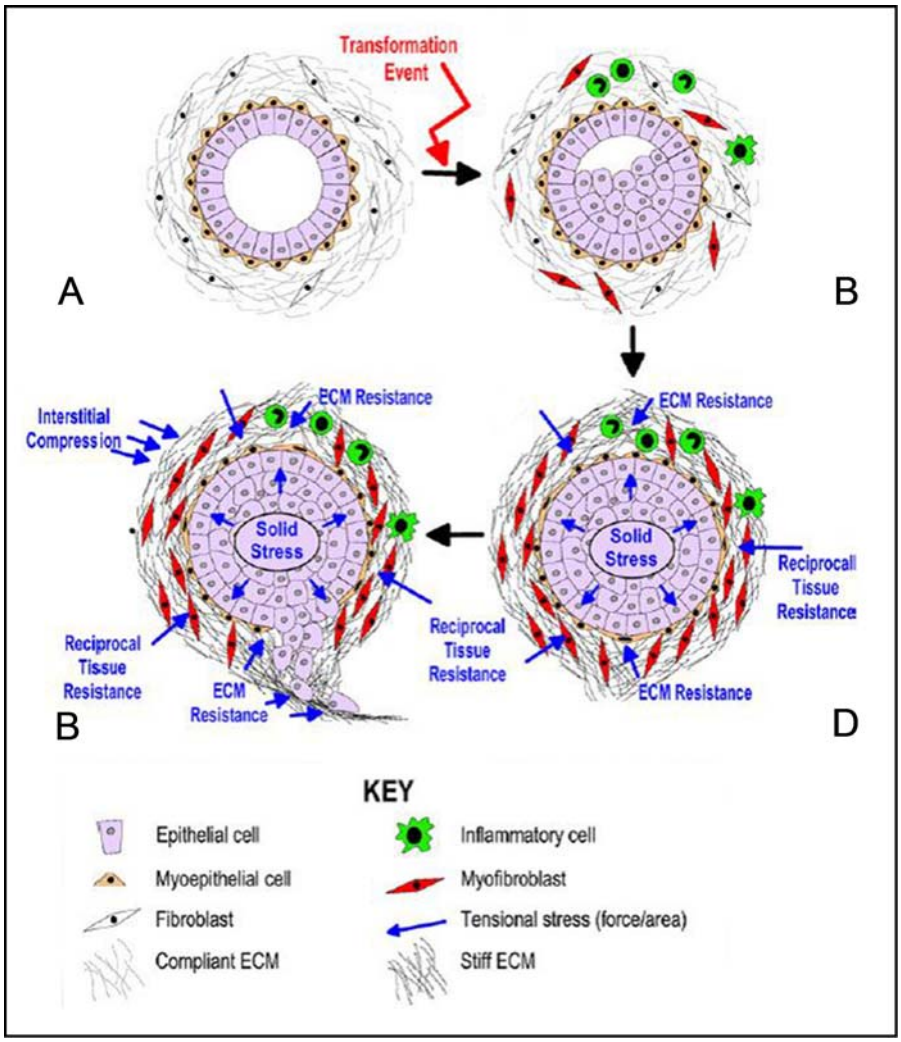

Fig.1.5: Tensional force and the normal and malignant breast
Cartoon highlighting the predicted types of tensional force that a normal and malignant breast might be expected to experience. A, B transformation event C,D proliferating pre-malignant luminal epithelial cells in the ducts exerting compression forces. The infiltrating immune cells and activated resident fibroblasts induce a desmoplastic response in the surrounding stroma. Adapted from (Paszek M.J. and Weaver V.M. 2004)

Experimental data suggest that this reciprocal tissue resistance can mediate cytoskeletal tensional forces and thus alter the behaviour of the tumor (cells growth, survival, motility and invasion) by regulating the activity of various biochemical signalling cascades. This forces can alter the conformations of proteins at the focal adhesions level, induce changes in the lipid packing in the membrane(Gilmore A.P. and Burridge K. 1995; Carrion-Vazquez M., Orr A.W. et al. 1999) and induce dynamic and random changes in the whole cellular cytoskeleton (Davies P.F. 1995; Helmke B.P. and Davies P.F. 2002).

For this reasons characterizing the mechanical properties of malignant cells in connection with the membrane and cytoskeleton organization is challenging for a deeper comprehension of the metastatic spreading process.

1.4 Aim of the study

The clinical, pathological and molecular classifiers of breast cancer are used to predict the progression of the disease and to assign the right therapeutic approach. Nevertheless, patients with the same cancer, in terms of subtype, stage and grade could present completely different clinical outcomes. Some patients recur and some do not. This dichotomy requires new tools able to better characterise each patient. Cancer cell mechanics is emerging as a topic of rapidly expanding scientific interest, since it represents an innovative approach to study this kind of disease. At the moment a wide variety of experimental biophysical techniques are commonly used to extract both local and global mechanical properties of living cells: in general, malignant cells respond either less elastic or less viscous to applied stresses, an even oppose lower resistance to deformation (Raz A. and Geiger B. 1982; Guck J. 2005) These tools are able to discriminate between cancerous and non cancerous cells.

The aim of this study was to investigate in vitro the mechanical and molecular properties of different cell lines related to different stages of breast cancer aggressiveness, using three different biophysical micromanipulation tools: Optical Tweezers, Atomic Force Microscopy and Microfluidic Optical Stretcher. Up to now, most of the studies related to the biomechanical properties of diseased cells have compared mechanical properties of tumour cells *versus* to normal ones or non-transformed cells (Lekka M., Laidler P. et al. 1999; Zhang G., Long M. et al. 2002; Guck J. 2005; Park S., Koch D. et al. 2005). In this thesis we investigated if biomechanical tools are able to sense the different stages of aggressiveness of breast cancer cells. To fulfil our proposal, we chose the cell line model for luminal A tumours, MCF-7, and basal tumours of the breast, MDA-MB-231. To compare our results and to investigate the reliability of our approaches we selected as model for normal cells the cell line HBL-100, which was developed from milk of 27-year-old Caucasian woman with no evidence of breast cancer lesions. Finally, we investigated on the actin cytoskeleton organization of cells by STimulation Emission Delpetion (STED) and confocal microscopy; and analyzed cell membranes lipid composition by MALDI Mass Spectroscopy (MALDI-MS). The aim was to associate the biomechanical analysis on

cells and their plasma membranes to possible alterations of cytoskeleton structure and membranes lipid composition.

2. MATERIALS AND METHODS

2.1 Cell Cultures

2.1.1 Cell lines description

According to the molecular classification described by Perou and colleagues (Perou C.M. 2000) (see section 1.2.2.5) two breast cancer cell lines from two different groups related to different aggressive behaviours were selected: MDA-MB-231 and MCF-7 cell lines. Finally a third breast cell line, HBL-100, which is immortalized but non-neoplastic was analyzed. These three immortal cell lines were used as model of human epithelial cells progressing toward malignancy.

Briefly, MDA-MB-231 (Fig 2.1, left) is an estrogen receptor independent breast cancer epithelial cell line derived from the pleural effusion of a cancer patient. It is widely used for breast cancer biology studies; it belongs to the Basal cell-like (BCL) or "triple negative" phenotype. As already described in section 1.2.2.5, this subtype has been associated with aggressive behaviour, poor clinical outcomes, lack of response to the usual endocrine therapies and shorter survivals when compared to other cancer subtypes. (Perou C.M. 2000; Foulkes WD 2003; Sotiriou C. 2003; Liu H. 2008) We used this cell type as a model of tumoral cell with high aggressive behaviour.

MCF-7 (Fig 2.1, central picture) is an estrogen receptor dependent breast cancer epithelial cell line widely used for studies of breast cancer biology and hormone mechanism of action. The cell line was originally derived at the Michigan Cancer Foundation from a malignant pleural effusion from a postmenopausal woman with metastatic breast cancer, who had been previously treated with radiation therapy and hormonal manipulation (Soule H., Vazquez J. et al. 1973). The cells express receptors for a variety of hormones including estrogen, androgen, progesterone, glucocorticoids, insulin, epidermal growth factor, insulin like growth factor, prolactin, and thyroid hormone (Lippman M., Osborne C. et al. 1977). It belongs to Luminal A cell-like tumour subtype which is associated with good prognosis and a less aggressive behaviour, compared to the BLC group (Sotiriou C. 2003)

Finally, HBL-100 (Fig 2.1, right) is an epithelial cell line developed and established in vitro, obtainedfrom the milk of an apparently healthy 27-year-old Caucasian woman after 3days from delivery (Polanowski F.P., Gaffney E.V. et al. 1976; Gaffney E.V. 1982). The milk donor was followed for several years with clinical and mammographic evaluations at regular intervals with no detectable breast lesion (Gaffney E.V. 1982; Ziche M. and Gullino P. 1982).

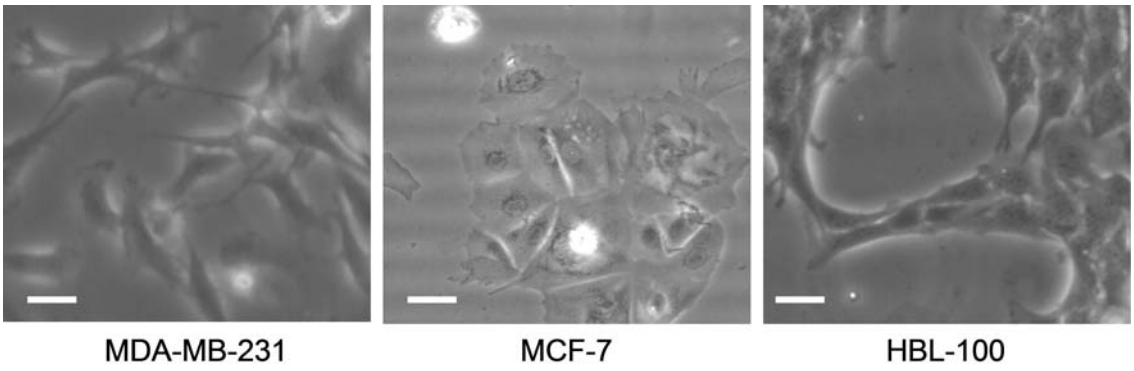

Figure 2.1: Optical Microscope image of the three cell lines.
Optical microscope image of the cell lines MDA-MB-231(left) MCF-7(centre) and HBL-100 (right) on adhesion on a Petri dish. Scale bar is 25μm.

Cell lines MDA-MB-231 and MCF-7 were kindly provided by Dr. Licio Collavin from the Molecular Oncology Unit at L.N.CIB, AREA Science Park (Trieste, Italy); cell line HBL-100 was kindly provided by Prof. Giuliana Decorti from the Biomedical Science Department at University of Trieste.

2.1.2 Cell cultures propagation and passaging

MDA-MB-231 and MCF-7, were cultured on adhesion and maintained in low glucose Dulbecco's modified eagle's medium (DMEM) with L-glutamine (Euroclone); HBL-100 were grown and mantained in RPMI 1640 medium with Stable L-glutamine (Euroclone). The culture mediums were used including 10% fetal bovine serum (FBS), 50 IU/mL of penicillin-streptomycin solution and 1mM Gentamicyn. Cell cultures were kept in an incubator at 37^{o}C with 5% of CO_2.

Cell passaging was performed with the same protocol for each cell type: adherent cells were incubated at 37^{o}C with a 1:10 diluited solution of 0,05% Trypsin/EDTA using a proper volume to cover the entire flask's surface: trypsin solution was incubated for 3-4 minutes until the cells detachment from the flask surface. Afterwards trypsin action was blocked by adding 1 mL of cell culture medium containing FBS (FBS contains alpha-1-antitrypsin which inhibits trypsin). The solution with cells in suspension was then removed from the flask, collected in a Falcon tube and centrifuged at 800 rpm for 4 mins. Cell pellet was resuspended in new warm medium, cells were counted in a Burker cell counting chamber and plated in new flasks in a proper concentration.

2.2 Methods used for local measurements of biomechanical properties of single cells

Among the variety of experimental biophysical probes that are currently used to extract mechanical properties of cancer cells, we chose the following approaches: Optical Tweezers (OT), Atomic Force Microscopy (AFM), and Microfluidic Optical Stretcher (MOS).

By OT, an optically trapped bead was used to grab the plasma membrane and pull a tether of several microns to measure the viscoelastic properties of the cell membrane. We measured tether stiffness, membrane bending rigidity and cell viscosity. A bead glued on the tip of the cantilever was used to locally indent the cell and measure the Young's Modulus. With both these approaches, OT and AFM, we were able to perform very local measurements and to test the mechanical properties of the cell membrane as well as the underlying region. OT tether membrane approach gives viscoelastic informations about cytoskeleton-membrane interaction (tether stiffness and viscosity, rupture force, membrane bending) while AFM gives elastic information about a larger region of the cell under bead indentation.

Cell detached from substrate and flowed in a microfluidic channel were trapped and stretched by two counter propagating laser beams by MOS. The deformation of the cells stretched by the radiation pressure of light was used as biomechanical parameter characterizing the cell as a whole body.

In conclusion, using three different approaches, we could evaluate different mechanical properties of a cell region or cell as a whole. The principles, the setups, and the experimental approaches are described in the following sections.

2.2.1 Locally membrane probing of the viscoelastic properties by Optical Tweezers (OT)

2.2.1.1 OT principle and applications to cell biomechanics

In 1970, Arthur Ashkin proved experimentally that micron-sized particles could be accelerated and trapped in stable optical potential wells, using only the force of radiation pressure from two counter propagating Gaussian beams (Ashkin A. 1970)

The single gradient beam, or Optical Tweezers, was demonstrated for stable three-dimensional trapping of dielectric particles by the same group in 1986 (Ashkin A., Dziedzic J.M. et al. 1986). Soon after, they demonstrated that viruses and bacteria could be trapped and manipulated without optical damage (Ashkin A. and Dziedzic JM.

1987). Then OT was used by Ashkin and colleagues to measure force generated by organelles transport (Ashkin A., Schutze K. et al. 1990) and by Block et al. to measure forces developed by single kinesin molecules (Block A.M., B. et al. 1990).

Since then the OT has rapidly developed in many different research areas such as biology, physics and chemistry (Ashkin A. 2006) and its success is rapidly increasing. This technique has proven to be effective because laser-based optical traps can precisely isolate and trap dielectric spheres, viruses, bacteria, living cells, organelles, small metal particles, and even strands of DNA. Two of the main uses in force spectroscopy have been the study of molecular motors and the physical properties of DNA. The use of OT to probe mechanical properties of larger structures such as cells and membranes has been increasing in the last decade. As technique for cell mechanics OT present several advantages:

1-probing by individual beads can be monitored in different regions of the cell;

2-measurements can be very local and occur over brief periods of time;

3- it probes the mechanics of the underlying cytoplasm or test the local viscoelastic properties of cell membranes (Sheetz M.P. and 2001)

The advantage of using OT in biological samples lies on the "contact-free" and lack of sample photodamage, by using a laser at wavelengths for which absorption of the biological matter is low. The typical wavelength used for biological applications is around 1 μm (infrared light), for which viability tests on cells have been made both on bacteria and eukaryotic cells (Neuman K.C., Chadd E.H. et al. 1999; Ericsson M., Hanstorp D. et al. 2000). Furthermore OT can be easily built on standard optical microscopes and do not need an extremely complex technology neither high costs.

A schematic represantation of the OT microscope is shown in Fig 2.2, left . The laser beam is focused by a microscope objective into the sample cell. Small particles diffusing in the fluid of the sample cell are confined toward the focus and trapped by the forces exerted by the laser beam. A high numerical aperture (NA) objective is necessary to obtain a 3D optical trapping. Low NA (NA< 0.9) allow only a 2D trapping confining the particles along the optical axis.

The trapping force (see Fig 2.2) is proportional to the laser power (W) , the refractive index of the medium (n_m) and a dimensionless efficiency coefficient (Q) which depends on the trapped object (shape and refractive index).

.

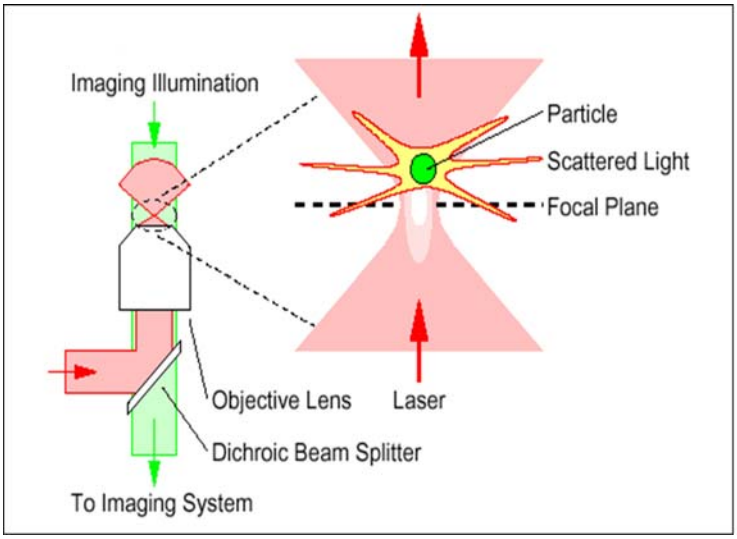

$$F = Q\frac{n_m W}{c}$$

F – trapping force
Q – dimensionless efficiency coefficient
W – power of the laser beam
$\mathbf{n_m}$ – refractive index of the medium
c – light speed

Figure 2.2: Schematic view of an optical trap.
(left) Represented in pink, a laser beam is reflected by a dichroic mirror and directed to an objective lens. Objective lens focus the laser and create an optical trap. The image system is indicated in green: white light crosses the objective lens, the dichroic mirror and continue its path to a camera (not shown) for the experiment videotracking. A particle is optically trapped. (right))The trapping force is proportional to the laser power (W) , the refractive index of the medium (n_m) and a dimensionless efficiency coefficient (Q) which depends on the trapped object .

To explain the 3D optical trapping mechanism, a simple explanation can be given for macroscopic spherical particles considering ray optics propagation and conservation of light momentum (Ashkin A., Dziedzic J.M. et al. 1986). A ray of light bends due to refraction through the bead, and hence the light linear momentum associated to the ray changes, as shown in Fig. 2.3 below. The change of light momentum P is transferred to the bead as force F.

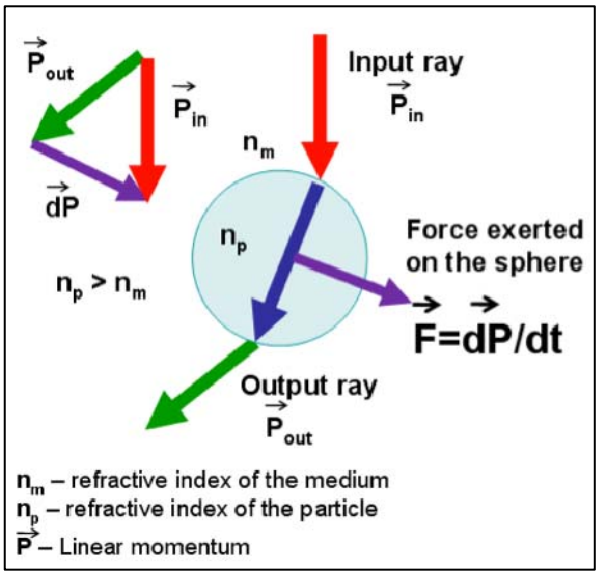

Figure 2.3: Force exerted by a ray of light on a spherical particle, as a consequence of the light momentum conservationchange of light momentum due to ray bending by refraction.

The directions of the resultant force exerted on the bead by two rays of a strongly focused beam is shown in Figure. 2.4 for three typical situations: on axis after and before the focus and out of axis. It can be seen that, for sufficiently high beam convergence angles, one expects a strong backward gradient component of the radiation pressure force.

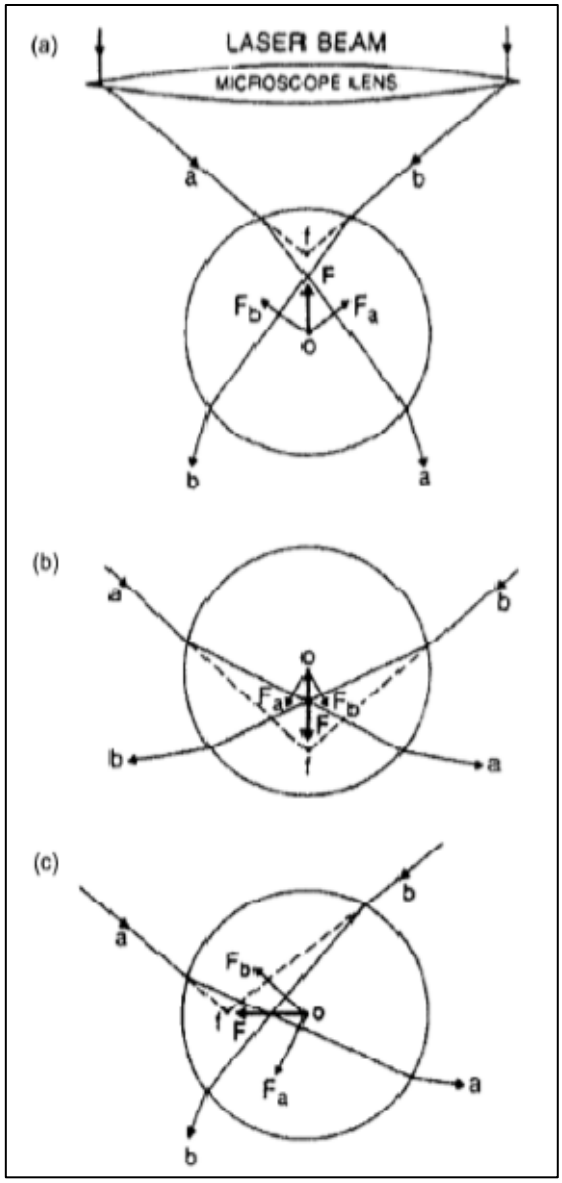

Figure 2.4:

Ray optics explanation of the stability of a tweezer trap for spherical particles large compared to the wavelength of the laser beam λ, for different displacements of the sphere relative to the beam focus at *f*.

Note the origin of the so-called "backward radiation pressure" in (a), which pulls the bead to the focus when the bead is on the optical axis after the focus.

If the bead is after the focus (b) the bead is pushed to the focus.When a bead is situated out of the optical axis (c) the resultant force pushes the bead to optical axis.

Taken from (Ashkin A. 1992)

The trapping mechanism for smaller submicrometer Rayleigh particles, can not be explained by the ray optics approach presented above. Optical trapping of particles as small as 30 nm has been demonstrated (Neuman K.C. and Block M. 2004). The trapping mechanism and the forces acting on such small particles can be derived considering the polarizability of the particle and the dipole induced by the gradient of light intensity (Ashkin A. 2006).

The explanation of the trapping mechanism above presented is pictorial and helps understanding optical trapping. However, it does not completely characterize the behaviour of the optical trap. The optical force is not the only force exerted on the trapped particle. A micrometer sized bead in water has an extremely low Reynolds number, which means that inertial forces play a negligible role in the bead's motion. The mass of such beads is tiny and their density often similar to that of water, so that, over short timescales at least, we can also disregard gravitational force. This means we need only to consider the following forces acting on a trapped object (see figure 2.5):

- **Restoring force** due to the optical trap:$F_r = \kappa \cdot x$where$x$is the displacement from the centre of the trap and κ is the trap stiffness.

- **Drag force** due to the viscosity of the medium: $F_d = \gamma(dx/dt)$ where γ is the drag coefficient and dx/dt is the velocity.

- **Thermal forces** (F_t) due to thermal energy (k_BT). This force varies randomly and results in the so called thermal or Brownian motion of the object.

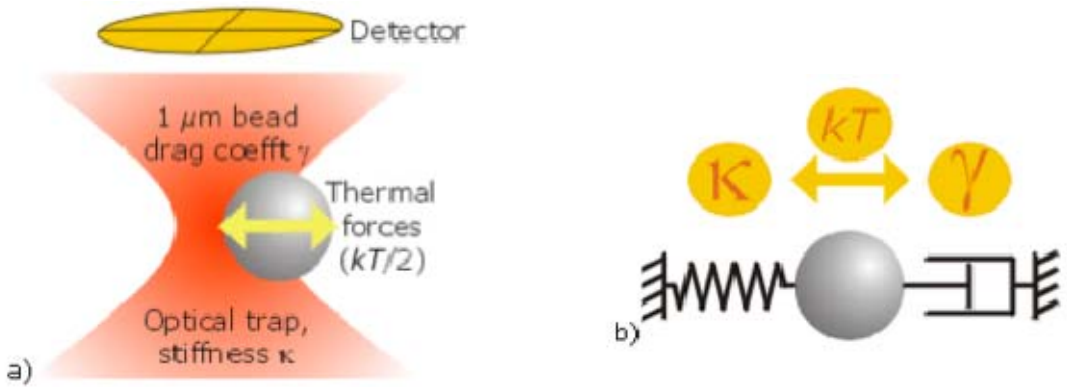

Fig. 2.5: Forces in an optical trap
(a) Schematic of a 1 μm bead diffusing in an optical trap. The bead's position is monitored with a detector, shown schematically above the trap. The forces acting on the bead are the restoring force due to the optical trap, stiffness κ; the viscous drag force on the bead, drag coefficient γ; and thermal forces due to the mean thermal energy ($k_BT/2$). (b) Mechanical model of the forces acting on the bead. The spring represents the restoring force due to the trap stiffness; the dashpot the damping due to viscous drag; and the arrows the random forces due to thermal energy. Taken from http://www2.bioch.ox.ac.uk/~oubsu/ebjknight/motion.html)

The forces acting on a freely diffusing but trapped particle at any moment can then be described by the equation:

$$F_t = F_r + F_d = \kappa \cdot x + \gamma(dx/dt) \qquad \textit{(eq.2.1)}$$

Optical tweezers have the useful property that the restoring force is linearly proportional to displacement (at least over positions near to zero). This linearity means that the strength of the trap can be represented simply by a stiffness value. We can also say, the trap is analogous to a simple spring i.e., it obeys Hooke's law. This linear or Hookean behaviour is one of the most useful properties of OT. As well as providing an obvious way of measuring very small forces, it simplifies the mathematical properties of the system, as described below.

Because the restoring force is proportional to displacement ($F = \kappa \cdot x$) and the work done to displace an object from the centre of the trap is given by $E=F \cdot x/2$, then the potential energy of an object is given by $E= \kappa \cdot x^2/2$. This results in what is often described as a parabolic "potential well". The mean thermal energy of an object is $k_BT/2$per degree of freedom, where k_B is Boltzmann's constant (1.4×10^{-23}J·K^{-1}), and T is the absolute temperature. At room temperature, $k_BT \approx 4$ pN·nm (1 pN·nm = 1zeptojoule or 10^{-21}J). However, the actual distribution of energy is exponential:

$$P=e^{-E/k_BT} \qquad \textit{(eq.2.2)}$$

(Boltzmann's law). This, together with the parabolic potential well, means that the distribution of positions over time tends to follow a Gaussian or normal distribution. Thus, if we observe a trapped object for long enough and record its position, then if we plot a histogram of positions it forms a Gaussian shape with a width determined by the temperature and trap stiffness. In fact, the variance $<x^2>$ of the position signal is given byk_BT/κ. In other words, if we know the temperature, we can use the variance as a measure of stiffness:

$$\kappa=k_BT/<x^2> \qquad \textit{(eq. 2.3)}$$

There are also other methods to calculate the trap stiffness. Two examples are the power spectra (Berg-Sorensen K. and Flyvbjerg H. 2004) and the Stokes drag (Singer W., Bernet S. et al. 2000) methods. However, for these methods, the viscosity of the solution of the trapped particle needs to be known. Since the culture of the cells is characterized by considerable viscosity fluctuations, impossible to be measured accurately, we have chosen equipartition method.

2.2.1.2 Custom built OT set up

We have built the custom inverted OT setup shown in Fig 2.6.

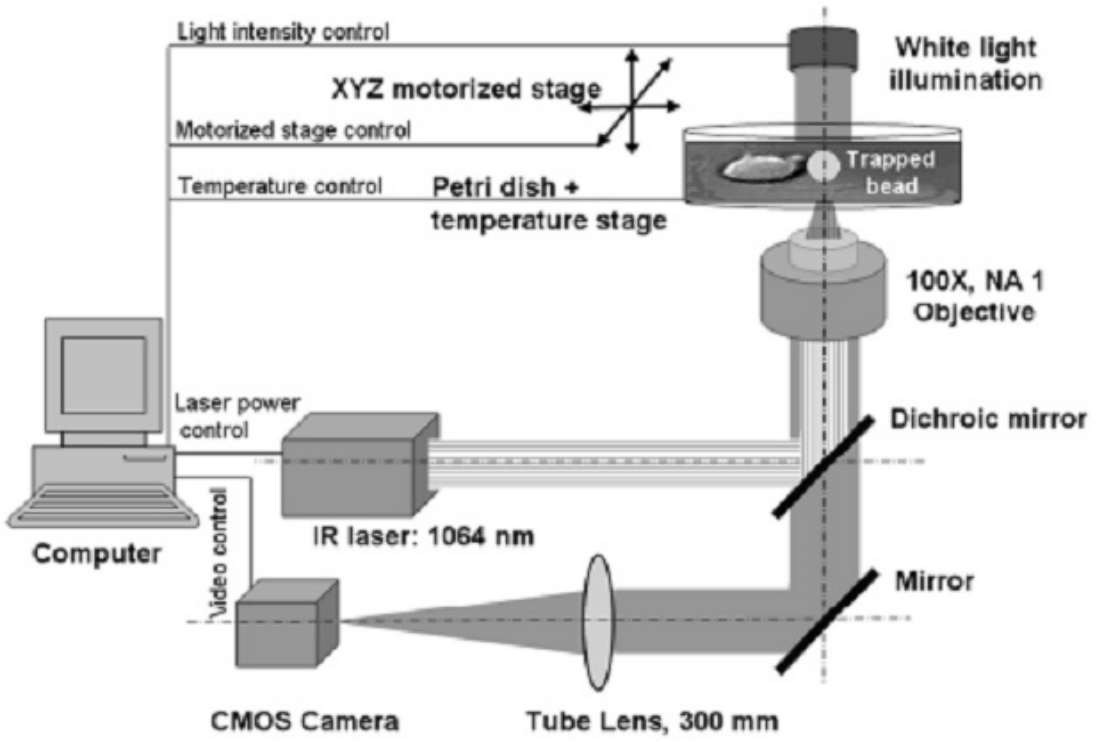

Figure 2.6: OT setup for force-elongation measurements.
The trapping IR laser beam is focused by the microscope objective to form an optical trap inside the sample cell (Petri-dish). The approached cell is observed in transmission by imaging it on the CMOS camera. The XYZ movement of the stage on which the Petri-dish is fixed, sample temperature, sample illumination, laser power, and sample imaging are remotely controlled. Taken from Tavano F. et al. 2011

The trapping laser beam is generated by a 1024 nm continuous wave single mode Yb fiber laser (YLM-5, IPG Photonics GmbH). The laser head has a built-in collimator providing a TEM00 collimated beam with the diameter D_b= 5 mm. Since the entrance pupil of the microscope lens (Olympus, 100X, NA 1, WD 1) has a diameter Dp = 3.6 mm, the laser beam overfills it, meeting the condition for an optimum trapping. The objective lens has a moderate numerical aperture (NA = 1, water immersion) which still provides a stable three-dimensional (3D) trapping. In turn, it has a relative long working distance (WD= 1 mm), allowing to move the trapped particle axially for hundreds of microns inside the sample cell. The alignment of the IR trapping beam is facilitated by a red guide laser beam (660 nm, 0.5 mW), emitted by the same source. Powers higher than 20 mW are necessary at the microbead location to obtain a stiff trap. Typically, the IR laser power at the output of the collimation head is regulated from 250 to 800 mW, allowing a trap stiffness k_{OT} > 0.1 pN/nm. The microbead is imaged by microscope objective and the tube lens on the sensor of the high speed CMOS camera (Fastec HiSpec-4, Adv. Im. Syst.) providing an acquisition velocity from 523 frames per second at full resolution (1696 x 1700 pixels) to 80 kfps at reduced resolution (128 x128 pixels). Note that the tube lens has a focal length (f= 300

mm) longer than the tube lens of a corresponding Olympus microscope (f= 180 mm). This allows an effective magnification, M= 167 X, higher than the nominal magnification (100X) allowed by the microscope objective with a normal tube lens. This longer focal length provides a better position detection sensitivity during microbead videotracking in the trap. Videotracking has been performed using the Particle Detector and Tracking Plugin of the open access NIH Software ImageJ (http://rsweb.nih.gov/ij/index.html). The plugin is based on an algorithm (Sbalzarini 2005) developed at ETH, Zurich, Switzerland and permits to follow the position of the microbead with a precision of about 5 nm. Videotracking calibration has been performed separately using stuck beads on coverslip and a 3-axis piezo–stage (Max314/M, Thorlabs/Optoprim). The movement of the sample during the experiments with the cells *in vitro* is instead carried out by a 3-axis DC motor stage with equipped with high resolution encoder (M-111 XYZ, Physik Instrumente PI) allowing 15 mm linear motion for each axis. This choice is required by the experimental working conditions where cell has to be quickly identified in a field of 12 mm in diameter

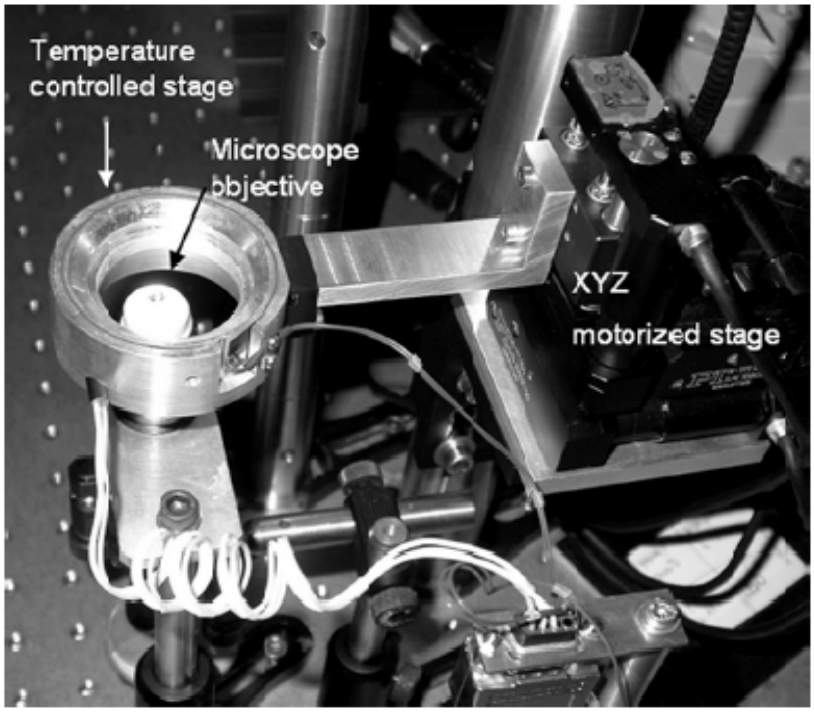

Figure 2.7: Picture of the custom-built OT setup
Partial picture of the setup, showing the sample cell environment. Components indicated: the temperature controlled stage, composed by a film resistance inserted in a ring of aluminium and a temperature sensor; the microscope objective is oriented toward the sample cell in an inverted microscope configuration; motorized stage XYZ. Taken from Tavano F., et al 2011

2.2.1.3.Cells preparation and beads functionalization

One day prior the OT experiments cells were plated on slightly modified Petri-dishes. We drilled a hole of 12 mm diameter in each Petri-dish and replaced the plastic by a glass 170 μm thick coverslip. This allowed a better propagation of the trapping beam and at the same time, the possibility to work also with microscope lenses with short WD. In order to have an adequate number of cells during experiments, 15-20x10^4 cells were seeded in a modified Petri-dish. To have uniformity in the experimental conditions 18 hours prior to experiments, Ara-C was added in the cell medium to a final concentration of 5um, in order to arrest cell cycle in the S-phase and perform the tether pulling experiments on cells in the same cell cycle phase.

During experiments, Petri-dish settled on a home made heating insert and kept at 37 ºC by a digital temperature controller (RSComponents) to maintain physiological conditions during experiments. There was no control of CO_2 concentration in the cell environment thus every Petri-Dish was used not more than 20-30 minutes to avoid pH alteration damages. To test the mechanical properties of cells on adhesion we used 1.5 um silica beads as probe. Beads were coated with COOH groups (Kisker-biotech, cat PSi- 1.5COOH) and functionalized with Bovine Serum Albumine (BSA) using the PolyLink Protein Coupling Kit (Bang Laboratories Inc., cat PL01N) following the manufacturer's protocol. Briefly, about 1.4 x 105 beads were incubated with 500 ng of BSA in the presence of 20 g L-1 EDAC (water-soluble carbodiimide) for 1h at room. Beads were usually prepared one or two days before the experiments and stored at 4^{o}C to avoid protein degradation. With an immunofluorescence staining with anti-BSA antibodies we confirmed that the coating was successful: BSA was present and its distribution on the bead was homogeneous.

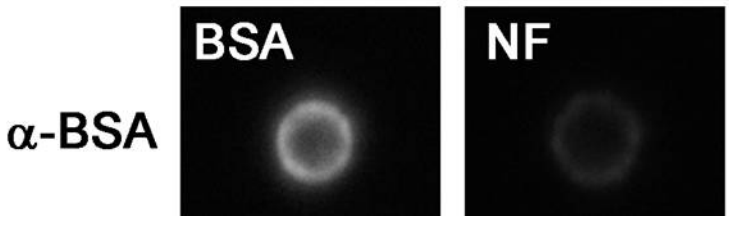

Figure 2.8 Immunofluorescence staining of BSA functionalized (left) and non functionalized (right) silica beads using α-BSA antibody. The test confirmed the BSA functionalization was successful and BSA was homogeneously distributed on the bead surface.

Beads used for pulling tethers were injected with a micropipette directly on cells some minutes before the experiment, to give beads time to float in the medium. When beads reach the focus point, we could visualize and trap them.

2.2.1.4. Tether membrane extraction and force-elongation measurement technique

The experimental approach used to extract a membrane tether by means of OT is described in this section and illustrated in Figure 2.9.

A silica microbead coated with Bovine Serum Albumine (BSA) is trapped by the laser beam focused through the microscope objective (100x, water). The cell of interest, laid on the culture dish, is then approached to get its membrane in contact with the microbead (Figure 2.9a, left). This is achieved by controlled x-y-z movements of the motorized stage. After few seconds of contact the coated bead is supposed to bind the surface membrane proteins and the tether can be extracted by moving laterally the stage at constant velocity (0.5 μm / s) (Figure 2.9a, centre). The tether is a membrane tube like with a diameter usually about 100 nm and hence it can not be visualized. To verify tether formation we switch off the laser and observe the movement of the microbead. If the microbead rapidly retracts to the cell the presence of the tether membrane is confirmed (Figure 2.9a, right). If the microbead simply diffuses around, it means that no tether has been created and the experiment should be repeated. During tether formation, both the cell and the bead are monitored by a CMOS camera working at a high acquisition frame rate (> 200 frames / s).

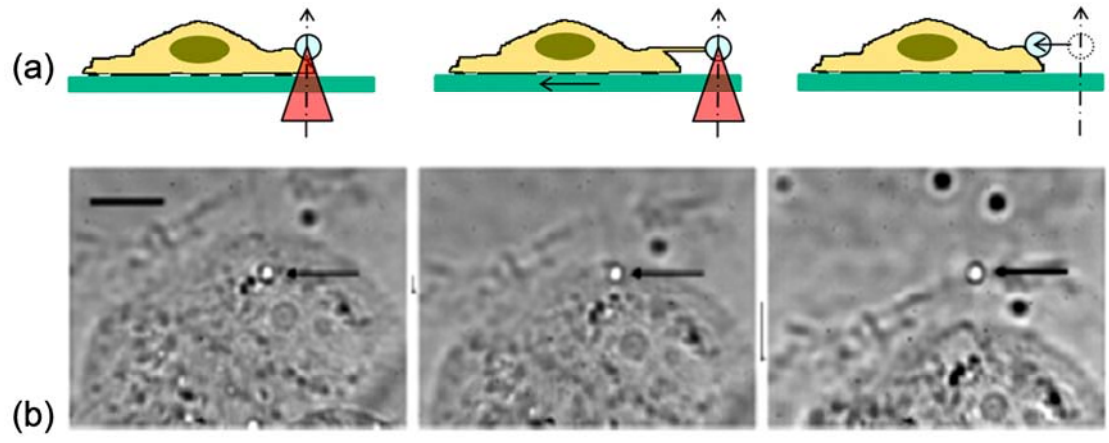

Figure 2.9 . Schematic of the experimental approach
Above:Sequence of three pictures showing the trapped bead in contact with the cell membrane (left), the cell translation during tether formation (centre), the bead retraction to the cell after laser is switched off. The laser is marked by the red triangle. Below: the focused laser creating the optical trap is marked by the red triangle. The third picture on the right shows the bead retraction to the cell after laser is switched off. Below: Sequence of three images showing the trapped bead in contact with the cell membrane (left) andthe cell translation during tether formation (centre and right). The size of the small vertical arrows oriented downward is proportional to the displacement. Scale bar is 10 μm.

Measurement of weak mechanical interactions (in the range from 10^{-1} to 10^{2} pN) using a trapped microbead as a probe is based on the fact that the force acting on a microsphere within an optical trap can be modelled as a Hookean spring (Svoboda K. 1994), provided the displacement from the optical trap is not too large:

$F=K_{ot}*X_b$ *(eq.2.4)*

where k_{OT} is the spring constant (trap stiffness) and X_b the displacement of the microbead. Thus, to get the force, the bead displacement X_b is measured by videotracking its image, which is formed on a high speed CMOS camera with high frame rate. The trap stiffness k_{OT} is calculated prior to each experiment by using the equipartition theorem method described in 2.2.1.1

During the pulling experiments, beside the bead displacement X_b we measured also the cell displacement, x(t). The calculated force is expressed as a function of elongation, F=F(x). The resulting plot is called Force-Elongation curve. All the FE curves have in common the presence of three regimes with distinct dominant behaviours: elastic, rupture, and viscous. A typical FE curve is shown in Figure 2.10.

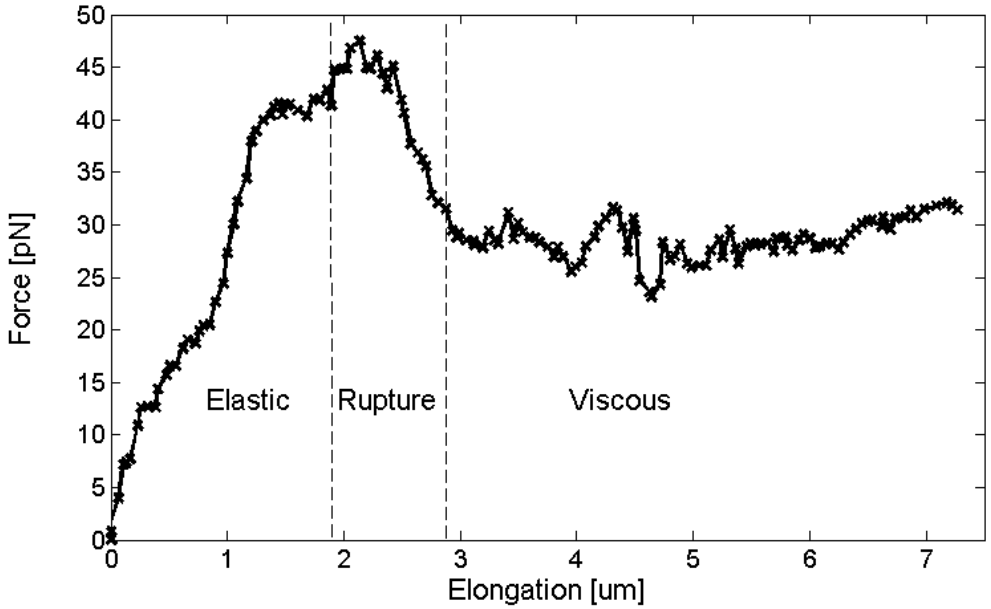

Figure 2.10: Force-elongation FE curve.
The curve is determined by measuring the force exerted on the bead when a tether membrane is formed. Note the presence of three distinct regions: 1- elastic regime, 2 – detachment of the membrane from the cytoskeleton, 3- viscous regime.

In the first part, the force increases almost linearly with the elongation, which is characteristic for an elastic regime. A maximum force is reached followed by relaxation in (2). This corresponds to the local separation of the membrane from the cytoskeleton. Finally, the force remains almost at a constant value which is characteristic for a

viscous behavior (3). The FE curve shown in Figure 2.10 is consistent with the assumption that the force necessary to pull a tether from membrane must overcome the membrane bending rigidity, the membrane tension membrane, the adhesion of the phospholipid membrane bilayer to the cytoskeleton and the viscous resistance of the phospholipid bilayer (Sheetz and Dai 1996; Raucher and Sheetz 1999; Sheetz, 2001). Forces of tens of pN are typically necessary to extract tethers (Hochmuth et al. 1996, Ermilov et al. 2005), which is well in the range of forces developed with OT.

The shape of our FE curve is similar to those reported previously in literature for cancer cells (Guo et al. 2004), neuronal cells and other types of cells (Hochmuth et al. 1996; Li et al. 2002; Ermilov et al. 2005). The data analysis to extract the parameters of interest to describe the local viscoelastic properties of cells is described in section 3.1.1.4.

2.2.2 Elastic modulus measurement for single cells by AFM

2.2.2.1. The Indentation technique

We used AFM to perform indentation experiments and determine the Young Modulus corresponding to a cell region. The indentation, δ, on the cell is given by the difference between the piezoelectric movement z, and the tip deflection x (figure2.11, right):

$$\delta = z + x \qquad (eq.2.5)$$

A bead was glued on the tip of an AFM cantilever. The cantilever was precisely moved down into the cell by a piezoelectric element while the deflection of the cantilever was measured by the laser beam deflection on the photodetector (figure 2.11, left) Both the deflection of the tip and the movement of the cantilever are measured with nanometer resolution (Franze K. 2011)

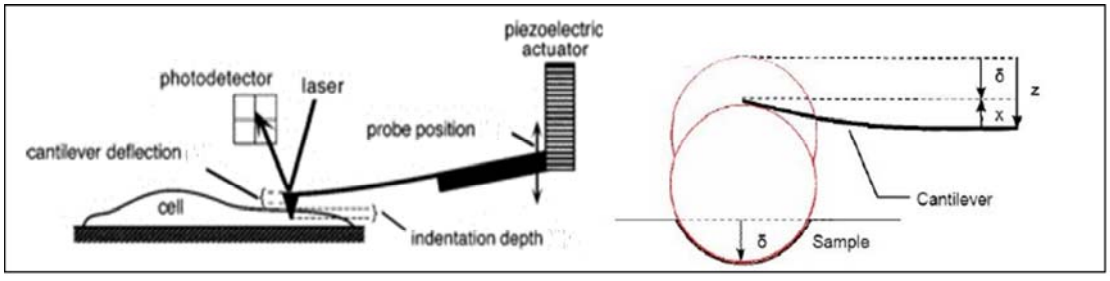

Fig. 2.11
(left) Cell indentation experiment with AFM. Cell is laying on adhesion while the cantilever indents cell surface. Deflection is measured by a laser beam reflected on the cantilever and is detect by a photodiode. (right) Sample indentation is described in detail: the cantilever is moved towards the sample by a distance z (height measured). The cantilever is bending into the opposite direction (x) whilst the sample is indented by δ . Finally δ is calculated by subtracting the cantilever deflection from the heigh measured. (jpk instruments)

For small deformations, the cantilever follows Hooke's law F = kx, where F is the force, x is the displacement from the equilibrium position, and k is the cantilever's spring constant (for biological samples usually 0.01–0.1 N/m). By recording cantilever deflection with higher frequency during the entire experiment, it is possible to derive the force during both the cantilever indentation in the cell and the cantilever retraction to the original position. Forces in the piconewton range can be measured with AFM (Munevar S., Wang Y. et al. 2001; Franze K., Gerdelmann J. et al. 2009). The data obtained by indentation measurements were plots of vertical cantilever deflection against tip-sample separation. An example is shown in Figure 2.12. To derive the Young's Modulus, the "extend" curves which relate to the indentation, but not the "retract" curves which relate to the retraction of the cantilever, were fitted in the Hertz (Hertz H. 1881) model by a dedicated JPK software, as described afterward in section 2.2.2.3.

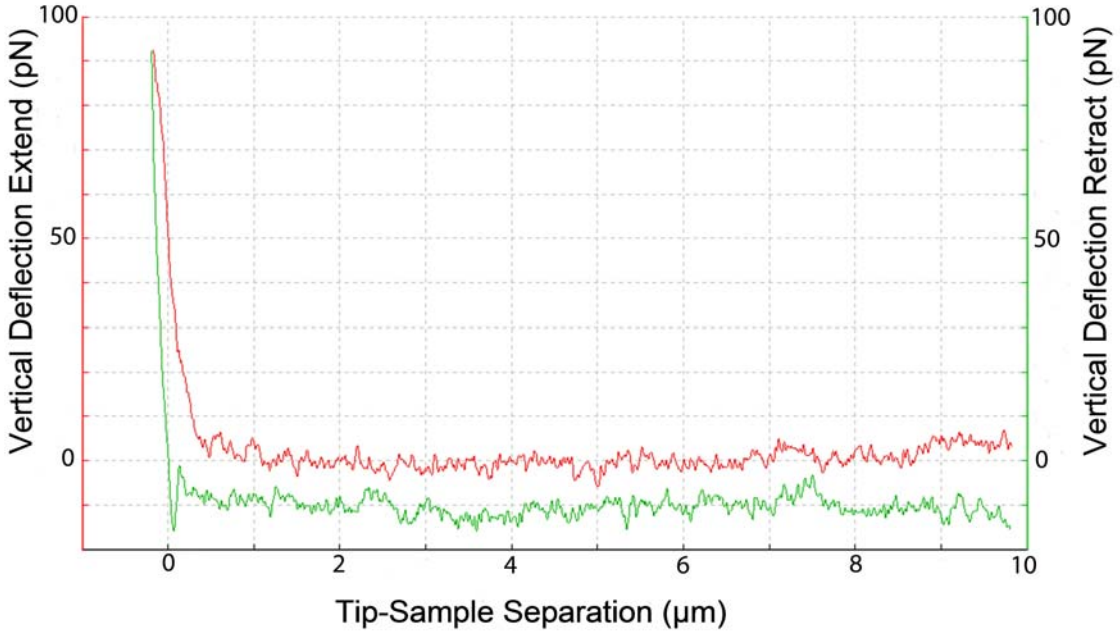

Figure 2.12: Example of curve resulting from and indentation experiment.
Cantilever vertical deflection Vs Tip-Sample separation during the extend (red) and the retract (green).The "extend" curve relates to the indentation, the "retract" curve relates to the retraction of the bead from the cell.

2.2.2.2 AFM setup and experimental approach

For our analysis, we used Nanowizard II AFM (JPK, Berlin, Germany) with a silicon nitride cantilever, V-shaped, 100 µm long and with a nominal spring constant of 37pN/nm from NANOWORLD (PNP-TR-TL-20). However, sharp tips exert a large stress s = F/A on the sample, where F is the force and A is the contact area. Thus, such probes are very likely to penetrate soft materials such as cell membranes and the underlying actin cortex already at small forces, limiting their application in biological

samples (Franze K. 2011) and invalidating elasticity measurements. For this reason, we used a bead glued on the tip of the cantilever (silica bead of 4.5 μm diameter , Kisker-biotech).

The cantilever was calibrated in liquid on a glass coverslip. Silica beads were first sonicated and a drop of 5 μl of them was dispersed on a glass coverslip. Also a drop of UV-curable glue was dispersed in the same glass coverslip, forming thin lines of glue close to the silica beads. The tipless cantilever was engaged on a clean area of the glass and then aligned on the top of a glue lines few microns far away from it. A force-curve with a set-point of 1nN and a z-length of 10 μm with a speed rate of 10 μm/s was performed to attach glue just on the end of the cantilever. The cantilever was then brought in contact with an isolated bead and a force-spectroscopy curve was obtained with a delay of 30 seconds between the extended and the retracted curve to permit the adhesion of the bead to the cantilever. Moreover a slow left-right movement was performed to facilitate the bead detachment from the substrate ant attachment to the cantilever.

The glue was cured with direct UV exposition (using an UV lamp with a DAPI filter) for 30 minutes. The cantilever with the bead was firstly calibrated in liquid and then used to acquire force-distance curves on the patterned area. The calibration was repeated at least 4 times to average the sensitivity values and to obtain a more precise spring constant value.

2.2.2.3. Data analysis to derive the elastic modulus: the Hertz Model

Data analysis has been made by applying the Hertz model on curves and calculating the apparent sample elasticity by automatic fitting of the JPK software, which give the possibility to derive the Young's Modulus (E).

The Hertz model assumes a linearly elastic, homogeneous, isotropic material, which does not necessarily apply to biological samples (Franze K. and Guck J. 2010; Chatelin S., Constantinesco A. et al. 2011). Furthermore, this model is only valid if the indentation depth is 5-10% than the sample's thickness (Engler A.J., Richert L. et al. 2004). If the indentation depth is larger, corrections for thin samples are required (Dimitriadis E.K., Horkay F. et al. 2002), otherwise the Young's modulus will be overestimated. Furthermore, while spherical probes provide reliable values, indenting cells with sharp tips results in higher Young's moduli (Carl P. and Schillers H. 2008) (and probably in cell damage). Thus, Young's moduli found in the literature should be interpreted with caution.

Nevertheless, if the experimental conditions and the data analysis are chosen carefully (Franze K. and Guck J. 2010; Chatelin S., Constantinesco A. et al. 2011), the Hertz model provides valuable information. To satisfy these conditions and to be able to use the Hertz model, we used a cantilever coated with a silica bead to avoid cell penetration and damaging; the indentation was 500 nm that can be considered neglectable compared to cell height.

As already mentioned above, E was derived from force-displacement curves obtained with the AFM, when the deflection of the AFM cantilever was monitored as it approached the sample. The standard Hertz model (Hertz H. 1881) describes the indentation of a silica bead with a specified radius (R) in a soft sample, predicting that the force *F* produced was:

$$F = \frac{E}{1-\upsilon^2}\left[\frac{a^2+R^2}{2} In \frac{R+a}{R-a} - aR\right] \qquad \textit{(eq.2.6)}$$

When the indentation δ was calculated as:

$$\delta = \frac{a}{2} \ln \frac{R+a}{R-a} \qquad \textit{(eq.2.7)}$$

Where α is the half-opening angle of the AFM tip (25) and ν is the Poisson's ratio, assumed to be 0.5 for cells.

E was obtained from the best linear fit of the force-distance curve.

2.2.3. Cell deformability measurements by Optical Stretcher (OS)

2.2.3.1 Microfluidic Optical Stretcher (MOS) principles

MOS is a novel laser tool which represents a recent advancement in cell manipulation and characterization techniques. It involves a dual-beam laser trap used to manipulate biological samples without mechanical contact nor bead attachment (Guck J., Ananthakrishnan R. et al. 2001; Lincoln B., Schinkinger S. et al. 2007). Most importantly, said method can be combined with a microfluidic system, which allows an automated serial, high-throughput measurement of the mechanical properties of cells in suspension (Lincoln B., Schinkinger S. et al. 2007).

Microfluidic Optical Stretcher is based on a double-beam trap in which two opposed, divergent and identical laser beams with Gaussian intensity profile trap an object in the middle. This trapping is stable if the total force on the object is zero. The condition is

fulfilled if the object that is positioned in the middle of the beams has a larger refractive index than the refractive index of the surrounding medium.

The principle of the OS is rather simple: when a Gaussian laser beam is incident on a dielectric object such as a cell, the momentum change and the resulting forces trap the object (figure 2.13, A) and tend to stretch it (figure 2.13, B) (Guck J., Ananthakrishnan R. et al. 2000). Stretching is observed as a measurable elongation of the cell along the laser axis. This stress is caused by a momentum transfer from the light to the interface, due to the change in refractive index (Ashkin A. and J.M. 1973). By increasing the laser power, these surface stresses can become sufficient to measurably deform a cell, while maintaining its position. If used for this purpose, a dual-beam laser trap is called an OS (Guck J., Ananthakrishnan R. et al. 2001).

More precisely, figure 2.13 describes the distribution of surface forces (thin blue arrows) induced when only one laser beam with Gaussian intensity profile incides from one side (indicated with large triangles) for a cell which is slightly below the laser axis and on the axis (C,D respectively) . The integration of these forces over the entire surface results in the net force (Fnet) shown as larger blue arrow. When two identical but counter propagating laser beams incide on a cell on axis, this create a stable trapping configuration and it is described in figure 2.13(E). The thin blue arrows represent the distribution of surface forces that act on the cell and stretch it. When the cell is displaced from the axis as shown in figure 2.13(F), the symmetry of the resulting force distribution is broken, giving the net force a restoring component perpendicular to the laser axis.

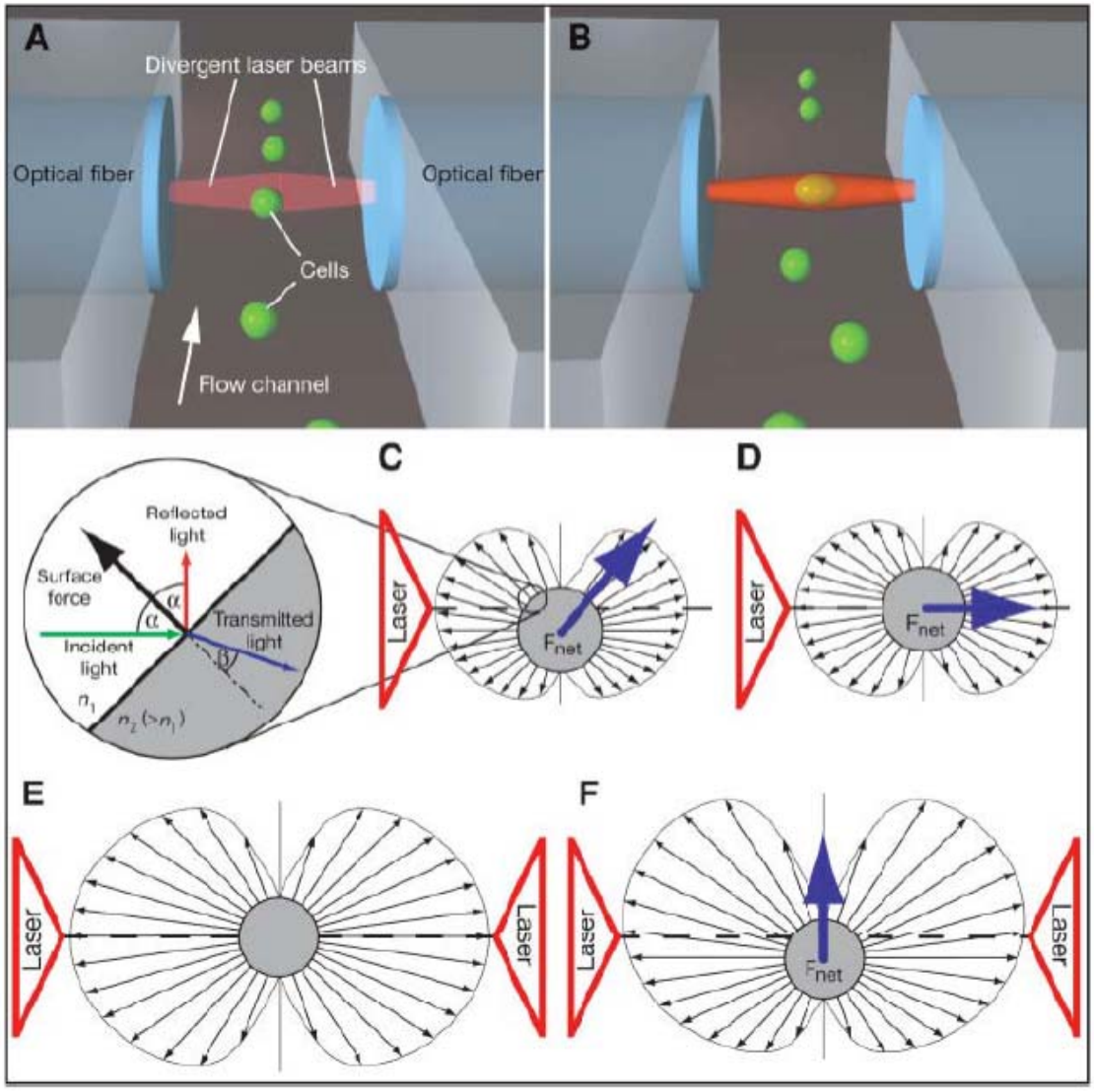

Figure 2.13: Optically induced surface forces lead to trapping and stretching of cells.
Cells flowing through a microfluidic channel can be serially trapped (A) and deformed (B) with two counterpropagating divergent laser beams. The distribution of surface forces (small arrows) induced by one laser beam with Gaussian intensity profile incident from the left (indicated with large triangles) for a cell that is (C) slightly below the laser axis and (D) on axis. In (E) the corresponding distributions for two identical but counterpropagating laser beams are shown for a cell on axis creating a stable trapping configuration. In (F) the broken symmetry of the resulting force distribution when the cell is displaced from the axis. Adapted from Guck J.2005

Since the laser beams in the optical stretcher are divergent and not focused light, powers as high as 1200 mW in each beam can be used, which lead to surface forces up to hundreds of pico-Newton without radiation damage to the cells.

2.2.3.2. MOS setup

The MOS setup used for our experiments has been design and built by the Softmatterphysics group of University of Leipzig (Germany). It consisted of two laser beams (λ= 1,064 nm) provided by two Ytterbium fiber lasers 5W YLM-5-1064 (IPG Photonics, Oxford, Massachusetts) with the laser guiding fibers aligned opposing one another. The fibers were align using a SU-8 (epoxy-based negative photoresist)

patterned structure and then positioned perpendicular to a square glass capillary flow channel, where cells flow. Soft clamps serve as a strain relief for the fibers and the capillary connectors. The setup is positioned onto the translatable microscope stage and connected to flow tubing. The trap is set inside the capillary where cells flow (see figure 2.14): the height is as low as possible without the divergent beams interfering with the channel floor. With fiber centered about 25 μm above the floor with a spot size (radius) of about 12 μm at the channel centre cells can be sequentially trapped without settling in the channel (Lincoln B., Schinkinger S. et al. 2007)

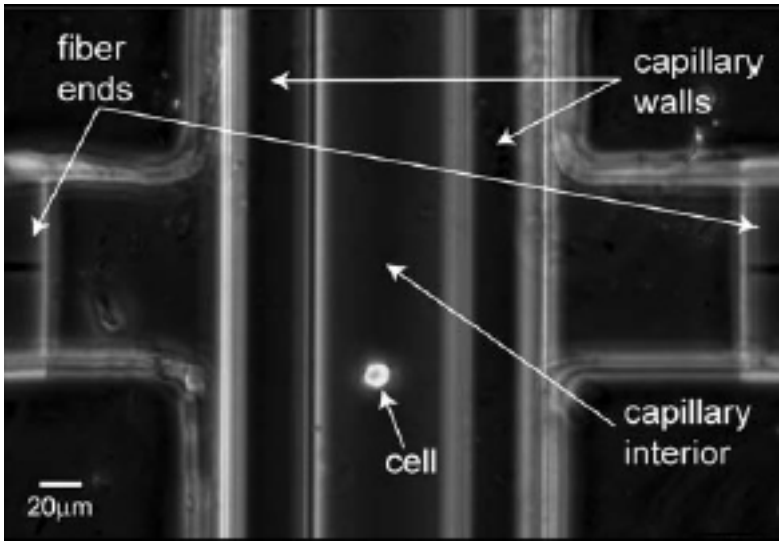

Figure 2.14 Phase contrast image of the capillary channel.
Fibers are align perpendicular to the capillary. A cell is flowing down the capillary. Scale bar is 20 μm. Illustration was taken and adapted from (Lincoln B., Schinkinger S. et al. 2007).

Flow was controlled by channel custom made computer controlled pressure driven pump system. The cell suspension is delivered via cryovial directly connected to the micro-fluidic system. Stage temperature was set up at 23^{o}C during experiments. During the stretching, due to a laser heating of 26^{o}C/W, the temperature was calculated to be in the range of 48,8^{o}C-54,2^{o}C during the 2 s of stretching. Cell deformation was recorded using video phase contrast microscopy on an inverted microscope (Axio.Observer Z1, Zeiss). These images, typically recorded at 30 frames/s with a digital CCD camera (A202k, Basler), were converted to contour data using a custom-made edge detection program (implemented in MatLab).

2.2.3.3 Sample preparation

Cells were grown normally in small flasks with the appropriate cell medium and trypsinized as described in section 2.1 some minutes prior to experiments they. Cells were counted using a Burker cell counting chamber and typically prepared in a density

range of 20− 50×10^4 cells/ml in order to assure that the cells can be found as regularly as possible within the flow while maintaining a reasonable distance between each one. A total volume of about 1 ml was standard for an experiment during which cells were serially trapped at low powers and deformed at higher powers (0.7–1.2 W per beam). The flow was stopped during each trap and deformation cycle.

2.2.3.4 Experimental Approach to measure cell deformability

Each cell was trapped with a laser power of 100 mW by each beam and subsequently stretched for 2 s with an higher laser power ranging from 866mW to 1200mW. The temporal development of the major axis was tracked for each individual cell and the relative axial extension or strain of each cell as a function of time in units of percent deformation $\gamma(t)$ was calculated

$$\gamma(t) = \frac{a(t) - a_0}{a_0} \times 100 \qquad \textit{(eq. 2.8)}$$

where $a(t)$ is the length of the major axis of the stretched cell, which is aligned with the beam axis, and a_0 is the lencth of major axis before stretching (average of the a values during the first second of the trap phase). An example of stretched cell is shown in fig. 2.15. In our analysis, we took in consideration the relative major axis extension as a cell classification parameter.

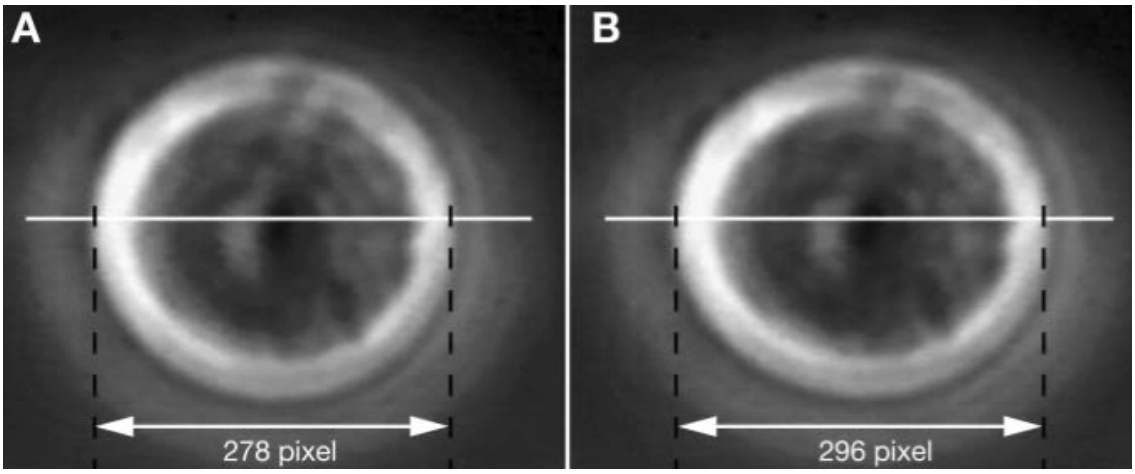

Figure 2.15:
Deformation of a cell in an optical stretcher. Cell deforms by 6.5 % along the laser axis, as determined by image analysis, when the light power is increased from 0.1 W (A) to 1.7 W (B) in both beams. Taken from Guck J. 2005.

Due to the small focal depth of the imaging system, only a cross section of the cells was imaged. After each experiment images were analyzed separately and converted to contour data using a custom-made edge detection program (implemented in Matlab)

partially based on the description in (Lincoln B., Schinkinger S. et al. 2007). Data have been analyzed in a phenomenological way and took in consideration only the optical deformability as a cell classification parameter (Lincoln et al. 2004; Guck et al. 2005). However depending on the application data could be potentially more rigorously modelled to obtain physical properties such as the frequency-dependant shear modulus of the cell (Wottawah et al. 2005).

2.3 Western Blot Analysis

2.3.1. Protein extraction

Proteins were extracted from cells using a Lysis Buffer for native proteins containing 50mM Tris-HCl pH 8.0, 0,4M NaCl, 1% NP40, proteases inhibitor 1X. The lysis buffer was freshly prepared prior to each extraction. Cell cultures were trypsinized as described in section 2.1 and cell pellets were washed 3 times with sterile PBS. Pellets were kept on ice and incubated for 4 minutes with cold lysis buffer, vortexed well for 1 minute and placed on ice .This cycle was repeated for 5 times until suspension looked homogeneous. The volume of lysis buffer used depends on the cell pellet volume. The smaller the lysis buffer volume the highest the final protein concentration, however too small volumes prevent proper cell lysis: typical extractions from 2-3 x 10^{6} cells required about 1 ml of Lysis Buffer.

After vortexing, the samples were centrifuged for 10 mins at 5000g at 4^{o}C and the supernatant containing the total protein extract was collected. During the protein extraction procedure the tubes containing cell pellets were kept on ice to avoid protein degradation.

Proteins were quantified by Bradford assay (Biorad) as suggested by the manufacturer Some aliquots were immediately used, the others were stored at -80^{o}C up to use. Prior to western blot analysis proteins were run in an SDS-PAGE to verify the success and the quality of protein extraction.

2.3.2.Western blot analysis

Ten micrograms aliquots of cell lysates were separated on denaturing 12% polyacrylamide gels and electroblotted onto nitrocellulose membranes (Millipore) Afterwards membranes were blocked with 5% non-fat milk powder in PBS or TBS containing 0,05% Tween 20 for 1 hour at room temperature, then the primary antibody was added and the membranes were incubated separately again for 1-2hours. The choice of PBS or TBS, the antibody concentration and the time of incubation were related to the antibody type we were going to use: for each antibody we followed the manifacture's protocol.

Primary Antibodies			
Protein	**Host/Ab Type**	**Diluition**	**Manifacturer**
CK 18	Rabbit Ronoclonal	1:5000	Millipore
CK8	Mouse Monoclonal	1:5000	Millipore
Vimentin	Goat Polyclonal	1:100	Millipore
E-Cadherin	Mouse purified antibody	1:5000	BD Bioscience Pharmigen
Integrin αVβ3	Mouse Monoclonal	1:1000	Millipore
Vinculin	Mouse Monoclonal	1:1000	Millipore

Table 2.1:
List of the primary antibodies used for immunoblotting experiments. Informations on antibody type, host, diluition, and manufacturer are reported

After incubation with the primary antibodies membranes were washed with PBS or TBS containing 0,05% Tween 20 (SIGMA) - 5 washings of 5 minutes each - and then incubated with the proper secondary antibody. We used horseradish peroxidise (HRP)-conjugated IgG (anti-mouse, anti-rabbit from DAKO or ImmunoPure Rabbit Anti-Goat IgG from Thermo Scientific dilution 1: 20000). After each antibody's incubation, the membranes were washed with PBS or TBS containing 0,05% Tween 20. Signals were developed using the enhanced chemiluminescence system (Luminata Forte Western HRP substrate, Millipore). After each experiment membranes were incubated again with a HRP-conjugate Beta actin antibody as positive control. Densiometric signal intensities of the detected spots were calculated with Image J software.

2.4 Super resolution cytoskeleton imaging by fluorescence microscopy

2.4.1 Cell staining preparation

Immunofluorescence was performed on the three cell lines analyzed MDA-MB-231, MCF-7 and HBL-100 to investigate their cytoskeletal organization.

To visualize the actin cytoskeleton structure the following protocol was used: cells were grown on coverslips, fixed in 3% paraformaldehyde for 20 minutes at room temperature and then washed for 5 minutes with 0.1M NH_4Cl in PBS. Permeabilization and blocking was performed by incubation in TritonX-100 0,1% in PBS+ 1% BSA for 1 hour at room temperature. To label the actin cytoskeleton cells were incubated with Phalloidin (Phalloidin-atto 590, attotech) at a diluition of 1:100 1hour at room temperature and washed 3 times with PBS and once with water prior to mount the coverslip.

2.4.2. Stimulated Emission Depletion (STED) super resolution imaging principle

The images were recorded with a custom-built STED microscope of the group of Prof. Stefan Hell from the Department of NanoBiophotonics of Max Planck Institute for Biophysical Chemistry in Göttingen, Germany. The set up (Bückers J., Wildanger D. et al. 2011), combines two pairs of excitation and STED laser beams, all stemming from a single supercontinuum laser source (Wildanger D., Rittweger E. et al. 2008; Wildanger D., Medda R. et al. 2009). Whereas the excitation wavelengths (570±2 nm and 650±2 nm) were selected from the supercontinuum using an acousto-optical tunable filter (AOTF, AA Opto-Electronic, Orsay Cedex, France) the STED wavelengths (720±10 nm, 755±15 nm) were extracted using prism monochromators ensuring strict wavelength selections. After filtering the appropriate wavelength ranges, the four beams were coupled into separate polarization-maintaining single mode fibers. At the fiber outputs the beams were collimated and sent to the objective lens. The corresponding excitation and STED beams were combined using dichroic mirrors to give two pairs of beams with orthogonal polarization. The beam pairs were then combined with a polarizing beam splitter cube and coupled into the objective lens (PL APO 100×/1.40–0.7 oil, Leica Microsystems, Wetzlar, Germany). Two vortex phase plates (RPC Photonics, Rochester, NY, USA.) placed into the STED beams followed by a superachromatic quarterwave plate (600–2700 nm, B. Halle GmbH, Berlin, Germany) placed at the back of the objective lens afforded ring-shaped STED foci with a zero-intensity minimum in their center.

To ensure spatial overlap of the excitation and the STED foci, the diffraction patterns („point spread functions PSFs") of the four beams were measured sequentially by recording scattered light from gold nanoparticles (80 nm) as they were scanned through the focal region. The alignment precision was on the order of 5 nm, i.e. below the resolution achievable with the setup.

Since all four laser beams originated from a single source, no pulse synchronization was necessary. Still, the simultaneous arrival of the excitation and the respective STED beam in the sample had to be adjusted by matching the optical path lengths for each pair of beams. On the contrary, the pairs of excitation and STED beams for the two colour channels were time-shifted by about 40 ns using optical fibers of different lengths. This pulse-interleaved acquisition scheme enabled the (quasi-)simultaneous recording of both colour channels: in addition to the spectral separation photons were assigned to a dye according to their arrival time at the detector. Due to the simultaneous recording of both colour channels hardly any shift of the sample was possible during the recording time.

The fluorescence from the two fluorophores was separated from the laser beams with a custom made multiband dichroic mirror (Chroma Technology, Rockingham, VT, USA). It was subsequently split up with a second dichroic mirror (Z635RDC, Chroma Technology) according to the maximum emission of the different dyes, and was finally cleaned up with bandpass and longpass filters (M620/40, M670/40 nm and Z660LP, all from Chroma Technology). The fluorescence was then focused into separate multimode optical fibers (Ø = 62.5 µm, Thorlabs, Dachau, Germany) which served as confocal pinholes. The fibers were attached to single-photon counting modules (SPC-AQRH-13-FC, Perkin Elmer, Salem, MA) which were connected to custom time gating electronics extracting the fluorescence signals following each of the excitation/STED pulse pairs. Optionally, for the acquisition of fluorescence lifetime data, the time trace of the fluorescent signals was measured by a time-correlated single-photon counting (TCSPC) module (SPC-730, Becker & Hickl GmbH, Berlin, Germany).

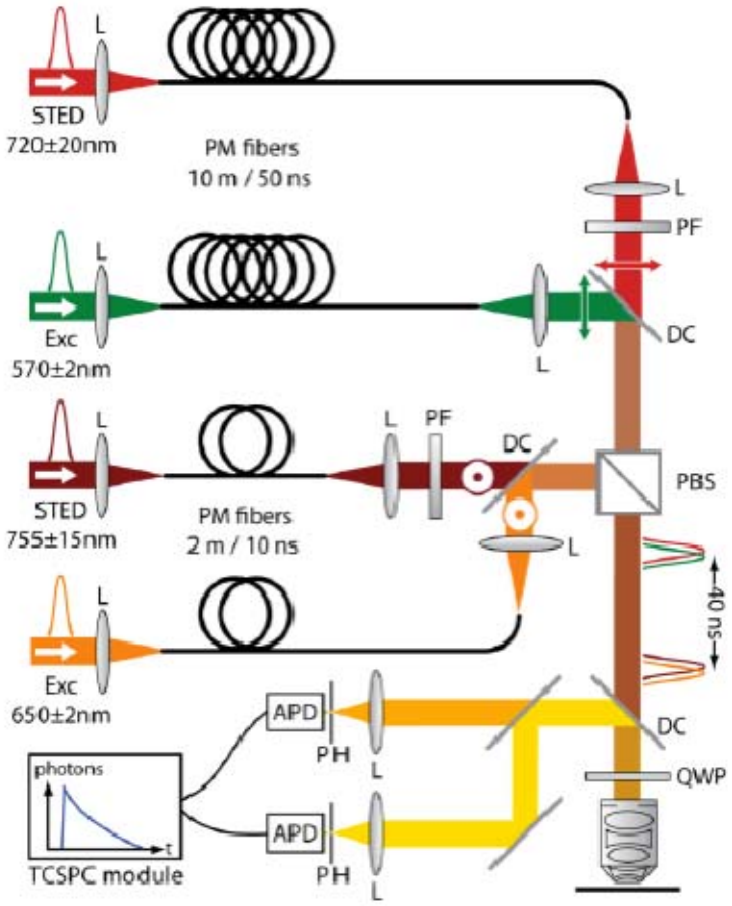

Figure 2.16
Setup of the multi-lifetime/multi-color STED microscope. (Bückers J., Wildanger D. et al. 2011)

2.5 MALDI-MS

We used matrix-assisted laser desorption and ionization (MALDI) mass spectrometry (MS) to characterize the lipid composition of cells. We performed semi-quantitative analysis to compare the lipid composition of the three different cell types and find out significative differences among them. MALDI-MS is a well established technique in the study of proteins but there is increasing evidence that MALDI MS is also very useful in lipid research, because it is fast, sensitive, it tolerates sample impurities to a relatively high extent and it provides very simple mass spectra without major fragmentation of the analyte (Fuchs B., Süß R et al. 2010).

2.5.1. MALDI-MS technique principles

The technique of mass spectrometry determines the elemental compositions and/or molecular structures of compounds by measuring the mass-to-charge (*m/z*) ratios of generated ions. Traditional "hard" ionization techniques have been used in lipid chemistry in early days, but the development of modern "soft" ionization methods

significantly facilitated the analysis of lipids and phospholipids. One of these is the MALDI technique that will be described in this section.

As indicated by its name, a typical MALDI-MS is based on a matrix that absorbs laser energy (Schiller J., Süss R. et al. 2006). IR and UV lasers that are normally used on commercially available MALDI devices. The use of matrix is essential in the design of MALDI in that it absorbs the laser energy, and prevents aggregation of the analytes. In most cases, an organic matrix solution is mixed with the analyte solution and afterwards crystallized on a metal "target" plate.

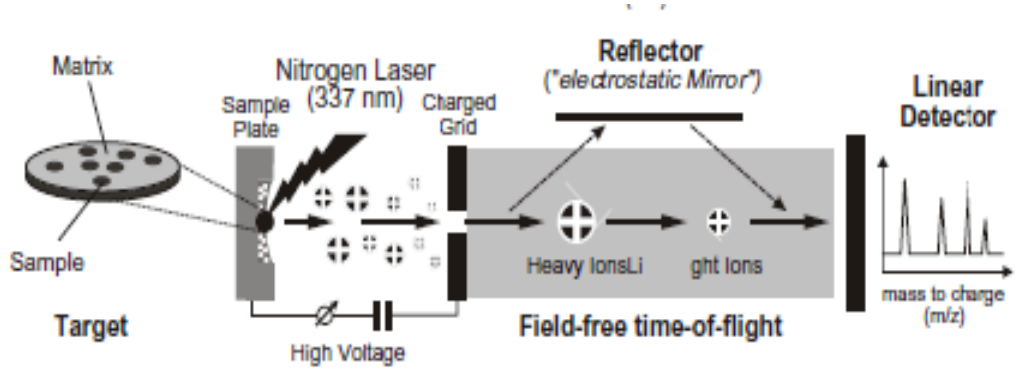

Figure 2.17
Schema of the processes occurring during the MALDI-TOF ionization process in the mass spectrometer). The influence of the detection using the ‘‘linear” and ‘‘reflector” mode is emphasized in the figure. Adapted from (Baldwin MA. 2005)

As shown in Figure 2.17, when the laser beam hits the sample, the matrix (which is in a large excess over the analytes) primarily absorbs the laser energy and evaporate together with the analytes. Singly charged molecular ions of the analytes are formed in this evaporated gas phase, when H^+ and other possible ions such as Na^+ are exchanged between matrix and analytes. Although multiply charged molecules can also be generated, they are more easily neutralized and less stable. This is the well-known "lucky survivor" model (Karas M., Glückmann M. et al. 2000)., Although not mandatory (MALDI can be also combined with a quadrupole, ion trap or Fourier transform ion cyclotron resonance (FTICR) analyzer), the most commonly used mass analyzer combined with a MALDI ion source is the time-of-flight (TOF). Formed molecular ions are accelerated in a strong electric field (normally about 20,000 V) and enter a field-free space through a charged grid with the same energy. Invertion of the direction of the electric field leads to the differentiation of positive and negative ions. In this space they fly in a speed according to their mass: light ions travel faster and arrive at the detector earlier than heavier ions. Using a "reflectron" that enhances the

flight path and is useful to compensate for differences in the initial velocities of the generated ions, mass resolutions of about 20000 and mass accuracies of the order of 20 ppm can be obtained (Hillenkamp F. and Peter-Katalinic J. 2007). As stated above, the matrix in a MALDI-MS is of great importance. A “good” matrix should have reasonable absorption properties at the laser wavelength (often 337 nm), good mixing properties with the analyte for homogeneous co-crystallization, reasonable high-vacuum stability and low yield of matrix ions that are generated by photochemical reactions such as "cluster" ion formation (Hillenkamp F. and Peter-Katalinic J. 2007). The last requirement is especially essential for lipid analysis, since typical lipid molecules generate ions with rather low mass.

2.5.2 MALDI setup description

For our experiments MALDI mass spectra were acquired on a Bruker Autoflex mass spectrometer. The system utilizes a pulsed nitrogen laser, emitting at 337 nm. The extraction voltage was 20 kV and gated matrix suppression was applied to prevent the saturation of the detector by matrix ions (Schiller J., Suss R. et al. 2007). 128 single laser shots were averaged for each mass spectrum. The laser strength was kept about ten percent above threshold to obtain optimum signal to noise ratio. In order to enhance the spectral resolution all spectra were acquired in the reflector mode using delayed extraction conditions.

2.5.3. Lipid extraction and sample preparation

In order to analyze the composition of cells, lipids were purified from cell pellets to remove salts and polar compounds such as proteins or carbohydrates.

More precisely, cells were trypsinized to detach them from flasks surface and centrifuged as described in section 2.1 and cell pellets were washed 3 times with sterile PBS to remove any medium or trypsin solution residues. Cell pellet was resuspended in PBS and cells were counted with a Bruker counting chamber. Cells suspension was diluited 2 millions of cells each. This procedure was performed for each of three cell lines (MDA-MB-231, MCF-7 and HBL-100). : Since lipid evaluation through MALDI-MS is a semi-quantitative analysis, it was crucial to analyse the same amount for each cell type.. Lipid extraction can be made directly after cells preparation: for practical reason in our case we kept cell pellets at -80^{o}C in falcon tubes for a couple of days prior lipid extraction. A well established extraction method was introduced by Bligh and Dyer (Bligh E.G. and Dyer W.J. 1959). For each cell pellet, 3,75 ml of 1:2

(v/v) CHCl3:MeOH were added followed by . 1,25 ml CHCl3 and finally 1,25 ml dH2O. After each solvent addition, the sample was vortexed for a long time. Then the sample was centrifuged at 1000 RPM in IEC table-top centrifuge for 5 min at room temperature to obtain a two-phase system: the aqueous phase remained on the top while the organic one at the bottom. Due to the solubility of lipids in apolar organic solvent, lipids are easily extracted into the organic (chloroform) layer. Impurities (such as inorganic salts) are readily purified from the lipid extracts, since they remain in the aqueous layer. The organic phase was recovered with a Pasteur pipette through the upper phase with gentle positive-pressure taking care that the upper phase could not get into the pipette tip. Although the use of chloroform is nowadays strongly discouraged because it represents a harmful solvent, the vast majority of work in the lipid field is still based on the use of chloroform. Although a lot of different extraction methods, for instance hexane and isopropanol or methyl-tert-butyl ether have been introduced, these techniques are not widely accepted so far.

Afterwards two aliquotes of each lipid mixture were separately mixed with two different matrices : 2,5-Dihydroxybenzoic acid (DHBfrom Fluka Chemie GmbH, Buchs, Switzerland) and 9-Aminoacridine(9-AA from Sigma-Aldrich Chemie GmbH, Steinheim, GermanyDHB). The mixture was added to the target, dryed and analyzed. The remaining lipid samples was storaged at -20^{o}C.

Since lipids and common matrices such as DHB and 9-AA are generally soluble in the same organic solvents, they are usually mixed together and applied on the target, where the solvent evaporates and matrix, typically in a 100-1000-fold molar excess, co-crystallizes with the analytes.

3. EXPERIMENTAL RESULTS

3.1 Biomechanical properties measurements

3.1.1 OT viscoelasticity measurements results

3.1.1.1 Custom built OT setup

The OT set up used in this work has been designed and built in the Optical Manipulation lab of CNR-IOM (Istituto Officina Materiali). The components and setup configuration are described in section 2.2.1.2.

The set up has been used to measure the local viscoelastic properties of human cell lines MDA-MB-231, MCF-7 and HBL-100 by membrane tether pulling experiments. The experimental approach is described in section 2.2.1.4.

3.1.1.2. Experimental data analysis: Force Elongation (FE) curve and its interpretation

Experimental data obtained by a single tether pulling experiments are plotted to derive a FE curve from which we can extract the local viscoelastic properties of the cell as described in section 2.2.1.4. A typical FE curve is shown in figure 2.10.

FE curve is consistent with the assumption that the force necessary to pull a tether from membrane must overcome the membrane bending rigidity, the membrane tension, the adhesion of the phospholipid membrane bilayer to the cytoskeleton and the viscous resistance of the phospholipid bilayer (Sheetz 1996, Raucher 1999, Sheetz 2001). The shape of our FE curve is similar to those previously reported in literature for cancer neuronal cells (Guo 2004) and other types of cells (Hochmuth 1996, Li 2002, Ermilov 2005).

The FE curve (see figure 2.10 in 2.2.1.4) has typically three regions:

(1) the elastic region, where the elastic regime dominates in the first part until the membrane separates from the cytoskeleton. In a first approximation, by linear fitting of this region of the curve, elasticity could be expressed by a single parameter, the tether stiffness k_T.

(2) the point of maximum force (F_T), where the membrane is supposed to detach from the cytoskeleton. This part is followed by a rapid dropping of the force;

(3) the viscous regime (V_T), indicated by a force value which remains constant until the depletion of the membrane reservoir allows tether elongation.

3.1.1.3. Analysis of the temperature dependence of the cell membrane visoelastic properties.

In order to investigate the cell membrane viscoelastic properties dependence with the temperature we have performed tether pulling experiments at two different temperatures: room temperature (25°C) and physiological temperature (37°C), for one of the cell types.

Experiments were performed with the metodology described in 2.2.1.4. We calculated the trap stiffness by acquiring the Brownian motion of the trapped bead for 2 seconds at 2 kfps, prior to each experiment. The laser power arriving at the sample was 5% from the laser power at the source: using a laser power of 800 mW we have obtained a trap stiffness kOT = 0.21 pN/nm in both X and Y directions.

During the tether formation, the image acquisition rate was reduced to 100 fps, keeping instead a larger frame, which allows to image also the cell.

In order to extract the viscoelastic feature of the cell from the FE curve we have calculated the following three parameters: tether stiffness(k_T), tether force (F_T), tether length (L_T) at F_T and tether viscosity(V_T). The k_T is given by the slope of the linear fit of the curve in the elastic regime with least squares method. The F_T is represented by the maximum force reached at the end of the elastic regime, when the membrane detaches locally from the cytoskeleton. Finally, the V_T is given by the ratio between the median value of the force in the third region and the velocity at which the stage is moved.

We have first measured a series of tethers formed from ten MDA-MB-231 cells at room temperature (25 ºC). Then, we repeated the same measurements for other ten cells, keeping the sample cell at the physiological temperature (37 ºC).

MDA-MB-231	k_T [pN/μm]	F_T [pN]	L_T [μm]	V_T [pN sec/μm]
$T = 25°C$	**17.7** ± 6.9	**41.5** ± 11.1	**3.8** ± 1.9	**53.1** ± 14.8
$T = 37°C$	**37.4** ± 13.9	**49.8** ± 14.4	**2.8** ± 1.8	**30.5** ± 14.6

Table 3.1
Mean values and standard deviations of the viscoelastic parameters measured for two series of ten MDAMB- 231 cells at room and physiological temperatures respectively.

The results, presented in Table 3.1, show a significant difference of the cell behaviour when the temperature is changed. At room temperature the tether membrane is less stiff than at physiological temperature, while the viscosity is higher. Expectedly, the tether force is higher, while the tether length is shorter for physiological conditions.

These results demonstrate that the temperature variation, even for short period (10-20 min) change significantly their viscoelastic properties, even if the morphology is not modified.

This conclusion has to be considered when measurements on different types of cells are performed, because the experimental conditions must be strictly identical.

3.1.1.4.Viscoelastic parameter extraction from FE curves using the Kelvin model

A linear fitting of the three regions of the FE curve could represents a first approximation for the elasticity, allowing the estimation of the tether stiffness and the viscosity. To get more information about the tether formation mechanism, we have analyzed in detail the FE curves and fitted them using a more complex model including two elastic components and a viscous element. Figure 2.9 shows that the FE curve is increasing monotonically but is not linear. Since the FE curve of pulling tether has the characteristics of viscoelastic solids (Li Z. 2002), it makes sense trying to use similar models to interpret it. One well-established model for viscoelastic solids is the Kelvin body, which has been also proposed to describe the viscoelastic properties of cells investigated by magnetic bead microrheometry (Bausch A. R. 1998) or tether pulling with AFM (Schmitz J., Benoit M. et al. 2008). Observing the shape of the FE curve we assume that the cell behaves like a Kelvin body also under tether pulling experiments with OT. The Kelvin mechanical model is represented in figure 3.1.The cell is thus described by three parameters: the spring constant, k_T, representing the tether stiffness, the spring constant, k_{Be}, representing the bending rigidity and the tension of the membrane and a dashpot with viscosity, V_T, representing the viscosity of the cell membrane (Sheetz M.P. and 2001).

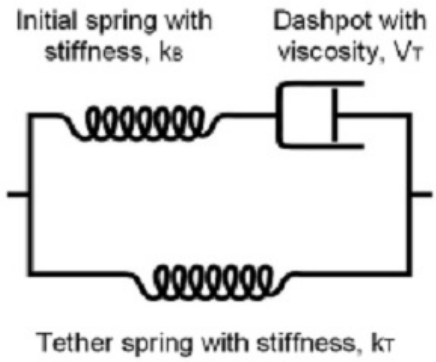

Figure 3.1: Kelvin body mechanical model adopted for cells. The Kelvin body consists of a spring with spring constant kT representing the tether stiffness, and parallel to this spring a series of a second spring with spring constant kBe representing the bending rigidity of the membrane and a dashpot with viscosity VT.

Transforming the differential equation for the Kelvin body into a time dependency of the force, under the boundary condition of a constant retraction velocity, and null force at the moment zero, one gets the following force-elongation equation (Schmitz 2008):

$$F(x) = k_T \cdot x + V_T \cdot v - V_T \cdot v \cdot \exp\left(-\frac{k_{Be} \cdot x}{V_T \cdot v}\right) \qquad \textit{(eq.3.1)}$$

where x is the elongation and v the extension velocity. Using this analytical relationship we have fitted the FE curves. The fit was made dividing the FE curve into different intervals: in each one the values of the Kelvin Body parameters have been changed as soon as the fitted curve differed too much from the experimental values. For each FE curve we calculated the mean values of the three parameters.

The membrane bending rigidity is related to the local deformation of the cell and expressed by the spring constant kBe: it is dominant at the beginning of the pulling decrease when the membrane tether almost detaches from the cytoskeleton, becoming insignificant when the tether membrane is detached. Tether stiffness, expressed by the spring constant k_T, is related to the adhesion points between the inter-membrane proteins and the cytoskeleton has a different behaviour. It increases to a maximum value before the rupture process begins. The tether stiffness is then reduced. The bending rigidity and membrane tension components are insignificant after the maximum force F_T is reached . This is consistent with the fact that the cell membrane is no more tensed. Analysing the viscosity values V_T for the different sub-regions one can see that there is a major contribution in the region after the rupture point, where the viscous flow is evident. Nevertheless, there are contributions also at the beginning of the pulling process, showing that a viscous regime, even if it is weak, should be coupled to the elastic regime. In conclusion, the interpretation of the FE curve with the Kelvin body model could provide additional information related to the mechanism of tether formation.

3.1.1.5.Comparative analysis of the local viscoelastic parameters extracted for the breast cell lines

Cells for tether pulling experiment were randomly selected as long as they had a healthy morphology. We pulled tethers in random positions between the top of the cell and the final edge. No tether was pulled a second time since it was reasonable that tether structure changes definitely in response to the first pulling. In some cases we repeated more than one measurement on the same cell, at different position, at least 5 micron far one to each other. Each experiment was performed at 37^{o}C, tethers of

several µm were pulled out with a velocity of 0.5 µm/sec. Experiments in which floating beads or cellular debris interfered with the bead during the tether pulling were invalidated and not considered.

Membrane tether pulling experiments on cell lines with different level of aggressiveness were performed on sample sizes of 8-10 cells. To reduce variability as much as possible we incubated cells in the presence of Ara-C for 18 hours prior to the experiment in order to synchronize cell cycle.

Using MATLAB we fitted experimental data with Kelvin body model to extract the three parameters: tether stiffness (K_T), membrane bending rigidity (K_{be}) and viscosity (V_T). We analyzed the parameters using the Data Analysis and Statistical Software STATA SE9.2.

Values of the elastic and viscous parameters extracted from the OT experiments are reported in Figures 3.2, 3.3 and 3.4

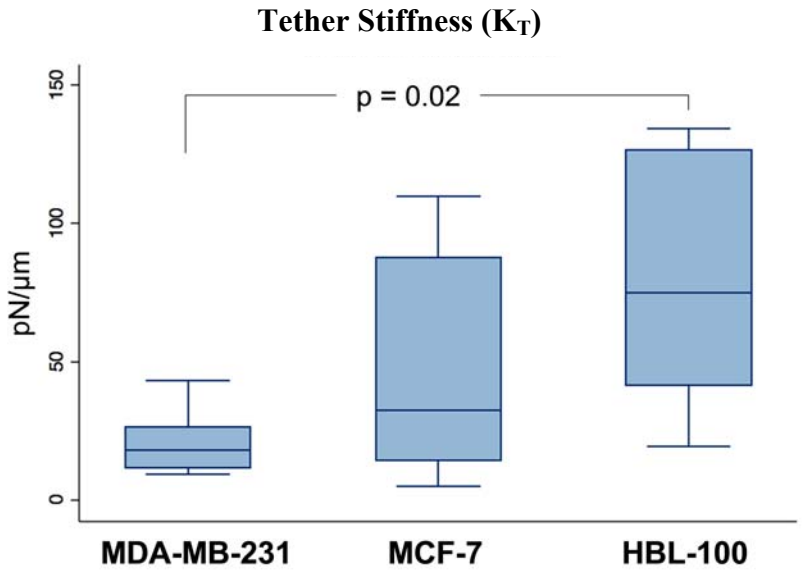

Tether Stiffness	MDA-MB-231	MCF-7	HBL-100
Median	18,1 pN/µm	32,5 pN/µm	75,0 pN/µm
Mean	20,7±11,6 pN/µm	48,04±41,3 pN/µm	76,7±42,9 pN/µm

Figure 3.2: Box plots representing the Tether Stiffness values of MDA-MB-231, MCF-7 and HBL-100 cell lines.
(a) Box plot representing the Tether Stiffness values (in pN/µm) of the three cell lines. Values were obtained with OT tether pulling experiments. The blue boxes contain values from the 25° percentile to the 75° percentile. Horizontal lines in the blue boxes represent the median value. (b) Table indicating the median and the mean values of Tether stiffness of the three cell lines. Significant p value has been reported above box plots.

The tethers stiffness mean value for the higher aggressive neoplastic cells, MDA-MB-231 (20,7 pN/µm) is 3,7 times lower than the tether stiffness mean value (76,7 pN/µm).

of HBL-100, the immortalized cell line. Despite the high standard deviations, significant differences were detected by ANOVA test between the two cell types MDA-MB-231 and HBL-100 (p=0,02).

MCF-7 cell type exhibits a tether stiffness value (48,04 pN/µm) which is in between the two groups of MDA-MB-231 and HBL-100. No significant differences were detected for this type of cell.

Membrane Bending Rigidity (K_{be})

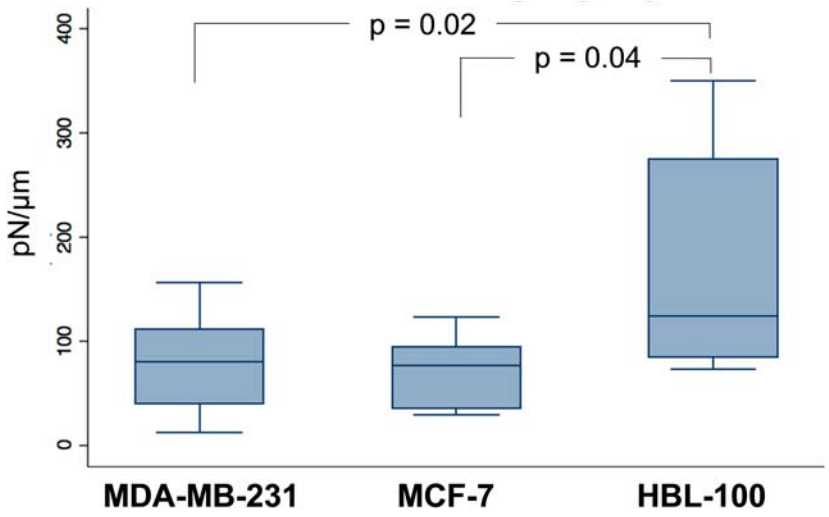

Membrane Bending Rigidity	MDA-MB-231	MCF-7	HBL-100
Median	80,8 pN/µm	77,5 pN/µm	125,0 pN/µm
Mean	71,2±34,7pN/µm	79,3±49,3pN/µm	175,4±104,2pN/µm

Figure 3.3: Box plots representing the Membrane Bending Rigidity values of MDA-MB-231, MCF-7 and HBL-100 cell lines.
(a) Box plot representing the Membrane Bending rigidity values (in pN/µm) of the cell lines. Values were obtained by OT tether pulling experiments. The boxes contain values from the 25^{o} percentile to the 75^{o} percentile. Horizontal lines in the blue boxes represent the median value. (b) Table indicating the median and the mean values of Membrane Bending Rigidity of the three cell lines. Significant, p value are reported above box plots.

The membrane bending rigidity of the breast cancer cell types MDA-MD-231 and MCF-7 showed lower values compared to the non-neoplastic (but immortalized) cells HBL-100.

In particular the membrane bending rigidity mean value of MDA-MB-231 (71,2 pN/µm) is 2,5 times lower that the one of HBL-100 (175,4 pN/µm). The ANOVA test confirmed that these values are significantly different with p=0,02.

The membrane bending rigidity mean value of MCF-7 (79,3 pN/µm) is 2,2 times lower that the one of HBL-100 (175,4 pN/µm). Again ANOVA test confirmed that these values are significantly different with p=0,004.

Membrane bending rigidity mean values of the two breast cancer cell types MDA-MB-231 and MCF-7 were comparable and no significant differences were detected between them.

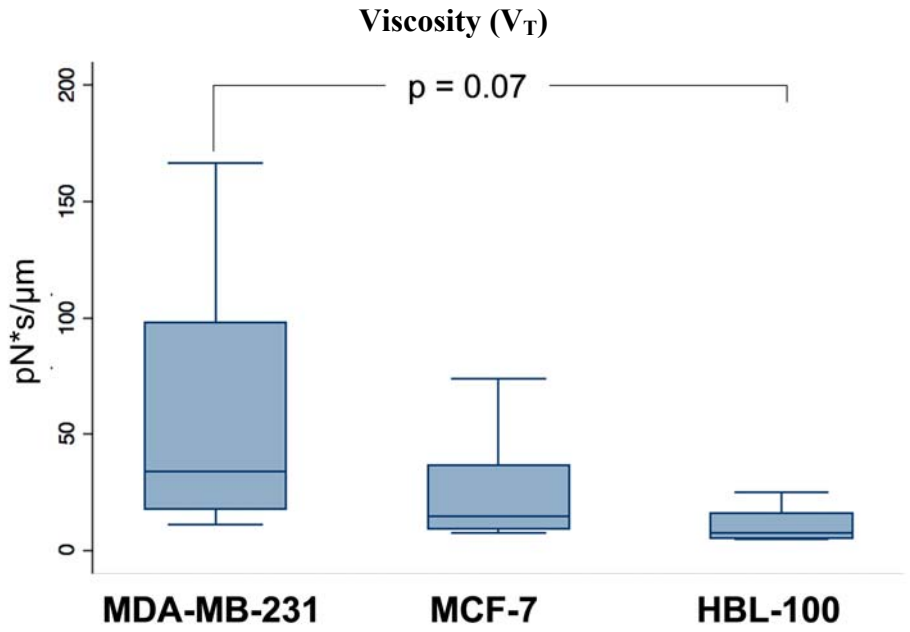

Viscosity	MDA-MB-231	MCF-7	HBL-100
Median	33,9 pN*s/µm	15,0 pN*s/µm	7,5 pN*s/µm
Mean	59,7 pN*s/µm	25,5 pN*s/µm	25,5 pN*s/µm

Figure 3.4: Box plots representing the Viscosity values of MDA-MB-231, MCF-7 and HBL-100 cell lines.
(a) Box plot representing the Viscosity values (in pN*sec/µm) of the three cell lines. Values were obtained by OT tether pulling experiments. The blue boxes contain values from the 25^{o} percentile to the 75^{o} percentile. Horizontal lines in the blue boxes represent the median value. (b) Table indicating the median and the mean values of Viscosity of the three cell lines. The value of p is reported above the box plots.

The viscosity values showed an inverse tendency with respect to the elastic parameters: the metastatic cells exhibit higher viscosity values if compared to the non-neoplastic cells.

HBL-100 showed a mean viscosity value (10,5 pN*s/µm) six times lower than MDA-MB-231 (59,7 pN*s/µm) and 2,5 lower than MCF-7 (25,5 pN*s/µm).

The difference between MDA-MB-231 and HBL-100 was not significant, but borderline (p=0.07).

To conclude, elastic parameters such as Tether Stiffness and Membrane Bending were higher in those cells associated to malignancy and high aggressive behaviour. On the contrary, viscosity showed an inverse tendency increasing with the progression of the malignancy and the aggressive behaviour of the tumour cell. We observed very high standard deviations suggesting that cell lines were very heterogeneous in terms of biomechanical properties and more experiments should be done to have significant statistical data and confirm our observations.

3.1.2 Elastic modulus by AFM

3.1.2.1.Comparative analysis of the parameters extracted for the three cell lines

Before AFM experiments, cells were cultured in the same conditions as described in section 2.1.2. Cells were plated on a glass coverslip at low density to have isolated and not overlapping cells, in order to facilitate the choice of the cell and clearly distinguish its morphology before the measurement. We selected cells randomly as long as they looked healthy and they had the typical morphology of their cell line. Probes were positioned under optical control in the region between nucleus and the edge of the cell, a constant approach velocity of 5μm/s during the extend and 10 μm/s during the extend was used.

Velocity during the extend was maintained consistent in each experiment: this is a crucial point because differences in indentation velocity brings variations in force indentation measurements. Higher velocities results in higher resistance of the sample material and over all interaction is more viscous. Thus, the higher is the loading rate, the smaller is the indentation at a given force and the higher is the apparent stiffness. Non consistent velocities in experiments would have invalidate the measurements.

Indentations were performed with a cantilever functionalized with a silica bead to avoid cell membrane damages caused by the sharp cantilever tip; the indentation depth was 500nm, which is 5-10% that the extimated cell thickness

To obtain a statistically significant Young's Modulus on each cell, we performed 25 measurements in different positions, distributed in a grid of 5μm x5μm on the cell surface. We analyzed 10 cells for each cell type (MDA-MB-231, MCF-7 and HBL-100) resulting in 250 measurements for each cell line.

Experiments were performed at room temperature (25^{o}C) with no CO_2 concentration control: to avoid temperature or pH acidification damages as much as possible we

changed sample every 30 minutes. To calculate the apparent cell elasticity the JPK software applied the Hertz model by automatic fitting and derived the Young's Modulus (E).

We used ANOVA test to see if there were significative differences between each cell line. Young's Modulus values are reported in figure 3.5:

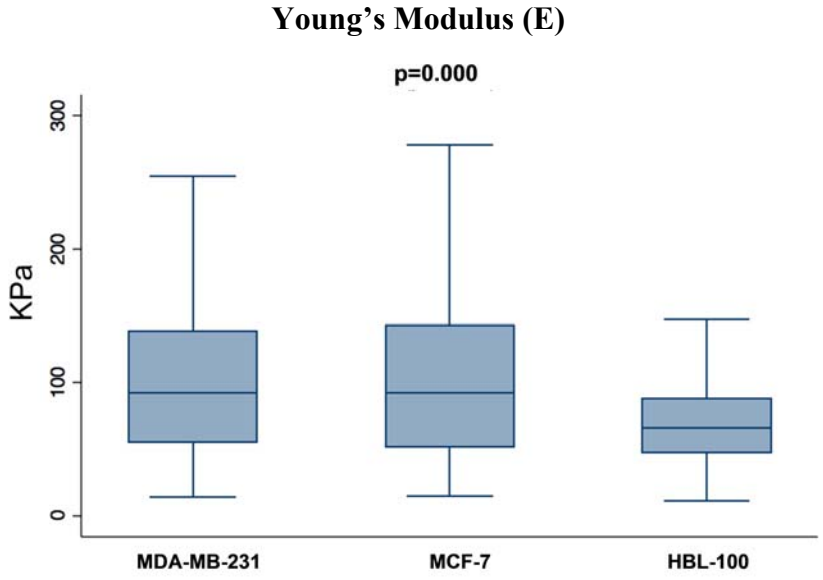

Young's Modulus	MDA-MB-231	MCF-7	HBL-100
Median	87,5 kPa	120,4 kPa	63,1 kPa
Mean	95,1±57,7 kPa	134,0±147,8	137,0±147,8 kPa

Figure 3.5: Box plots representing the Young's Modulus values of MDA-MB-231, MCF-7 and HBL-100 cell lines.
(a) Box plot representing the Viscosity values (in pN*sec/µm) of the three cell lines. Values were obtained by AFM indentation experiments. The blue boxes contain values from the 25^{o} percentile to the 75^{o} percentile. Horizontal lines in the blue boxes represent the median value. (b) Table indicating the median and the mean values of Viscosity of the three cell lines. Where ANOVA test showed significativity, p value has been reported above box plots.

Looking at the median Young's Modulus values we may conclude that higher Youngs Modulus values and higher resistance to deformation are associated with breast cancer cells MDA-MB-231 and MCF-7 compared to the immortalized HBL-100 cell line. Nevertheless mean values are not coherent. Young's Modulus values were quite spread, we observed very high standard deviations suggesting that cell lines were very heterogeneous in terms of biomechanical properties. Despite ANOVA test showed that differences were significative a net discrimination in terms of elasticity is difficult.

3.1.3 Cell deformability measurements by MOS

We tried to analyze the three cell types by the measurement of their time-dependent response to a stress using MOS.

The cell types MDA-MB-231, MCF-7 and HBL-100 were analyzed each in separate measurement series. Cells were prepared as previously described in section 2.2.3.2 and connected to the microfluidic system: subsequently each cell was trapped with a laser power of 100 mW from each beam, and deformed for 2 s with a laser power of 866 mW, 1033 mW or 1200 mW from each beam. The laser power was chosen randomly by an alghoritm. As described in section 2.2.3.4 the evaluated parameter was the relative axial extension $\gamma(t)$ of each cell as a function of time in units of percent deformation,

In figure 3.6 the plot of the average relative axial deformation of each cell type in response to the stretching by different laser powers. Cell deformation is proportional to the force applied on the cell

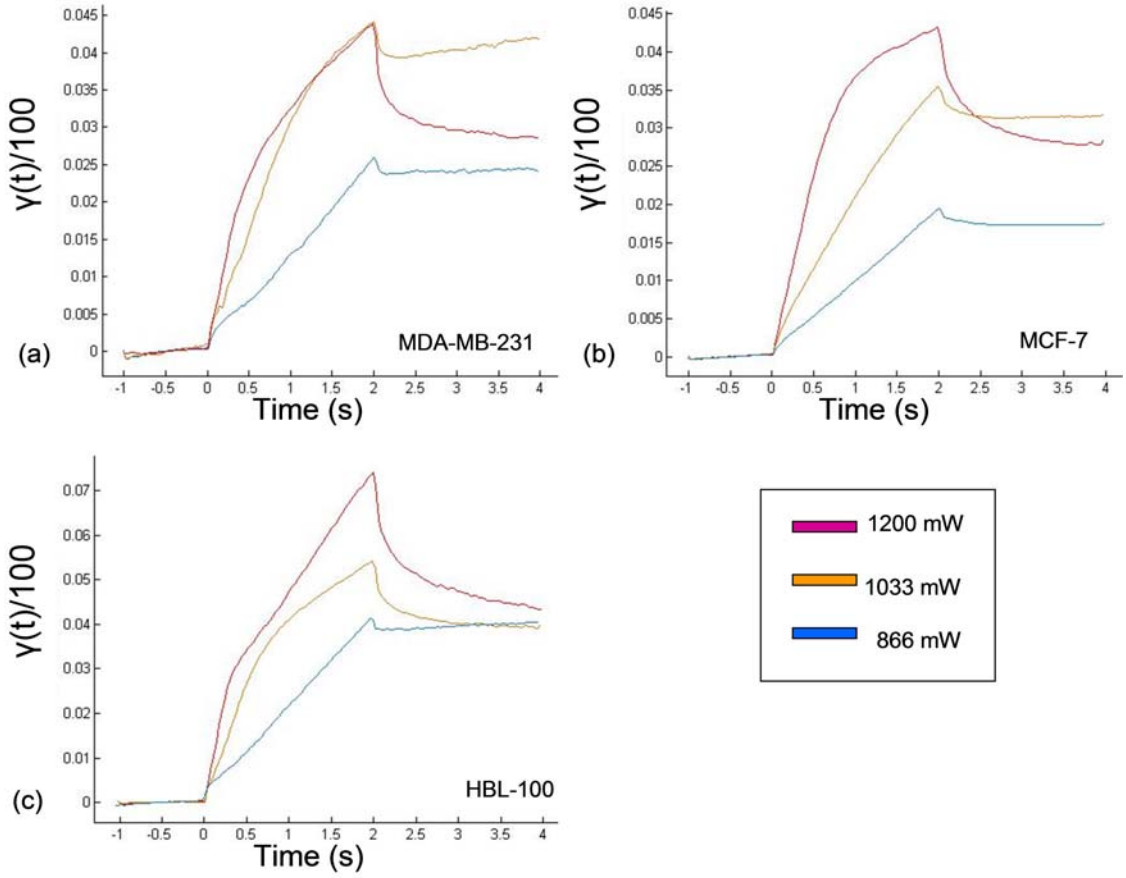

Figure 3.6.
Plots of the average relative axial deformation of (a) MDA-MB-231(b) MCF-7 (c) HBL-100 as a function of time for different laser powers: 1200 mW (violet curve), 1033 mW (yellow curve) and 866 mW (blu curve)

Since cell response to stress is different in relation to the entity of the stretching we analyzed and compared the relative axial deformation of the three cell types at three different laser powers: 866mW, 1033 mW and 1200mW

The average relative axial extension for each cell type can be used to show the different average response from the three populations.

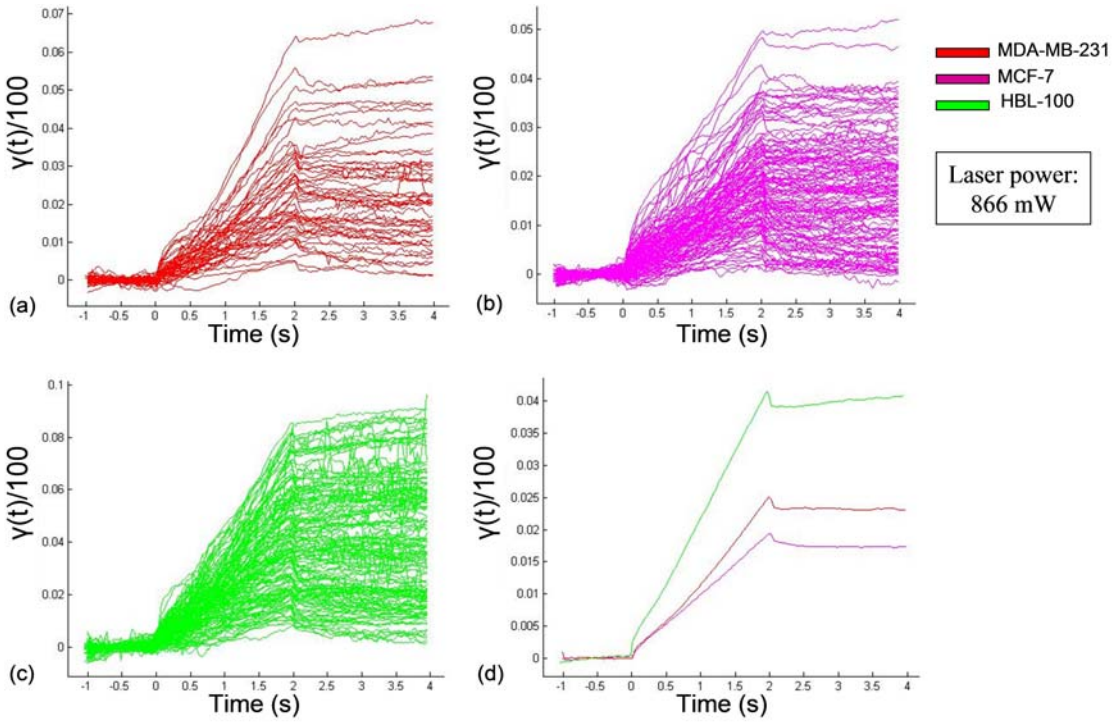

Figure 3.7.
Plots of the relative axial deformation as a function of time of (a) 71 individual MDA-MB-231 cells (b) 131 individual MCF-7 cells and (c) 141 individual HBL-100 cells trapped at 100 mW and stretched for 2 s at laser power of 866 mW. Finally (d) plot of the average relative axial deformation of MDA-MB-231 (red curve), MCF-7 (violet curve) and HBL-100 (blue curve) cells.

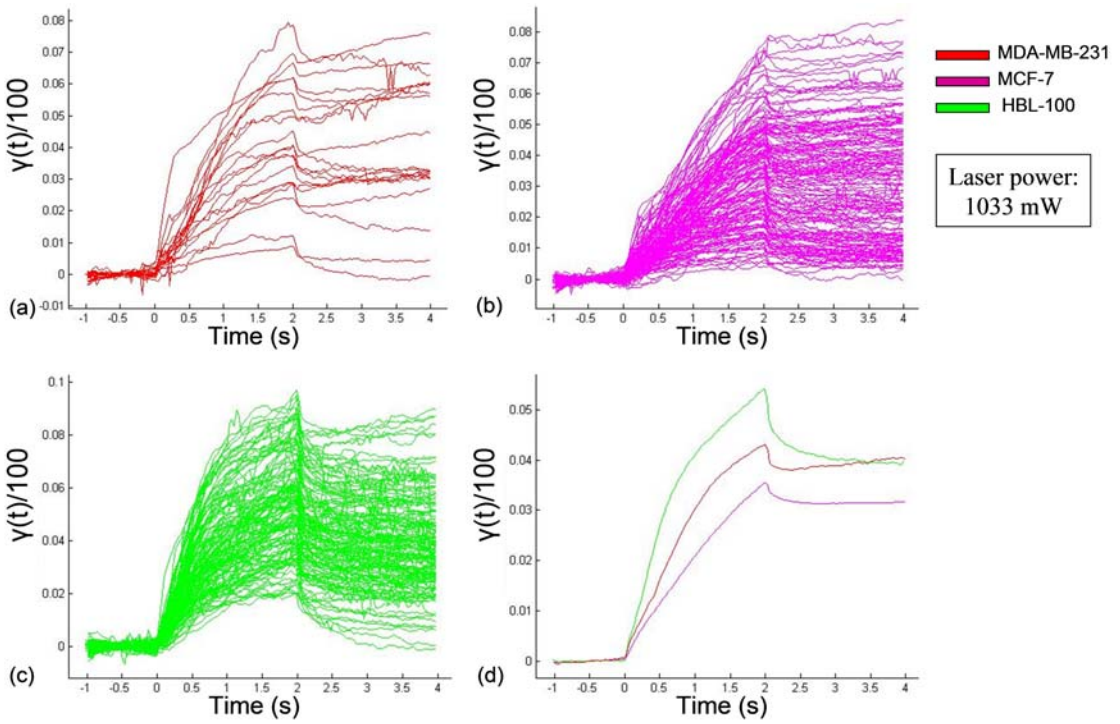

Figure 3.8:
Plots of the relative axial deformation as a function of time of (a) 40 individual MDA-MB-231 cells (b) 161 individual MCF-7 cells and (c) 141 individual HBL-100 cells trapped at 100mW and stretched for 2 s at laser power of 1033 mW. Finally (d) plot of the average relative axial deformation of MDA-MB-231 (red curve), MCF-7 (violet curve) and HBL-100 (blue curve) cells.

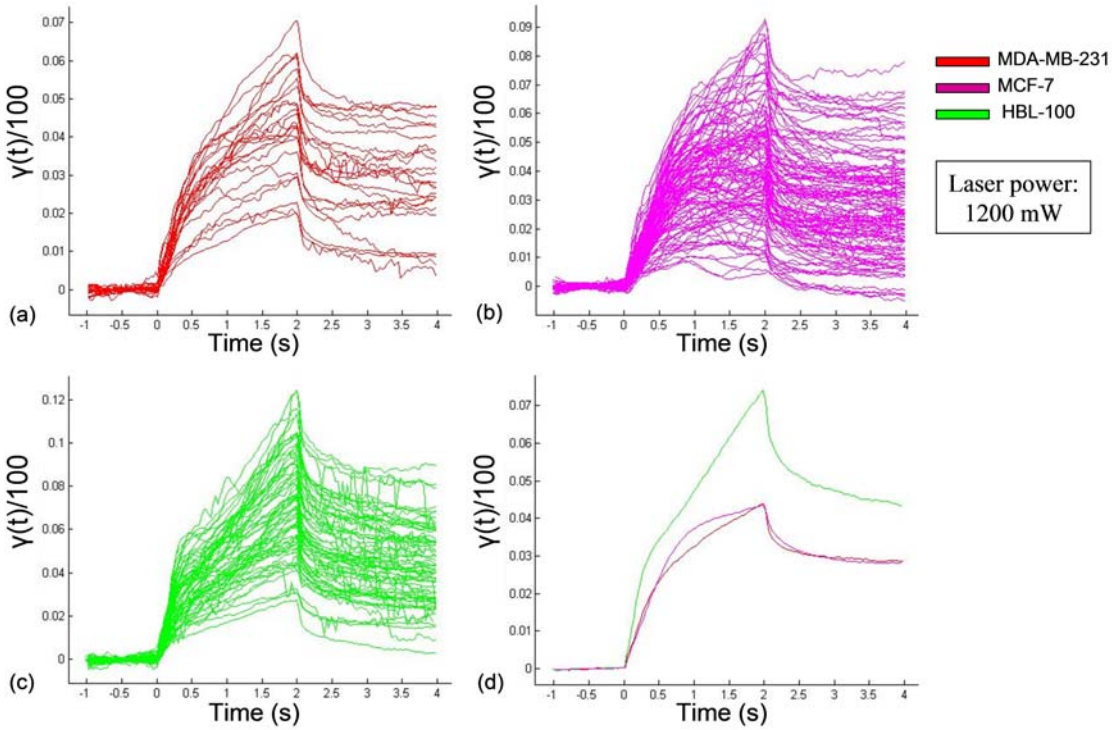

Figure 3.9
Plots of the relative axial deformation as a function of time of (a) 24 individual MDA-MB-231 cells (b) 118 individual MCF-7 cells and (c) 67 individual HBL-100 cells trapped at 100 mW and stretched for 2 s at laser power of 1200 mW. Finally (d) plot of the average relative axial deformation of MDA-MB-231 (red curve), MCF-7 (violet curve) and HBL-100 (blue curve)

In both the stretching experiments using 866 mW and 1033 mW as laser power, MCF-7 cells exhibit more resistance to deformability compared with MDA-MB-231. If higher stretching force (1200 mW) is used, MDA-MB-231 and MCF-7 resistance to deformability is comparable.

HBL-100 showed to be more deformable than the other two cell types for the different stretching force.

3.2 Proteomic analysis results by Western Blotting

We performed immunoblot analysis on the whole protein extracts of the three cell types: MDA-MB-231, MCF-7 and HBL-100. Protein extraction and western blot analysis procedures are described in 2.3. In order compare the expression patterns of the three cell types we performed semi-quantitative analysis by loading on SDS-PAGE the same amount of proteins (10 mg). Each Western Blot analysis was repeated three times in the same experimental conditions to verify results' repeatability. We tested the expression patterns of 6 proteins:

1. E-cadherin, which is involved in the cell-cell adhesion. Its down-regulation is related to epithelial mesechymal transition and neoplastic transformation Heimann R., Lan F.S. et al. 2000 Siitonen S.M., Kononen J.T. et al. 1996).
2. Cytokeratins 8/18, which is a marker for the discrimination between luminal and basal tumours of the beast (Delgallo W.D., Rodriguez J.R.P. et al. 2009)
3. Vimentin. Intermediate filaments are involved in cell transformation and malignant progression (Gilles C., Polette M. et al. 2003; Korsching E., Packeisen J. et al. 2005)
4. Integrin αvβ3 and Vinculin, which are involved in the Cell-Extracellular Matrix (ECM) interactions and thus are related to cell adhesion and cell migration.

Since MDA-MB-231 and MCF-7 are widely used and well-characterized cell models, their E-Cadherine, CK8/18 and Vimentin expression patterns are well known. The aim of these analyses was to verify the expression patterns of the same markers in HBL-100 and obtain information on its status. On the other hand, the expression patterns of Integrin αvβ3 and Vinculin could be useful to further characterize the malignancy status of the three cell types. HBL-100 is an immortalized cell line derived from milk of an apparently healthy woman. This cell line has been widely used as low aggressiveness model or 'healthy' control, however no clear data are available on the molecular classification of this cell line. In the present study we search the abovementioned markers in this cell type in order to provide a molecular classification for the comparison with biomechanical data.

3.2.1 Analysed molecular markers

E-Cadherin

E-cadherin is a trans-membrane glycoprotein, which interacts with several proteins collectively termed Catenins, that bind the actin cytoskeleton. E-cadherin mediates cell–cell adhesion and cell–extracellular matrix adhesion (Berx G. and Van Roy F. 2001). Lost of E-cadherin protein is a hallmark of Epithelial Mesenchymal Transition (EMT), which is typical of embryonic development and cancer progression (Thiery J.P. 2002; Thiery J.P. 2003).

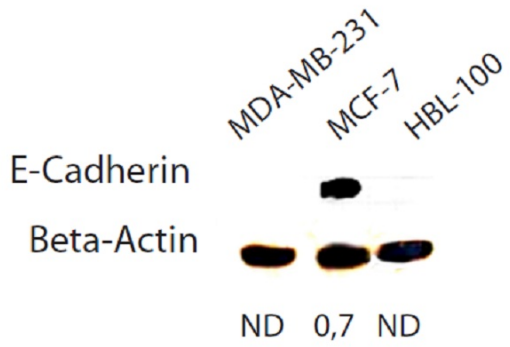

Figure 3.10: Protein expression pattern of E-cadherin
Protein expression patterns of E-Cadherin (135 kda)in the three breast cell lines MDA-MB-231 MCF-7 and HBL-100. 10 mg of proteins from the whole cell protein lysates were loaded, separated by SDS PAGE and stained by immunoblotting with primary and secondary antibodies. B-actin (42 kDa) was used as control. Numbers below pictures represent the ratio of the densiometric signal intensitiy of the detected protein Vs the densiometric signal intensity of actin. ND, not detected.

The immunoblot revealed positivity only for MCF-7 cell line, while MDA-MB-231 and HBL-100 resulted negative. This data was confirmed even in the replica of our experiments.

CK 8/18

Cytokeratins are proteins involved in the typical intermediate filaments, which characterize the epithelial cells' cytoskeleton. In particular Cytokeratin 18 (CK18) together with its partner Cytokeratin 8 (CK8) are the most common products of the intermediate filament gene family (Omary M.B. et al. 1992).

They are usually used as molecular markers to distinguish Luminal carcinomas from Basal –like carcinomas. Luminal carcinomas strongly express luminal cytokeratins (CK8 ⁄ 18). Basal-like carcinomas exhibit weak or focal positivity for CK8 ⁄ 18 (Delgallo W.D., Rodriguez J.R.P. et al. 2009)

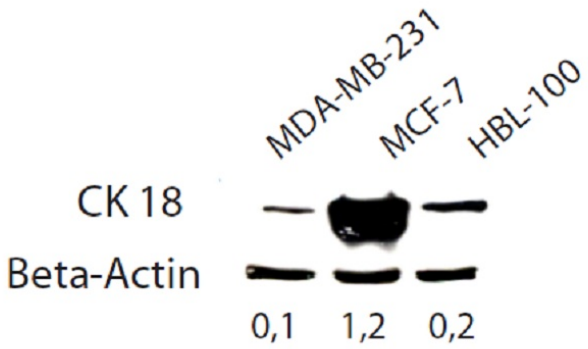

Figure 3.11: Protein expression pattern of CK18
Protein expression patterns of CK18 (48kDa) in the three breast cell lines MDA-MB-231 MCF-7 and HBL-100. 10 mg of proteins from the whole cell protein lysates were loaded, separated by SDS PAGE and stained by immunoblotting with primary and secondary antibodies. B-actin (42 kDa) was used as control. Numbers below pictures represent the ratio of the densiometric signal intensitiy of the detected protein Vs the densiometric signal intensity of actin. ND, not detected

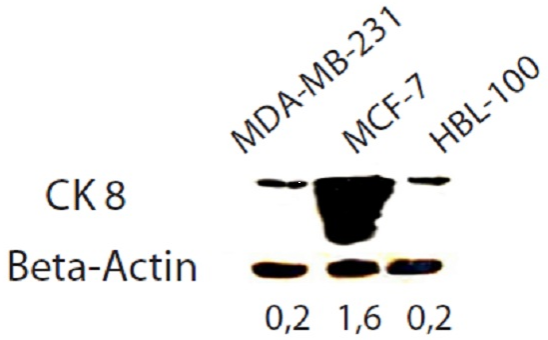

Figure 3.12: Protein expression pattern of CK8
Protein expression patterns of CK8 (55kDa) in the three breast cell lines MDA-MB-231 MCF-7 and HBL-100. 10 mg of proteins from the whole cell protein lysates were loaded, separated by SDS PAGE and stained by immunoblotting with primary and secondary antibodies. B-actin (42 kDa) was used as control. Numbers below pictures represent the ratio of the densiometric signal intensitiy of the detected protein Vs the densiometric signal intensity of actin. ND, not detected

Cytokeratins 18 and 8 resulted positive in all the analysed cell lines, with a higher expression level for MCF-7 cells in comparison to MDA-MB-231 and HBL-100. Since cytokeratins are usually found in pairs comprising a type I (basic) cytokeratin and a type II (acidic) cytokeratin, the similar amount of CK8 and CK18 detected in this experiment is in agreement with their structure.

Vimentin

Vimentin is a intermediate filament (IF) protein, which forms part of the cytoskeleton and it is typically expressed in mesenchymal cells: its expression in epithelial cells is a hallmark of EMT. Expression of vimentin has been described in breast carcinomas (Azumi N. and Battifora H. 1987; Kokkinos M.I., Wafai R. et al. 2007) and aggressive

breast cancer cell lines (Gilles C., Polette M. et al. 2003). Higher vimentin expression level correlates well with up-regulated migration and invasion of cancer cells (Gilles C., Polette M. et al. 2003; Korsching E., Packeisen J. et al. 2005). The transfection of the non-invasive human breast cancer cell line (MCF7) with vimentin gene led to accelerated invasiveness (Hendrix M.J., Seftor E.A. et al. 1997).

.

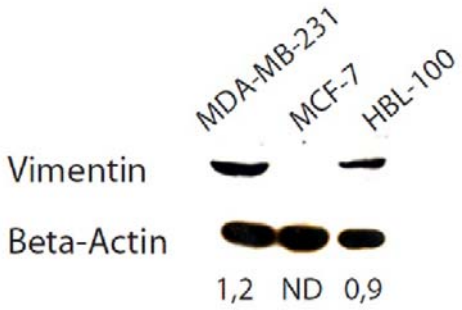

Figure 3.13: Protein expression pattern of Vimentin
Protein expression patterns of Vimentin (57kDa) in the three breast cell lines MDA-MB-231 MCF-7 and HBL-100. 10 mg of proteins from the whole cell protein lysates were loaded, separated by SDS PAGE and stained by immunoblotting with primary and secondary antibodies. B-actin (42 kDa)was used as control. Numbers below pictures represent the ratio of the densiometric signal intensitiy of the detected protein Vs the densiometric signal intensity of actin. ND. Not detected

Our experiments revealed positivity to Vimentin in MDA-MB-cells and HBL-100. On the contrary MCF-7 cells were negative for Vimentin. The expression level of Vimentin in MDA-MB-231 was higher than in HBL-100 cells (ratio 1,2 vs 0,9, respectively).

Integrin αvβ3

The integrins constitute a family of trans-membrane receptor proteins composed of heterodimeric complexes of non-covalently linked α and β chains. They are linked to the actin cytoskeleton involving talin, vinculin, and α-actinin as intermediaries. Integrins function in cell-cell and cell-extracellular matrix (ECM) adhesive interactions and transduce signals from the ECM to the cell interior and vice versa. Integrins mediate the ECM influence on cell growth and differentiation, and are involved in cell migration, cell invasion, cell intra- and extra-vasation.

Integrins have been found on virtually every cell and tissue studied. During development, integrins are ubiquitously expressed. They regulate morphogenetic cell movements and migration; and are especially numerous during gastrulation, neurulation, and histogenesis (Albelda S.M. and Buck C.A. 1990). Integrin expression levels tend to decrease gradually during differentiation as adult structures emerge.

Expression of integrin $\alpha_v\beta_3$ is associated with progression of a variety of human tumours and it is expressed in some of the most aggressive tumour cells in a variety of cancers including also breast cancers (Mizejewski G.J. 1999).

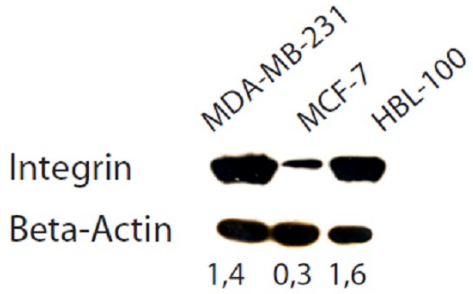

Figure 3.14 Protein expression pattern of Integrin $\alpha_v\beta_3$
Protein expression patterns of $\alpha_v\beta_3$ integrin (130kDa) in the three breast cell lines MDA-MB-231 MCF-7 and HBL-100. 10 mg of proteins from the whole cell protein lysates were loaded, separated by SDS PAGE and stained by immunoblotting with primary and secondary antibodies. B-actin (42kDa) was used as control. Numbers below pictures represent the ratio of the densiometric signal intensitiy of the detected protein Vs the densiometric signal intensity of actin. ND, not detected

Integrin $\alpha_v\beta_3$ were highly expressed in MDA-MB-231 and HBL-100 cells, in MCF-7 the protein was detectable, but at lower expression level. The intensity of Integrin in MDA-MB-231 and HBL-100 was similar as reported in Fig 3.14.

Vinculin

Vinculin is a cytoplasmic actin-binding protein and represent the major connection of adhesion sites to the actin cytoskeleton via integrins. Vinculin is enriched in focal adhesions and adherens adherens junctions and has a critical function in governing cell-matrix adhesion, promoting focal adhesion formation by regulating integrin clustering, force generation and cell migration (Peng X., Nelson E.S. et al. 2011) . Cells depleted of Vinculin have reduced adhesion to a variety of ECM proteins, fewer and smaller adhesions compared with wild type cells, alterations in cell migrations (Coll J.L., Ben-Ze'ev A. et al. 1995; Volberg T., Geiger B. et al. 1995; Saunders R.M., Holt M.R. et al. 2006)

Figure 3.15: Protein expression pattern of Vinculin
Protein expression patterns of Vinculin (117 kDa) in the three breast cell lines MDA-MB-231 MCF-7 and HBL-100. 10 mg of proteins from the whole cell protein lysates were loaded, separated by SDS PAGE and stained by immunoblotting with primary and secondary antibodies. B-actin (42 kDa) was used as control. Numbers below pictures represent the ratio of the densiometric signal intensitiy of the detected protein Vs the densiometric signal intensity of actin. ND, not detected

Vinculin showed to have a similar expression pattern of Integrin $\alpha_v\beta_3$ in the analyzed cell types. Vinculin was highly expressed in MDA-MB-231 and HBL-100 in comparison to MCF-7. The intensity ratios detected for Vinculin in MDA-MB-231 were similar to those detected in HBL-100 (0,7 vs 0,6, respectively).

Molecular marker	MDA-MB-231	MCF-7	HL-100
E-cadherin	-	++	-
CK 8	+	++	+
CK 18	+	++	+
Vimentin	+	-	+
Integrin αvβ3	+	-	+
Vinculin	+	-	+
++ positive (high expression) + positive (low expression) - negative			

Table 3.2: Western Blot results.
Summary of the molecular markers expression patterns in MDA-MB-231, MCF-7 and HBL-100 cell lines. Symbols "+ "and "–" means positive and negative result, respectively. When all three cell lines are positive for a certain molecular markers symbols "++" and "+" discriminate samples with higher or lower expression respectively.

3.3 Super resolution imaging: comparative analysis of the cytoskeleton morphology of the breast cell lines

We investigated the actin cytoskeleton structure of cell types by immunostaining with Phalloidin 590 (attotech). Cells were fixed, stained and imaged with STED microscopy as described in 2.4. Images were acquired with pixel sizes of 20 nm × 20 nm and a pixel dwell-time of 1 ms. In addition to the STED images, confocal images were recorded (Fig. 3.16).

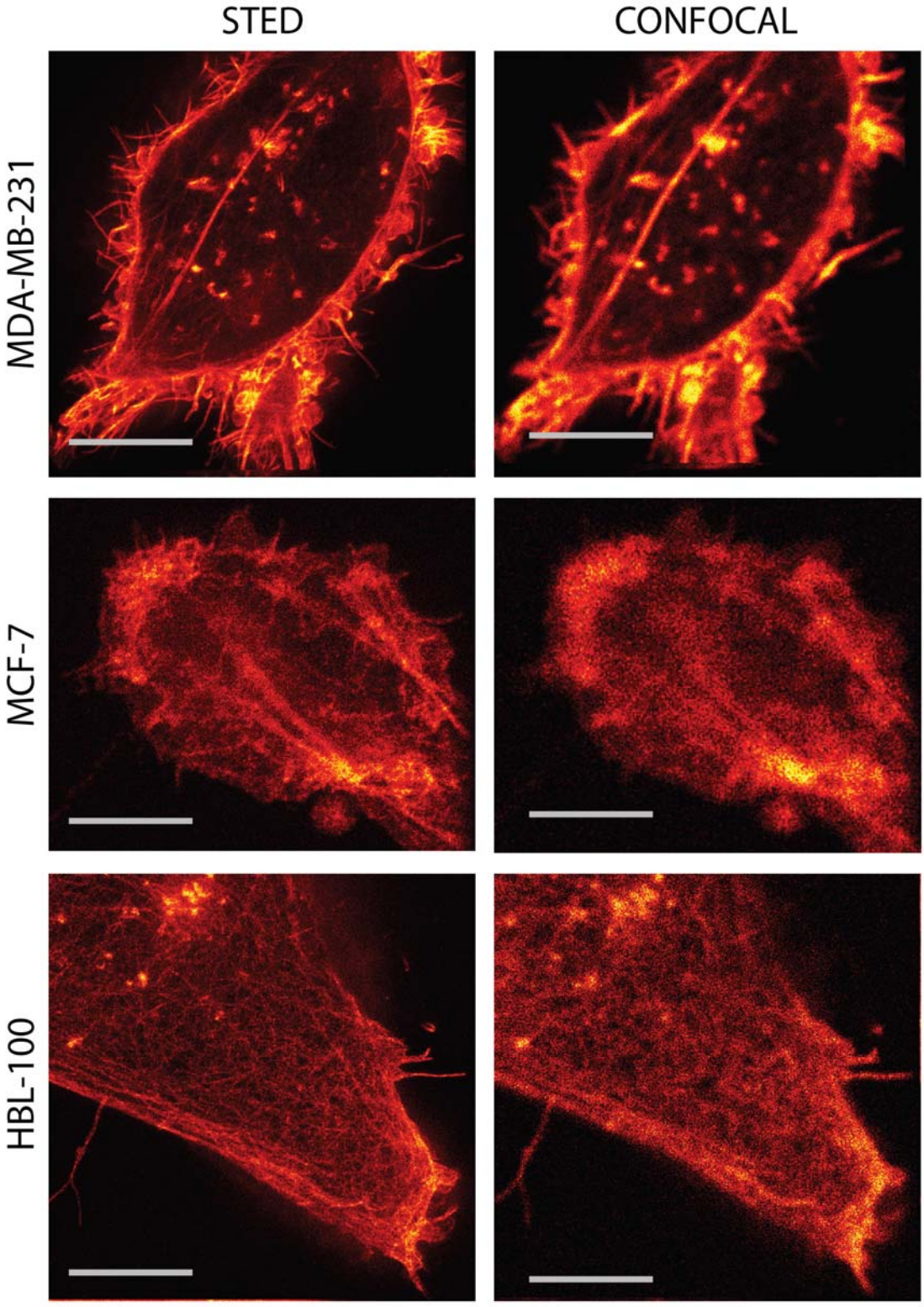

Figure.3.16: Comparative actin cytoskeleton imaging by STED and Confocal microscopy
Actin cytoskeleton of MDA-MB-231 cells (above), MCF-7 cells (centre) and HBL-100 cells (below) was marked by Phalloidin 590. Cells were imaged with STED microscopy (left) and Confocal microscopy (right). Scale bar is 5um.

Cytoskeleton imaging clearly revealed a miss-regulation in the organization of the actin filaments in cancer cells MDA-MB-231 and MCF-7 compared to HBL-100. This difference can be observed from both STED and Confocal imaging, details are particularly clear for STED.

HBL-100 exhibited an actin network with thin filaments homogeneously distributed under the cell surface. MDA-MB-231 and MCF-7 exhibited thicker filaments, a less homogeneous network and the presence of actin drifts. In particular, MDA-MB-231 cells showed very thick and abundant actin filaments confined at the edge of the cells; spot like actin accumulations in the cell body.

3.4 MALDI-MS analysis of the cells lipid composition

We analyzed the whole lipid extracts from the three cell lines MDA-MB-231, MCF-7 and HBL-100 by means of MALDI-MS. We performed semi-quantitative analysis by applying the same amount of lipids on the matrix and comparing the spectra. Experiments were repeated twice, using in parallel 2,5-dihydroxybenzoic acid (DHB) and 9-aminoacridine (9-AA) as matrix.

DHB is used predominantly for lipid studies. The application of DHB offers the possibility to record both positive- and negative-ion spectra from the same sample, but due to its acidic property (pK=2.97 in water)(Schiller J., Suss R. et al. 2007), it shows lower suitability in negative-ion mode. This is disadvantageous because the detection of the individual lipid classes in the positive-ion mode varies significantly, and it has been noted that the presence of lipids with quaternary ammonia groups, such as in phosphatidylcholines (PCs), lyso-phosphatidylcholines (LPCs) as well as sphingomyelins (SMs), may lead to the suppression of the signals of other lipid classes, such as phosphatidylethanolamines (PEs), in a lipid mixture (Petkovic M., Schiller J. et al. 2001)

9-AA is more suitable than DHB for negative-ion mode measurements, under which lipid classes such as PEs can be analysed without the suppression effect in the presence of PCs in positive-ion mode. This highlight of 9-AA comes from its basicity (pK_9.99 in water) (Schiller J., Suss R. et al. 2007).

Therefore, to be able to detect different lipid classes and have a complete overview of the cells lipid composition we performed our experiments in parallel using both matrixes.

MALDI-MS spectra with matrix DHB and 9-AA are reported in figures 3.16 and 3.17.

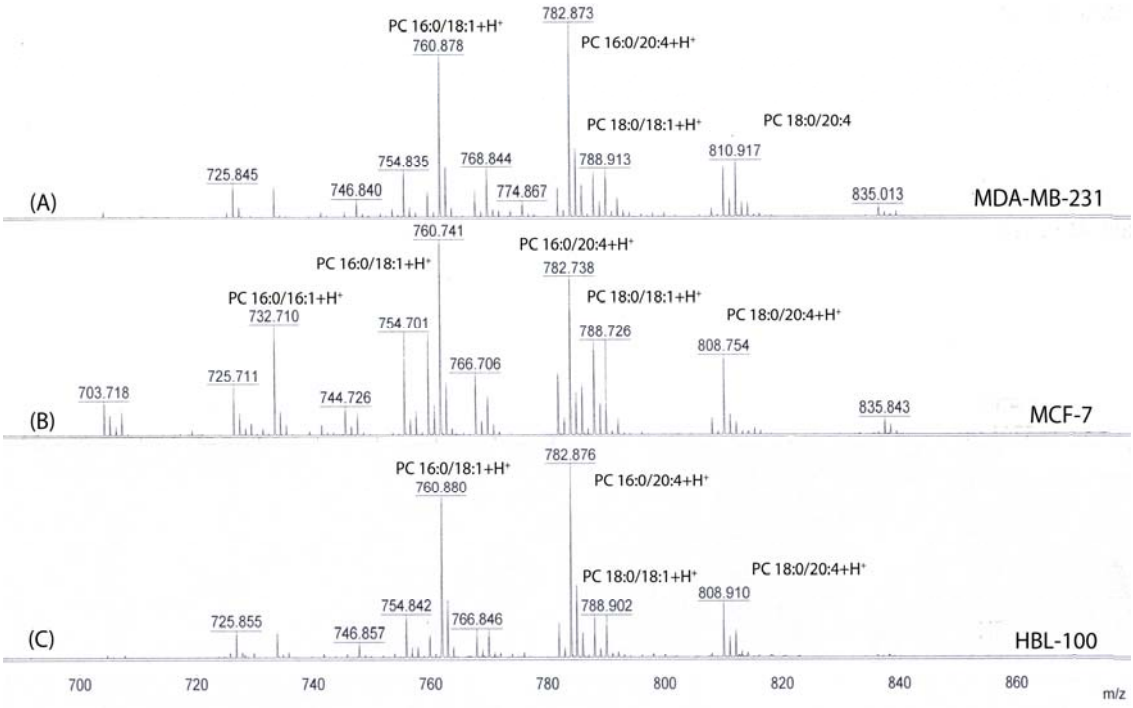

Figure 3.17
Positive ion MALDI-MS spectra with DHB matrix of (a) MDA-MD-231 (b) MCF-7 and (c) HBL-100 cells lipid extracts.

As expected, the Positive ion MALDI-MS spectra obtained with DHB matrix were dominated by Phosphatidyl-choline (PC) signals. In these spectra no significant differences were found among the three cell types, as reported in Fig 3.17.

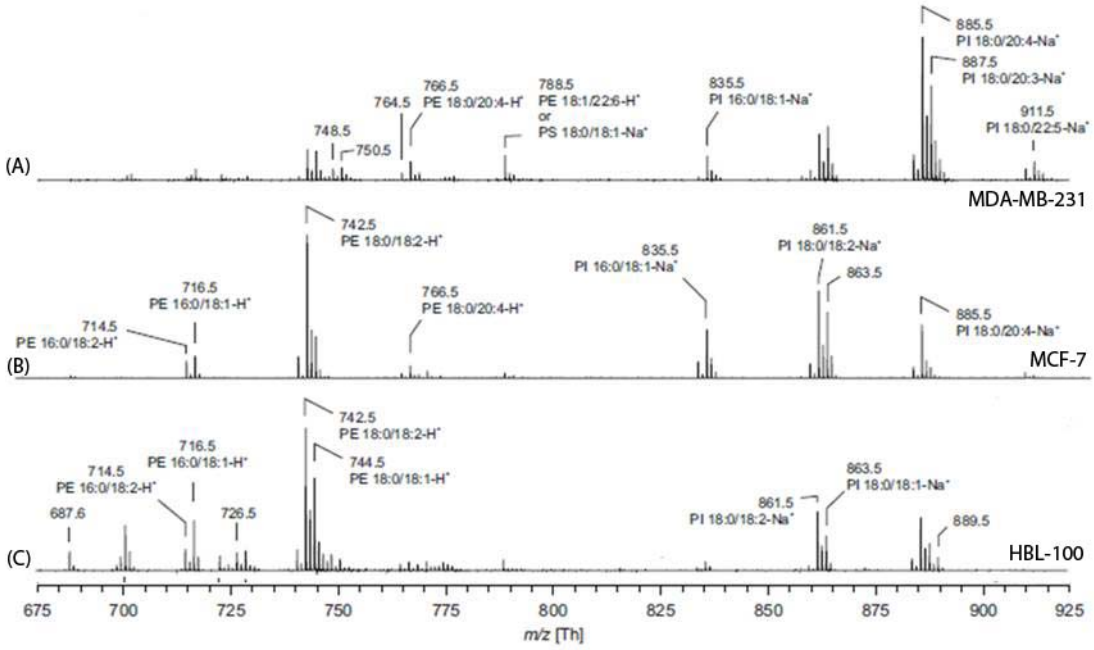

Fig 3.18
Negative ion MALDI-MS spectra with 9-AA matrix of (a) MDA-MD-231 (b) MCF-7 and (c) HBL-100 cells lipid extracts.

As shown in Fig 3.18, the negative ion MALDI –MS spectra obtained with 9-AA matrix showed some differences at the level of some PEs and some PIs. In particular, spectra corresponding to MCF-7 and HBL-100 were similar when compared to MDA-MB231. Main differences observed in MDA-MB-231 spectrum were an higher expression of the Phosphatidylinositols PI 18:0/20:4-Na^+ and PI 18:0/20:3 Na^+ and lower expression of the Phosphatidylethanolamines PE 18:0/18:1-H^+ and PE 18:0/18:2-H^+

A detailed assignment of the peaks detected in our spectra is listed in **Appendix**

4. COMPARATIVE DISCUSSION ON THE DIFFERENCES BETWEEN THE BIOMECHANICAL PROPERTIES OF THE BREAST CELL LINES

We have built an Optical Tweezers (OT) setup in which a trapped microbead is used to grab the cell plasma membrane and pull a tether of several microns to measure the viscoelastic properties of the cell membrane. We first investigated on temperature dependence of the cell viscoelastic properties. The results obtained from experiments performed at room temperature and physiological temperature show a considerable variation of the viscoelastic properties. Afterwards, a more detailed analysis of the FE curves has been proposed using the Kelvin model. From these analyses some viscoleastic characteristics, such as tether stiffness, tether force, viscosity of the cell membranes can be extracted.

We used this experimental technique and this data analysis approach to measure and compare the local viscoelastic properties of two breast cancer cell lines, MDA-MB-231 and MCF-7, as tumour models of breast cancer related to different aggressiveness. A third immortalized cell line HBL-100, derived from the milk of an apparently healthy woman was used as control.

Afterwards we further investigate on the mechanical properties of the cell lines using other two experimental techniques that are currently used to extract mechanical properties of cancer cells: Atomic Force Microscopy (AFM), and Microfluidic Optical Stretcher (MOS). With AFM we locally indented cells with a bead attached to the cantilever to measure the Young's Modulus. Both OT and AFM perform local measurements to test the mechanical properties of the cell membrane as well as the underlying region. OT tether membrane approach gives viscoelastic information about cytoskeleton-membrane interaction while AFM gives information on the elasticity only, but measurement involves a larger region of the cell under bead indentation. Finally, we used MOS to further characterize the cell as a whole body: cells in suspension were deformed by the radiation pressure of light. In conclusion, we used three different approaches to evaluate different mechanical properties of the analysed cells.

Up to now, most of the studies related to the biomechanical properties of neoplasticcells have compared mechanical properties of tumour cells *versus* to normal ones or non-transformed cells (Lekka M., Laidler P. et al. 1999; Zhang G., Long M. et al. 2002; Guck J. 2005; Park S., Koch D. et al. 2005). The aim of the present study was to investigate if mechanical properties of cells were able to discriminate between cancer cells related to different aggressive behaviours. Our data strongly support the fact that biomechanical measures, despite the experimental approach used, are able to significantly discriminate between tumour and control. By the use of these three

different approaches we obtained different information: in the case of AFM and MOS the results were comparable, since both revealed that HBL-100 cells were more deformable than cancer breast cancer cells. On the contrary, OT revealed that cancer cells exhibited a less stiff plasma membrane and lower membrane bending rigidity than control cell type. These different behaviours could be explained with the nature of the measurements.: MOS and AFM compress the entire cell or only a region respectively, involving a larger region, if compared to OT measurements. In membrane tether pullings a much restricted cell region and its underlying region are involved, thus the measures are more local taking in consideration also the viscous component of the plasma membrane.

If these measurements were able to discriminate tumour and control, they could not discriminate different types of tumours of the same origin, but with different aggressiveness. We observed very high standard deviations suggesting that cell lines were heterogeneous in terms of biomechanical properties and a net discrimination in terms of elasticity was difficult. However, a trend could be observed: in all three cases if we consider the two breast cancer cells taken together, MCF-7 showed to be weakly more resistant to deformation compared to MDA-MB-231 that are more aggressive.

In particular, our results from OT experiments showed that lower tether stiffness and membrane bending rigidity values were associated to breast cancer cells MDA-MB-231 and MCF-7, while higher values were significantly associated to HBL-100 cell line. As already mentioned there was no significant discrimination between the two breast cancer cell lines, but an increase of tether stiffness in MCF-7 compared to MDA-MB-231 could be observed as a trend. Viscosity, compared to elastic parameters, exhibited an inverse tendency: highest viscosity values were observed in the more aggressive cell line MDA-MB-231, values gradually decreased with an evident trend in MCF-7 and in HBL-100, but with no significant differences.

We interpret the Force- Tether Elongation curves derived from our OT experimental data with the assumption that the force necessary to pull a tether from membrane must overcome the membrane bending rigidity, the membrane tension, and also the adhesion of the phospholipid membrane bilayer to the cytoskeleton and the viscous resistance of the phospholipid bilayer (Sheetz and Dai 1996; Raucher and Sheetz 1999; Sheetz, 2001). Thus, plasma membrane structure and composition, is supposed to give a strong contribute to viscoelastic properties of cells. Thus far, the lipid metabolism of cancer

has been predominantly investigated at the level of genes and many of these have been shown to affect tumorigenesis. Nevertheless, the precise molecular composition of lipids in tumours remains generally poorly characterized (Hilvo M., Denkert C. et al. 2011).

It is known that activation of lipid metabolism is an early event in carcinogenesis and a central hallmark of many cancers, including breast cancer (Chajes V., Lanson M. et al. 1995). Thus, we investigated on possible alterations in the lipid membrane composition of cells, that could eventually be correlated to these alterations in the viscoelastic properties of cells. To fulfil this proposal we used matrix-assisted laser desorption and ionization (MALDI) mass spectrometry (MS) to characterize the lipid composition of cells with semi-quantitative analysis, and compare the results for the different cell types. Despite MALDI-MS is a well established technique in the study of proteins, it is also very useful in lipid research, because it is fast, sensitive, and provides very simple mass spectra without major fragmentation of the analyte (Fuchs B., Süß R et al. 2010).

From our results, we could not observe any significant difference at level of PCs (Phosphatidylcolines). However, MDA-MB-231 exhibited a significant downregulation of PEs (Phosphatidyletanholamines) and upregulation of PIs (Phosphatidyliinositoles) , compared to the loess aggressive MCF-7 and the control cell line HBL-100. Our results are supported by a previous paper (Hilvo M., Denkert C. et al. 2011) in which a study based on breast cancer tissues reported a striking difference in the lipid profiles between the breast tumour and normal tissue samples. Membrane phospholipids including PEs, and PIs, were altered in tumors. Interestingly, the altered phospholipid metabolism of the tumour samples was related to ER status and tumour grade. These results suggest that the alterations in lipid metabolism could be directly involved in the alterations of the viscoelastic properties of membrane cancer cells. However, this observations needs to be confirm with further experiments.

Taking in consideration the two other biomechanical tools used to probe cell mechanical properties, AFM and MOS, we could observe a certain coherence in the results. Young's Modulus values, that are measuring the resistance to deformability of the three cell types obtained by AFM were quite spread thus a net discrimination in terms of elasticity was difficult. However we could observe a trend: the less aggressive cancer cells MCF-7 showed higher median values of Young's Modulus, and thus a major resistance to deformability, than the highly aggressive MDA-MB-231 cells. The

same has been seen in MOS results: MCF-7 showed higher deformation rates compared to MDA-MB-231.

Both AFM and MOS observed differences were not significant, however these results suggest a trend , which is supported by previous studies here reported. Distinct cell lines from both human and murine tumours have been assessed in terms of their elastic responses to force stimulation by AFM; namely, human bladder (Lekka M., Laidler P. et al. 1999) , prostate (Faria E.C., Ma N. et al. 2008), breast (Cross 2007), mesothelial (Cross S.E., Jin Y.S. et al. 2008), cartilage (Darling E.M., Zauscher S. et al. 2007) and blood (Rosenbluth M.J., Lam W.A. et al. 2006) as well as murine ovarian (Carl P. and Schillers H. 2008) and fibroblast cells (Nikkhah M., Strobl J. et al. 2010). All groups have suggested that cancerous cells are "softer" or deform at a higher rate than their "normal" or non transformed counterparts by means of their respective elastic moduli. Previous measurements with MOS have shown that optical deformability was sensitive to monitor the changes during the progression of mouse fibroblasts and human breast epithelial cells from normal to cancerous and even metastatic state, showing transformed cells more deformable than their normal counterparts. (Guck J. 2005).

Our data agree with those studies since we were able to significantly group tumour cells *versus* control, but our MOS results showed that the control cell lines HBL-100 had significantly higher deformability rates compared to cancer cells. The same was observed with AFM, but in this case the difference was not significant.

The biomechanical measures we performed in this study strongly suggested that HBL-100 are a cell type with a deformation pattern dissimilar from "normal" cell. This observation was confirmed by the analysis of different molecular biomarkers.

We verified by immunoblotting the expression patterns of some molecular markers associated to malignancy progression and to epithelial to mesenchymal transition (CK8/18, Vimentin, E-cadherin); and two proteins involved in cell-adhesion and cell migration (Integrin αvβ3 and Vinculin). As expected we confirmed the low aggressive status of MCF-7 compared to MDA-MB-231. However HBL-100 marker expression pattern was identical to MDA-MB-231, thus more similar to an aggressive cancer cell line rather than a non cancerous control.

HBL-100 were positive for Vimentin, which expression in epithelial cells is a hallmark of EMT. Data on vimentin reactive cells in benign and malignant breast tissue have been described by many authors suggesting its usefulness in identifying cases with clinically aggressive behaviour of tumours and poorer prognosis (Zajchowski D.A.,

Bartholdi M.F. et al. 2001; Korsching E., Packeisen J. et al. 2005), (Raymond W.A. and Leong AS-Y. 1989), (Raymond W.A. and Leong AS-Y. 1989). It may be explained by correlation of vimentin expression and estrogen receptor negativity (Sommers C.L., Walker-Jones D. et al. 1989; Domagala W., Lasota J. et al. 1990), high Ki-67 level (Domagala W., Lasota J. et al. 1990) and poor differentiation of tumours (high grade) (Domagala W., Wozniak L. et al. Am J Pathol 1990). Only few reports are in opposite, as they showed that vimentin expression did not predict patient survival (Heatley M.K., Ewings P. et al. 2002).

Also from the results of the cytokeratins 8/18 immunoblotting, MDA-MB-231 and HBL-100 showed to have similar patterns. Cytokeratins 8/18 are considered markers of malignancy: they are usually used as molecular markers to distinguish Luminal carcinomas from Basal –like carcinomas, that are usually more aggressive (Delgallo W.D., Rodriguez J.R.P. et al. 2009). As expected MCF-7 strongly expressed both cytokeratins CK8 / 18 and MDA-MB-231 exhibited weak positivity; similar to MDA-MB-231 HBL-100 exhibited weak positivity.

Regarding E-Cadherine, both HBL-100 and MDA-MB-231 resulted negative. This is a protein which exerts an evident invasion-suppressing role in tumour cell lines and in vivo tumour model systems (Vleminckx K., Vakaet Jr L. et al. 1991; Frixen U.H., Behrens J. et al. 1991.): forced expression of E-cadherin decreased proliferation of different mammary carcinoma cell lines (Meiners S., Brinkmann V. et al. 1998; St Croix B., Sheehan C. et al. 1998.). E-cadherin is expressed in normal adults in luminal epithelial cells. Temporary down-regulation of E-cadherin was found in budding lobules invading the stroma of breast tissue (Daniels C., Strickland P. et al. 1995). In breast cancer partial or total loss of E-cadherin expression correlates with loss of differentiation characteristics, acquisition of invasiveness potentiality, increased tumor grade, metastatic phenotype and poor prognoses (Heimann R., Lan F.S. et al. 2000) (Siitonen S.M., Kononen J.T. et al. 1996).

Finally, HBL-100 (and MDA-MB-231) showed positivity for Integrin αvβ3 and Vinculin. The integrins are trans-membrane receptors linked to the actin cytoskeleton, involving vinculin as on of its intermediaries. Thus, both these proteins are involved in cell-cell and cell-extracellular matrix (ECM) interactions, cell mobility and migration. Detailed studies of integrin expression in benign breast lesions (fibroadenoma or papilloma) and mammary carcinomas show patterns of integrin type and distribution that are altered in comparison with normal breast tissue (Mizejewski G.J. 1999) In

particular in breast carcinomas $\alpha_v\beta_3$ mediates bone metastasis through the enhanced cell adhesion (Felding-Habermann B. and al. 2001; McCabe N.P., De S. et al. 2007). In their study, Desgrosellier et al. (Desgrosellier J.S., Barnes L.A. et al. 2009) compared $\alpha_v\beta_3$ expression in multiple matched pairs of primary tumors and lymph node metastases from breast cancer patients: interestingly several cases were observed in which $\alpha_v\beta_3$ expression was enriched in the lymph node metastases in comparison with the primary tumor. In ”in vitro” studies, high $\alpha_v\beta_3$ expression in breast tumors was positively correlated with the cell's ability to endothelial adhesion and migration, thus increasing the metastatic potential (Mizejewski G.J. 1999). Furthermore, $\alpha_v\beta_3$ integrin co-localizes with the ECM metalloproteinase-MMP2 on the surface of invasive melanoma cells thereby facilitating tumor cell invasion by degradation of the ECM (Koukoulis G.K., Howeedy A.A: et al. 1993). Taken together these information suggest $\alpha_v\beta_3$ integrin in breast cancer as a marker of the metastatic phenotype.

The fact that HBL-100 presented markers of aggressiveness is in agreement with previous papers. It has been seen in 2006 by Sheridan and colleagues that both MDA-MB-231 and HBL-100 possessed a large (>30%) CD44+/CD24- subpopulation. CD44 and CD24 have been shown to regulate invasion and metastasis of breast cancer cells either positively or negatively. Although most studies have shown CD44-mediated invasion of breast cancer cells (Bourguignon L.Y. 2001; Hill A., McFarlane S. et al. 2006), Lopez and coworkers (Lopez J.I., Camenisch T.D. et al. 2005) showed inhibition of breast cancer metastasis by this molecule. Similarly, CD24 has been shown to promote (Baumann P., Cremers N. et al. 2005) or inhibit (Schabath H., Runz S. et al. 2006) invasion and metastasis of breast cancer cells. Sheridan and colleagues found out that breast cancer cells with CD44+/CD24- subpopulation express higher levels of pro-invasive genes and have highly invasive properties, even if this phenotype seems to be not sufficient to predict capacity for pulmonary metastasis (Sheridan C., Kishimoto H. et al. 2006) A possible explanation for this discrepancy could be the problem related to cell culturing process. Cell lines, infact, are widely used since they are easy to handle and represent an unlimited self-replicating source that can be grown in almost infinite quantities. However, cell lines undergo to genotypic and phenotypic drift while becoming immortalized, and from their continual culture and subpopulations may arise and cause phenotypic changes over time by the selection of specific clones (Burdall Sarah E. 2003) changing the characteristic of the cell line.

HBL-100 was developed from milk of an apparently healthy 27-year-old Caucasian woman obtained on day 3 after delivery (Polanowski F.D. et al. 1976; Gaffney E.V, 1982; Caron de Fromentel C. et al. 1985. The milk donor was followed for several years with clinical and mammographic evaluations at regular intervals with no detectable breast lesion (Gaffney E.V. 1982). From literature data emerged that at low number of passages (below P 35), when the cells were inoculated by different routes into adult nude mice, no tumors were obtained. By contrast, carcinomas consistently appeared when the cells were tested at passage 103 or later (Ziche M. et al. 1982) Furthermore, it was shown that during the course of their progression toward neoplastic transformation, the HBL-100 cells displayed an increasing capacity to induce angiogenesis and a loss of fibrin clot retraction activity, properties both associated with the malignant phenotype (Ziche M. et al. 1982). For these reason we used HBL-100 between passage 9 to 25, in which HBL-100 cells are supposed to represent an early stage of the neoplastic progression. Nevertheless, biomechanical and proteomic characterization describes HBL-100 as a cancer cell type at a late and not early stage of the neoplastic progression.

A second explanation that could explain the HBL-100 aggressive behaviour is related to its nature. HBL-100 are derived from the milk of a donor demonstrate that they are not referred to the breast in a general situation, but particular, which is related to the production of milk. There is emerging evidence that the mammary epithelium is arranged as a hierarchy that spans from stem cells to differentiated hormone-sensing, milk-producing and myoepithelial cells. It is well established that estrogen is an important mediator of mammary gland morphogenesis and exposure to this hormone is associated with increased breast cancer risk (Stinql J. 2011). Mammary gland development occurs in three distinct stages during the lifetime of the female mammal: in embryonic, pubertal and reproductive life. At each of these developmental stages, different signalling molecules induce changes in both the epithelium and the surrounding stroma. However, it is during pregnancy that the most dramatic changes occur, resulting in a massive increase in the number of epithelial cells and in their function. Pregnancy initiates the development of a new epithelial lineage, the alveolar cells, which form the milk-producing lobuloalveolar structures. These cells become redundant at the end of lactation and are removed in an exquisitely controlled process of tissue remodelling coupled with extensive cell death. All of these events require not only steroid hormones but also sequential signalling by cytokines (Watson C.J. et al.

2011) The HBL-100 cell lines are so far representative of the lactation period and this fact could represent a possible explanation for the molecular pattern detected in these cells.

To further investigate on cell types and their nature, and to find out a possible correlation between their malignancy status and their mechanical properties, we used the cytoskeleton structure and organization as a parameter to discriminate the cell types.

The driving force that contrasts membrane protrusion is localized in the polymerization of submembrane actin filaments. Cytoskeleton imaging by STED microscopy could group the two breast cancer cells MDA-MB-231 and MCF-7 showing a deregulation in the organization of the actin filaments compared to HBL-100. The control cell line showed an actin network with thin filaments homogeneously distributed under the cell surface. On the other hand MDA-MB-231 and MCF-7 exhibited thicker filaments, a less homogeneous network and the presence of actin drifts.. This deregulation was expected, since malignant cancer cells utilize their intrinsic migratory ability to invade adjacent tissues and to metastasize (Yamaguchi H. and Condeelis J. 2007). This difference among the breast cancer cell lines and the control ,suggested the non neoplastic nature of HBL-100 supporting the hypothesis that its anomalous biomechanical characteristics and molecular pattern are due to its nature of epithelial cells related to an exceptional situation as lactation, and not to a real malignant nature.

5. FINAL REMARKS AND CONCLUSIONS

One of the most debated issue in oncology nowadays is the biomechanical characterization of tumour cells and its relationship with the progression of the disease. Tumour invasion and metastatization are strictly correlated with alterations in cell adhesion, migration properties and thus in cell mechanics. To give some contribution to this topic we studied three cell lines with different characteristics, representing different stages of the progression through malignancy: two breast cancer cell lines, one more aggressive than the other, and one cell line supposed to be from normal breast lactating cell.

The cell lines were submitted to physical stimulation by membrane tether pulling experiments with Optical Tweezers (OT), indentation experiments by Atomic Force Microscopy (AFM) and optical deformability tests by Microfluidic Optical Stretcher (MOS). To better explain the physical results we characterized the cell lines by protein biomarkers expression pattern analysis and investigated on the actin cytoskeleton organization and structure. Furthermore, phospholipid composition of cell membrane was studied by MALDI-MS analysis.

We can conclude that our results are suggesting:

1. The different biomechanical experimental approaches used in this work characterize different aspects of cell mechanical properties and thus could help for a extensive analysis of the cell mechanics. Membrane tether formation by OT is a local measure which gives visco-elastic information about cytoskeleton-membrane interaction; indentation experiments by AFM gives information on the elasticity only, but involves a larger region of the cell; MOS test the whole cell deformation by the radiation pression of light. With three experimental approaches we were able to evaluate different mechanical properties related to cell membrane or to the entire cell.

2. These experiments could discriminate between normal and tumour cells, but were unable to discriminate tumour cells with difference in aggressiveness.

3. We were able anyway to show a trend among the tumour cell types: membrane tether pulling experiments with OT showed that the less aggressive cell line have stiffer membranes and thus to be more resistant to membrane deformation compared with

the more aggressive ones; indentation experiments with AFM and optical deformability tests with MOS showed that the less aggressive cells have higher resistance to deformation compared to the more aggressive ones.

4. We could better explain the differences between cells comparing mechanical analysis with expression patterns of some molecular markers associated to epithelial differentiation (CK8/18), markers associated to epithelial to mesenchymal transition (E-cadherin and vimentin), markers involved in cell migration and adhesion (integrin άvβ3 and vinculin). We confirmed the neoplastic nature of the breast cancer cell lines considered, and their aggressive status. However, the mechanical and protein expression analysis of the control cell line suggested a pattern dissimilar from a "normal" non tumorigenic cell line.

5. We explained the anomalous behaviour of the control cells with its nature: the cell line was derived from the milk of an apparently healthy milk donor. We suppose its anomalous characteristics are due to fact that it is representative of an exceptional situation such as lactation, mimicking malignant nature.

6. Actin cytoskeleton images by STED (Stimulated Emission and Depletion) and confocal microscopy confirmed the non malignant nature of the control cell line. We could associate an homogeneous and ordered actin filament organization to the control cell line and observed a more dysregulated actin filaments organization in the tumour cell lines

7. Phospholipids analysis gave us some major results that could explain differences in membrane stiffness: downregulation of some PEs (Phosphatidylethanolammines) and upregulation of some PIs (Phosphatidylinositoles) were found in the more aggressive cell lines associated to softer membrane.

Our results are completely preliminary and need further confirmation in breast and other tumour cell lines.

BIBLIOGRAPHY

Abner A.L., Collins L., et al. (1998). "Correlation of tumor size and axillary lymph node involvement with prognosis in patients with T1 breast c a r c i n o m a . ." Cancer **83**: 2502-2508.

Adami H.O., Sparen P., et al. (1989). "Increasing survival trend after cancer diagnosis in Sweden: 1960-1984." **81**: 1640-1647.

Albelda S.M. and Buck C.A. (1990). "Integrins and other cell adhesion molecules." FASEB J. **4**: 2868-2880.

Allioux-Guerin, M., Icard-Arcizet D., Durieux C., Henon s., Gallet F., Mevel J. C., Masse M.J., Tramier M., Coppey-Moisan M. (2009). "Spatio-temporal analysis of cell response to a rigidity gradient: A quantitative study by multiple optical tweezers." Biophysical Journal **96 (1)**: 238-247.

Andre F. and P. L. (2006). "Molecular classification of breast cancer: implications for selection of adjuvant chemotherapy." Nature Clinical Practice Oncology **3**(11): 621-632.

Anon. (1992). "Systemic treatment of early breast cancer by hormonal, cytotoxic, or immune therapy. 133 randomised trials involving 31,000 recurrences and 24,000 deaths among 75,000 women. Early Breast Cancer Trialists' Collaborative Group." Lancet **339**: 1-15.

Ashkin A. (1970). "Acceleration and trapping of particles by radiation pressure." Physical Review Letters **24**(4): 156-159.

Ashkin A. (1992). "Forces of a single-beam gradient laser trap on a dielectric sphere in the ray optics regime." Bipophys. J. **61**: 569-582

Ashkin A. (2006). "Optical Trapping and Manipulation of Neutral Particles Using Lasers." Ed. World Scientific Publishing Company. Physics - Optics & Light

Ashkin A., Dziedzic J.M., et al. (1986). "Observation of a single-beam gradient force optical trap for dielectric particles." Opt. Lett. **11**: 288-290.

Ashkin A., Dziedzic J.M., et al. (1986). "Observation of a single-beam gradient force optical trap for dielectric particles." Optics Letters **11**(5): 288-290.

Ashkin A. and Dziedzic JM. (1987). "Optical trapping and manipulation of viruses and bacteria." Science **235**(4795): 1517-1520.

Ashkin A. and D. J.M. (1973). "Radiation Pressure on a Free Liquid Surface." Phys. Rev. Lett. **30**: 139-142.

Ashkin A., Schutze K., et al. (1990). "Force Generation of organelle transport measured in vivo by an infrared laser trap." Nature **348**(6299): 346-348.

Azumi N. and Battifora H. (1987). "The distribution of vimentin and keratin in epithelial and nonepithelial neoplasms. A comprehensive immunohistochemical study on formalin and alcohol fixed tumors. ." Am J Clin Pathol **88**: 286-96.

Baldwin MA. (2005). "Mass spectrometers for the analysis of biomolecules." Meth Enzymol **402**: 3–48.

Balzi D., Buiatti E., et al. (1993). "Summary of the results by site. In: Cancer in Italian Migrant Populations." International Agency for Research on Cancer: Lyon **IARC Scientific Publication No 123**: 193-292.

Baumann P., Cremers N., et al. (2005). "CD24 expression causes the acquisition of multiple cellular properties associated with tumor growth and metastasis. ." Cancer Res **65**: 10783-10793.

Bausch A. R. (1998). "Local measurements of viscoelastic parameters of adherent cell surfaces by magnetic bead microrheometry." Biophys. J. **75**: 2038–2049.

Berg-Sorensen K. and Flyvbjerg H. (2004). "Power spectrum analysis for optical tweezers." Review of Scientific Instruments,
75: 594–612.

Bertucci F. and Birnbaum D. (2008). "Reasons for breast cancer heterogeneity." François Bertucci and Daniel Birnbaum* **7**(6).

Berx G. and Van Roy F. (2001). "The E-cadherin/catenin complex: an important gatekeeper in breast cancer tumorigenesis and malignant progression
" Breast Cancer Res
3: 289–293

Bligh E.G. and Dyer W.J. (1959). "A rapid method of total lipid extraction and purification." Can. J. Biochem. Physiol. **37**: 911-917.

Block A.M., L. S. B., et al. (1990). "Bead movement by single kinesin molecules studied with optical tweezers." Nature **348**: 348 - 352

Bourguignon L.Y. (2001). "CD44-mediated oncogenic signaling and cytoskeleton activation during mammary tumor progression." J. Mammary Gland Biol Neoplasia **6**: 287-297.

Bückers J., Wildanger D., et al. (2011). "Simultaneous multi-lifetime multi-color STED imaging for colocalization analyses
" OPTICS EXPRESS **19,**(4).

Bückers J., Wildanger D., et al. (2011). "Simultaneous multi-lifetime multi-color STED imaging for colocalization analyses." Optics Express **19**(4).

Burdall Sarah E., H. A. M., Lansdown Marck RJ., Speirs Valerie (2003). "Breast cancer cell lines: friend or foe?" Breast Cancer Research **5**: 89-95.

Carl P. and Schillers H. (2008). "Elasticity measurement of living cells with an atomic force microscope: data acquisition and processing." Pflugers Arch **457**: 551-559.

Carl P. and Schillers H. (2008). "Elasticity measurement of living cells with an atomic force microscope: data acquisition and processing." Pflugers Arch-Eur J Physiol Rev **457**: 551-559.

Carlson R. H. G., Gabel C.V., et al. (1997). "Self-sorting of white blood cells in a lattice." Phys. Rev. Lett. **79**: 2149-2152.

Caron de Fromentel C., Nardeux P.C., et al. (1985). "Epithelial HBL-100 Cell Line Derived from Milk of an Apparently Healthy Woman Harbours SV40 Genetic Information." Experimental Cell Research **160**: 83-94.

Carrion-Vazquez M., Orr A.W., et al. (1999). "Mechanical and chemical unfolding of a single protein: A comparison." Proc Natl Acad sci USA **96**(7): 3694-3699.

Chajes V., Lanson M., et al. (1995). "Membrane fatty acids of breast carcinoma: contribution of host fatty acids and tumor properties." Chajes V, Lanson M, Fetissof F, L. huillery C, Bougnoux P. Membrane
fatty acids of breast carcinoma: contribution of host fatty acids and
tumor properties. Int J Cancer 1995;63:169–75. **63**: 169–75.

Chatelin S., Constantinesco A., et al. (2011). "Fifty years of brain tissue mechanical testing: from in vitro to in vivo investigations." Biorheology **47**: 255-276.

Choquet, D., Felsenfeld D.P., and Sheetz M. P. (1997). "Extracellular matrix rigidity causes strengthening of integrin-cytoskeleton linkages." Cell **88(1)**: 39-48.

Chu K.C., Tarone R.E., et al. (1996). "Recent trends in U.S. breast cancer incidence, survival, and mortality rates." J. Natl Cancer Inst **88**: 1571-1579.

Coll J.L., Ben-Ze'ev A., et al. (1995). "Targeted disruption of vinculin genes in F9 and embryonic stem cells changes cell morphology, adhesion, and locomotion." Proc. Natl. Acad. Sci. USA. 92:9161–9165 **92**: 9161–9165.

Commission, T. E. (1996). "European Guidelines for Quality Assurance in Mammography Screening.
." ed. The European Commission: Luxembourg **2nd ed.**

Contesso G., Mouriesse H, et al. (1987). "The importance of histologic grade in longterm prognosis of breast cancer: a study of 1,010 patients, uniformly treated at the Institut Gustave-Roussy." J Clin Oncol **5**: 1378-1386.

Cross S., Jin Y.S., et al. (2007). "Nanomechanical analysis of cells from cancer patients." Nature Nanotechnology **2**: 780-783.

Cross S.E., Jin Y.S., et al. (2008). "AFM-based analysis of human metastatic cancer cells." J Nanotechnol **19**: 1-8.

Cross, S. E., Jin Y.S., Rao J., and Gimzewski J.K (2007). "Nanomechanical analysis of cells from cancer patients." Nat Nanotechnology **2 (12)**: 780-783.

Daniels C., Strickland P., et al. (1995). "Expression and functional role of E- and P-cadherin in mouse mammary ductal morphogenesis and growth." Dev Biol **169**: 511-519.

Darling E.M., Zauscher S., et al. (2007). "A thin-layer model for viscoelastic, stress-relaxation testing of cells using atomic force microscopy: do cell properties reflect metastatic potential." Biophysics
J Cell Biol
92: 1784-91.

Davies P.F. (1995). "Flow-mediated endothelial mechanotransduction." Physiol Rev **75**(3): 519-560.

Delgallo W.D., Rodriguez J.R.P., et al. (2009). "Cell blocks allow reliable evaluation of expression of basal (CK5/6) and luminal (CK8/18) cytokeratins and smooth muscle actin (SMA) in breast carcinoma." Cytopathology **21**: 259–266.

Desgrosellier J.S., Barnes L.A., et al. (2009). "An integrin alpha(v)beta(3)-c-Src oncogenic unit promotes anchorage-independence and tumor progression." Nat Med **10**: 1163-1169.

Dimitriadis E.K., Horkay F., et al. (2002). "Determination of elastic moduli of thin layers of soft material using the atomic force microscope." Biophys J **82**: 2798-2810.

Domagala W., Lasota J., et al. (1990). "Vimentin is preferentially expressed in human breast carcinomas with low estrogen receptor and high Ki-67 growth fraction." Am J Pathol **136**: 219-227.

Domagala W., Wozniak L., et al. (Am J Pathol 1990). "Vimentin is preferentially expressed in high grade ductal and medullary, but not in lobular breast carcinomas." Am J Pathol **137**: 1059-1064.

du Toit R.S., Locker A.P., et al. (1989). "Invasive lobular carcinomas of the breast--the prognosis of histopathological subtypes.
." Br J Cancer **60**: 605-609.

Ellis I.O., Galea M., et al. (1992). "Pathological prognostic factors in breast cancer. II. Histological type. Relationship with survival in a large study with longterm follow-up." Histopathology **20**: 479-489.

Elston C.W. and E. I.O. (1991). "Pathological prognostic factors in breast cancer. I. The value of histological grade in breast cancer: experience from a large study with long-term follow-up." Histopathology **19**: 403-410.

Engler A.J., Richert L., et al. (2004). "Surface probe measurements of the elasticity of sectioned tissue, thin gels and polyelectrolyte multilayer films: correlations between substrate stiffness and cell adhesion." Surf Sci **570**: 142-154.

Ericsson M., Hanstorp D., et al. (2000). "Sorting out Bacterial Viability with Optical Yweezers." Journal of Bacteriology **182**(19): 5551-5555.

Faria E.C., Ma N., et al. (2008). "Measurement of elastic properties of prostate cancer cells using AFM.
." Analyst **133**: 1498-500.

Felding-Habermann B. and e. al. (2001). " Integrin activation controls metastasis in human breast cancer." Proc Natl Acad Sci U S A. **98**: 1853–1858.

Fisher B., Dignam J., et al. (1999). "Tamoxifen in treatment of intraductal breast cancer: National Surgical Adjuvant Breast and Bowel Project B-24 randomised controlled trial." Lancet **353**: 1993- 2000.

Fisher E.R., Anderson S., et al. (1993). "Pathologic findings from the National Surgical Adjuvant Breast Project protocol B-06. 10-year pathologic and clinical prognostic discriminants.
." Cancer **71**: 2507-2514.

Foulkes WD, S. I., Chappuis PO et al. (2003). "Germline BRCA1 mutations and a basal ephitelial phenotype in breast cancer." J Natl Cancer Inst(95 (19)): 1482-1485.

Franze K. (2011). "Atomic force microscopy and its contribution to understanding the development of the nervous system." Current Opinion in Genetics and Development **21**: 530-537.

Franze K., Gerdelmann J., et al. (2009). "Neutrite branch retraction is caused by a threshold-dependent mechanical impact." Biophysical Journal **97**: 1883-1890.

Franze K. and Guck J. (2010). "The biophysics of neuronal growth." Rep Prog Phys. **73**.

Frixen U.H., Behrens J., et al. (1991.). " E-cadherin-mediated cell–cell adhesion prevents invasiveness of human carcinoma cells." J Cell Biol **113**: 173-185.

Fuchs B., Süß R, et al. (2010). "An update of MALDI-TOF mass spectrometry in lipid research." Proggress in Lipid research **49**: 450-475.

Gaffney E.V. (1982). “HBL-100 A cell line established from human breast milk”Cell Tissue Res **227**: 563.

Geiger T.R. and P. D.S (2009). "Metastasis mechanisms." Biochimica et Biophysica Acta **1796** 293-308.

Gilles C., Polette M., et al. (2003). "Transactivation of vimentin by beta-catenin in human breast cancer cells." Cancer Res **63**(63): 2658-64.

Gilmore A.P. and Burridge K. (1995). "Cell adhesion. Cryptic sites in vinculin." Nature **373**: 197.

Goldhirsch A., Glick J.H., et al. (1998). "Meeting highlights: International consensus panel on the treatment of primary breast cancer." **90**: 1601-1608.

Guck J., Ananthakrishnan R., et al. (2001). "The Optical Stretcher: A Novel Laser Tool to Micromanipulate Cells." Biophysical Journal **81**: 767-784.

Guck J., Ananthakrishnan R., et al. (2000). "Optical Deformability of Soft Biological Dielectrics
" Phys. Rev. Lett. **84**: 5451-5454

Guck J., S. S., Lincoln B., Wottawah F., Ebert S., Romeyke M., Lenz D., Erickson H.M., Ananthakrishnan R., Mitchell D., Kas J., Ulvick S., and Bilby C. (2005). "Optical deformability as an inherent cell marker for testing malignant trasformation and metastatic competence." Biophysical Journal **88(5)**: 3689-3698.

Gupta G.P. and Massaguè . (2006). "Cancer Metastasis: Building a Framework." Cell **127**: 679-695.

Heatley M.K., Ewings P., et al. (2002). "Vimentin expression does not assist in predicting survival in ductal carcinoma of the breast." Pathology 2002, 34:230-2. **34**: 230-232.

Heidemann S.R. and Wirtz D. (2004). "Towards a regional approach to cell mechanics." TRENDS in Cell Biology **14**(4): 160-166.

Heimann R., Lan F.S., et al. (2000). "Separating favorable from unfavorable prognostic markers in breast cancer: the role of E-cadherin." Cancer Res **60**: 298-304.

Helmke B.P. and Davies P.F. (2002). "The cytoskeleton under external fluid mechanical forces: hemodynamic forces acting on the endothelium." Ann Biomed Eng **30**(3): 284-296.

Hendrix M.J., Seftor E.A., et al. (1997). "Experimental coexpression of vimentin and keratin intermediate filaments in human breast cancer cells results in phenotypic interconversion and increased invasive behavior." Am J Pathol **150**: 483-495.

Hertz H. (1881). " Ueber die Berührung fester elastischer Körper." J Reine Angew Math **92** 156–171.

Hill A., McFarlane S., et al. (2006). "Cortactin underpins CD44-promoted invasion and adhesion of breast cancer cells to bone marrow endothelial cells. ." Oncogene
25: 6079-6091.

Hillenkamp F. and Peter-Katalinic J. (2007). "MALDI-MS, a practical guide to instrumentation, methods
and applications." Wiley-VCH, Weinheim **Chap. 7**.

Hilvo M., Denkert C., et al. (2011). "Novel Theranostic Opportunities Offered by Characterization of Altered Membrane Lipid Metabolism in Breast Cancer Progression." Cancer Res **71**: 3236-3245.

Hochmuth M. R., S. J. Y., Dai J., and Sheetz M.P. (1996). "Deformation and flow of membrane into tethers extracted from neuronal growth cones." Biophysical Journal **70 (1)**: 358-369.

Hochmuth, M. R. (2000). "Micropipette aspiration of living cells." Journal of Biomechanics **33(1)**: 15-22.

Huang H., S. J., Jonas M., Barresi R., So P.T.C., Campbell K.P. and Lee R-T. (2005). "Cell stiffnes and receptors: evidence for cytoskeletal subnetworks." American Journal of Phhysiology- Cell Physiology **288(1)**: C72-C80.

Isaacs C., Stearns V., et al. (2001). "New prognostic factors for breast cancer recurrence." Semin Oncol **28**: 53-67.

Jemal A., Siegel R., et al. (2008). "Cancer statistics, 2008." CA Cancer J. Clin **58**: 71-96.

Karas M., Glückmann M., et al. (2000). " Ionization in matrix-assisted laser desorption/ionization: singly charged molecular ions are the lucky survivors." J. Mass Spectrom. **35**: 1-12.

Kliewer E.V. and Smith K.R. (1995). "Breast cancer mortality among immigrants in Australia and Canada." Breast cancer mortality among immigrants in Australia and Canada **87**: 1154-1161.

Kokkinos M.I., Wafai R., et al. (2007). "Vimentin and epithelial-mesenchymal transition in human breast cancer-observations in vitro and in vivo." Cells Tissues Organs . **185**: 191-203.

Korsching E., Packeisen J., et al. (2005). "The origin of vimentin expression in invasive breast cancer: epithelial-mesenchymal transition, myoepithelial histogenesis or histogenesis from progenitor cells with bilinear differentiation potential?." J Pathol **206**(206): 451-457.

Koukoulis G.K., Howeedy A.A:, et al. (1993). "Distribution of tenascin, cellular fibronectins and integrins in the normal, hyperplastic, and neoplastic of the breast." J. Submicrosc Cytol Pathol **25**: 283-295.

Krouskop T.A., Wheeler T.M., et al. (1998). "Elastic Moduli of Breast and prostate tissues under compression." Ultrason Imaging **20**(4): 260-274.

Kumar, S. and V. M. Weaver (2009). "Mechanics, malignancy, and metastasis: The force journey of a tumor cell." Cancer Metastasis Rev. **28 (1-2)**: 113-127.

Kundu T., Bereiter-Hahn J., et al. (2000). "Cell property determination from the acoustic microscope generated voltage versus frequency curves.
." Biophys. J. **78**: 2270-2279.

Lekka M., Laidler P., et al. (1999). "Elasticity of normal and cancerous human bladder cells studied by scanning force
microscopy." Eur. Biophys. J. **28**(4): 312-316.

Li Q.S., Lee G.Y.H., et al. (2008). "AFM indentation study of breast cancer cells." Biomechanical and Biophysical Research Communications **374**: 609-613.

Li Z. (2002). "Membrane tether formation from outer hair cells with optical tweezers." Biophys J
82: 1386-1395.

Lincoln B., Erickson H.M., et al. (2004). " Deformability-based flow cytometry." Cytometry A. **59A**(2): 203-209.

Lincoln B., Schinkinger S., et al. (2007). "Reconfigurable microfluidic integration of a dual beam laser trap with biomechanical applications." Biomed Microdevices **9**: 703-710.

Lippman M., Osborne C., et al. (1977). "In vitro model systems for the study of hormone-dependent human
breast cancer." N Engl J Med **296**: 154-159.

Liu H., F. Q., Zhang et al. (2008). "Basal-HER2 phenotype shows poorer survival than basal-like phenotype in hormone receptor-negative invasive breast cancers." Hum Pathol(39 (2)): 167-174.

Lopez J.I., Camenisch T.D., et al. (2005). "CD44 attenuates metastatic invasion during breast cancer progression." Cancer Res **65**: 6755-6763.

MacKintosh, F. C. and C. F. Schmidt (1999). "Microrheology." Elsevier **4**(4): 300-307.

Martinez V., Azzopardi J.G., et al. (1979). "Invasive lobular carcinoma of the breast: incidence and variants." Histopathology
3.

McCabe N.P., De S., et al. (2007). "Prostate cancer specific integrin alphavbeta3 modulates bone metastatic growth and tissue remodeling. ." Oncogene **26**: 6238–6243.

Meiners S., Brinkmann V., et al. (1998). "Role of morphogenetic factors in metastasis of mammary carcinoma cells." Oncogene **16**: 9-20.

Mizejewski G.J. (1999). "Role of Integrins in Cancer: Survey of Expression Patterns
" Exp Biol Med
222(2): 124-138.

Munevar S., Wang Y., et al. (2001). "Traction Force microscopy of migrating normal and H-ras transformed 3t3 fibroblasts." Biophysical Journal **80**: 1744-1757.

Neuman K.C. and Block M. (2004). "Optical Trapping." American Institute of Physics **75**(9): 2787-2809.

Neuman K.C., Chadd E.H., et al. (1999). "Characterization of Photodamage to Escherichia coli in Optical Traps." Biophysical Journal **77**: 2856-2863.

Nikkhah M., Strobl J., et al. (2010). "The cytoskeletal organization of breast carcinoma and fibroblast cells inside three dimensional (3-D) isotropic silicon microstructures." Biomaterials **31**: 1-10.

Nixon A.J., Schnitt S.J., et al. (1996). "Relationship of tumor grade to other pathologic features and to treatment outcome of patients with early stage breast carcinoma treated with breast-conserving therapy
" Cancer **78**: 1426-1431.

Omary MB, Baxter GT, Chou CF, et al. (1992). "PKC epsilon-related kinase associates with and phosphorylates cytokeratin 8 and 18". J. Cell Biol. **117** (3): 583–93).

Osborne C.K. (1998). "Steroid hormone receptors in breast cancer management
" **51**: 227-238.

Park S., Koch D., et al. (2005). "Cell Motility and Local Viscoelasticity of Fibroblasts." Biophys J **89**(6): 4330-4342.

Parkin D.M., Bray F., et al. (2001). "Estimating the world cancer burden: Globocan 2000." Int J Cancer **94**: 153-156.

Paszek M.J. and Weaver V.M. (2004). "The Tension Mounts: Mechanics Meets Morphogenesis and Malignancy." Journal of Mammary Gland Biology and Neoplasia **9**(4): 325-342.

Peng X., Nelson E.S., et al. (2011). "New insights into vinculin function and regulation
" Int Rev Cell Mol Biol. **287**: 191-231.

Pereira H., Pinder S.E., et al. (1995). "Pathological prognostic factors in breast cancer. IV: Should you be a typer or a grader? A com - parative study of two histological prognostic features in operable breast carcinoma." Histopathology **27**: 219-226.

Perou C.M., S. T., Eisen MB, et al. (2000). "Molecular portraits of human breast tumour." Nature (406): 747-752.

Petkovic M., Schiller J., et al. (2001). "Detection of individual phospholipids in lipid mixtures by matrix-Assisted Laser Desorption/Ionization
Time-of-Flight Mass Spectrometry: Phosphatidylcholine Prevents the Detection of Further Species." Anal. Biochem. **289**: 202-216.

Plewes D.B., Bishop J., et al. (2000). "Visualization and quantification of breast cancer biomechanical properties with magnetic resonance elastography." Phys Med Biol **45**(6): 1591-1610.

Polanowski F.P., Gaffney E.V., et al. (1976).”Cultures of normal human mammary cells” In Vitro **12**: 328.

Radmacher, M., Fritz, M., Kacher M., Cleveland J.P., and Hansma P.K. (1996). "Measuring the viscoelastic properties of human platelets with the atomic force microscope." Biophysical Journal **70 (1)**: 556-567.

Rakha E.A., Putti T.C., et al. (2006). "Morphological and immunophenotypic analysis of breast carcinomas with basal and myoepithelial differentiation." J. Pathol **208**: 495-506.

Raymond W.A. and Leong AS-Y. (1989). "Co-expression of cytokeratins and vimentin intermediate filament proteins in benign and neoplastic breast epithelium." J Pathol (157): 299-306.

Raz A. and Geiger B. (1982). "Altered organization of cell-substrate contacts and membrane-associated cytoskeleton in tumor cell variants exhibiting different metastatic capabilities." Cancer Res. **42**(5183-5190).

Remmerbach, T. W., F.Wottawah, Dietrich J., Lincoln B., Witterkind C. and Guck J. (2009). "Oral cancer diagnosis by mechanical phenotyping." Cancer Research **69(5)**: 1728-1732.

Rosen P.P., Groshen S., et al. (1989). "Pathological prognostic factors in stage I (T1N0M0) and stage II (T1N1M0) breast carcinoma: a study of 644 patients with median followup
of 18 years. ." J Clin Oncol **7**: 1239-1251.

Rosenbluth M.J., Lam W.A., et al. (2006). "Force microscopy of nonadherent cells: a comparison of leukemia cell deformability
" Biophysics J **90**: 2994-3003.

Rotsch C. and Radmacher M. (2000). "Drug-induced changes of cytoskeletal structure and mechanics in fibroblasts: an atomic force microscopy study. ." Biophys. J. **78**(520-535).

Sastre-Garau X., Jouve M., et al. (1996). " Infiltrating lobular carcinoma of the breast. Clinicopathologic analysis of 975 cases with reference to data on conservative therapy and metastatic patterns
" Cancer **77**: 113-120.

Sastre-Garau X., Jouve M., et al. (1996). "Infiltrating lobular carcinoma of the breast. Clinicopathologic analysis of 975 cases with reference to data on conservative therapy and metastatic patterns.
." **77**.

Saunders R.M., Holt M.R., et al. (2006). "Role of vinculin in regulating focal adhesion turnover." Eur. J. Cell Biol. **85**: 487–500.

Schabath H., Runz S., et al. (2006). "CD24 affects CXCR4 function in pre-B lymphocytes and breast carcinoma cells." J. Cell Sci **119**: 314-325.

Schiller J., Suss R., et al. (2007). "The suitability of different DHB isomers as matrices for the MALDI-TOF MS analysis of phospholipids: which isomer for what purpose?" Eur. Biophys. J. **36**: 517-527.

Schiller J., Süss R., et al. (2006). "Recent applications of

MALDI-TOF mass spectrometry and 31P NMR spectroscopy in phospholipid research." Fut. Lipid **1**: 115-125.

Schmitz J., Benoit M., et al. (2008). " The viscoelasticity of membrane tethers and its importance for cell adhesion." Biophys. J. **95**: 1448-1459.

Sheetz M.P. and (2001). "Cell control by membrane – cytoskeleton adhesion." Nat. Rev. Mol. Cell. Biol. **2**: 392-396.

Sheridan C., Kishimoto H., et al. (2006). "CD44+/CD24- breast cancer cells exhibit enhanced invasive properties: an early step necessary for metastasis." Breast Cancer Research **8**: R59.

Shures, S. (2007). "Biomechanics and biophysics of cancer cells." Acta Biomaterialia **3** 412-438.

Siitonen S.M., Kononen J.T., et al. (1996). "Reduced E-cadherin expression is associated with invasiveness and unfavorable prognosis in breast cancer." Am J Clin Pathol **105**: 394-402.

Silverstein M.J., Lewinsky B.S., et al. (1994). "Is it different from infiltrating duct carcinoma? ." Cancer **73**: 1673-1677.

Singer W., Bernet S., et al. (2000). "Three-dimensional force calibration of optical tweezers." Journal of Modern Optics **47**(14-15): 2921-2931.

Slamon D.J., Clark G. M., et al. (1987). "Human breast cancer: correlation of relapse and survival with amplification of the HER-2/neu oncogene
" Science **235**(4785): 177-182.

Sleep, J., D. Wilson, R. Simmons, and W. Gratzer. (1999). "Elasticity of the red cell membrane and its relation to haemolytic disorders" Biophys. J. **77(6)**: 3085-3095.

Sommers C.L., Walker-Jones D., et al. (1989). "Vimentin rather than keratin expression in some hormone independent breast cancer cell lines and in oncogene-transformed mammary epithelial cells. ." Cancer Res **49**: 4258-4263.

Sorlie T., Perou C.M., et al. (2001). "Repeated observation of breast tumor subtypes in independet gene expression profiles from a population-based study." Proc Natl Acad sci USA **100**(14): 8418-8423.

Sotiriou C., N. S., McShane LM., et al. (2003). "Breast cancer classification and prognosis based on gene expression profiles from a population-based study." Proc Natl Acad sci USA(100 (18)): 10393-10398.

Soule H., Vazquez J., et al. (1973). "A human cell line from a pleural effusion derived from a
breast carcinoma. JNCI 51: 1409-1413, 1973." JNCI **51**: 1409-1413.

St Croix B., Sheehan C., et al. (1998.). "E-Cadherin-dependent growth suppression is mediated by the cyclin-dependent kinase inhibitor p27KIP1." J Cell Biol **142**: 557-571.

Stinql J. (2011). "Estrogen and progesterone in normal mammary gland development and in cancer" Horm Cancer 2(2):85-90

Suresh, S. (2007). "Nanomedicine: elastic clues in cancer detection." Nature Nanotechnology **2(12)**: 748-9.

Svoboda K. (1994). "Biological Applications of Optical Forces." Annu. Rev. Biophys. Biomol.Struct. **23**: 247-285.

Tavano F., Bonin S., Pinato G., Stanta G., Cojoc D. (2011) "Custom Built Optical Tweezers for Locally Probing the Viscoelastic Properties of Cancer Cells" International Journal of Optomechatronics **5:3** 234-248

Tavassoli F. A. (2003). "World Health Organization classification of Tumours: Pathology and Genetics of Tumours of the Breast and Female genital Organs." WHO: Geneva 2003: 9-19.

Tavassoli F. A. and Devilee Peter. (2000). "WHO Classification of the Breast and Female Genital Organs." IARC Press: Lyon 2000.

Thiery J.P. (2002). "Epithelial-mesenchymal transitions in tumour progression." Nat Rev Cancer 2002 **2**: 442-454.

Thiery J.P. (2003). "Epithelial-mesenchymal transitions in development and pathologies." Curr Opin Cell Biol **15**: 740-746.

Thoumine, O., and Ott A. (1997). "Time scale dependent viscoelastic and contractile regimes in fibroblasts probed by microplate manipulation." Journal of Cell Science **110(9)**: 2109-2016.

Toikkanen S., Pylkkanen L., et al. (1997). "Invasive lobular carcinoma of the breast has better short- and long-term survival than invasive ductal carcinoma." Cancer **76**: 1234-1240.

Verlag, S. (2002). "AJCC Cancer Staging Manual." Sixth ed. Springer Verlag: New York.

Veronesi U., Viale G., et al. (2005). "Rethinking TNM: Breast cancer TNM classification for treatment decision-making and research." The Breast **15**(1): 3-8.

Vleminckx K., Vakaet Jr L., et al. (1991). "Genetic manipulation of E-cadherin expression by epithelial tumor cells reveals an invasion suppressor role." Cell **66**: 107-119.

Volberg T., Geiger B., et al. (1995). " Focal adhesion formation by F9 embryonal carcinoma cells after vinculin gene disruption." J. Cell Sci. **108**: 2253–2260.

Wang N., Butler J. P., et al. (1993). "Mechanotransduction across the cell surface and through the cytoskeleton.
." Science **260**(1124-1127).

Ward K.A., Li W.I., et al. (1991). "Viscoelastic properties of transformed cells: role of tumor cell progression and metastasis formation." Biorheology **28**: 301–13.

Watson C.J, Oliver C.H., Khaled W.T. (2011) "Cytokine signalling in mammary gland development" J.Reprod Immunol **88**(2):124-129

WHO (2000). "World Health Organisation 1997-1999. World Health Statistics Annual.
." http://www who int/whosis.

Wildanger D., Medda R., et al. (2009). "A compact STED microscope providing 3D nanoscale resolution." J. Microsc. **236**(1): 35-43.

Wildanger D., Rittweger E., et al. (2008). "STED microscopy with a supercontinuum laser source." Opt. Express **16**(13): 9614-9621.

Winchester D.J., Chang H.R., et al. (1998). "A comparative analysis of lobular and ductal carcinoma of the breast: presentation, treatment, and outcomes." J Am Coll Surg **186**: 416-422.

Winchester D.J., Chang H.R., et al. (1998). "A comparative analysis of lobular and ductal carcinoma of the breast: presentation, treatment, and outcomes." **186**: 416-422.

Wottawah F., Schinkinger S., Lincoln B., Ananthakrishnan R., Romeyke M, Guck J., Käs J. (2005) "Optical rehology of biological cells" Phys Rev. Lett. 94: 98-103

Zahalak G. I., McConnaughey W.B., et al. (1990). "Determination of cellular mechanical properties by cell poking, with an application to leukocytes." J. Biomech. Eng. **112**: 283-294.

Zajchowski D.A., Bartholdi M.F., et al. (2001). " Identification of gene expression profiles that predict the aggressive behavior of breast cancer." Cancer Res **61**(61): 5168-5178.

Zhang G., Long M., et al. (2002). "Mechanical properties of hepatocellular carcinoma cells." World J Gastroenterol **8**: 243–246.

Ziche M. and Gullino P. (1982)."Angiogenesis and neoplastic progression in vitro" J Natl Cancer Inst **69**: 483-487

Ziegler R.G., Hoover R.N., et al. (1993). "Migration patterns and breast cancer risk in Asian-American women. ." J Natl Cancer Inst **85**: 1819-1827.

APPENDIX

Assignment of the *m/z* values detected within this work	
Peak Position	**Assignement**
714,5	PE 16:0/18:2-H^+
716,5	PE 16:0/18:1-H^+
732,6	PC 16:0/16:1+H^+
742,5	PE 18:0/18:2-H^+
744,5	PE 18:0/18:1-H^+
760,6	PC 16:0/18:1+H^+
766,5	PE 18:0/20:4-H^+
782,6	PC 16:0/20:4+H^+
788,6	PC 18:0/18:1+H^+
788,5	PE 18:1/22:6-H^+
788,5	PS 18:0/18:1 Na^+
808,7	PC18:0/20:4+H^+
810,9	PC 18:0/20:4+H^+
835,5	PI 16:0/18:1-Na^+
861,5	PI 18:0/18:2-Na^+
863,5	PI 18:0/18:1-Na^+
885,5	PI 18:0/20:4-Na^+
887,5	PI 18:0/20:3 Na^+
911,5	PI 18:0/22:5-Na^+

ACKNOWLEDGEMENTS

The work described in this thesis was carried out at the Optical Manipulation Lab at IOM-CNR (Trieste, Italy) and the Molecular Histopathology Lab at the Dipartimento Universitario Clinico di Scienze mediche, chiururgiche e della salute (Cattinara Hospital, Trieste) under the supervision of Dr. Serena Bonin.

I would like to extend my sincere gratitude to:

Dr Serena Bonin, my academic supervisor for her assistance, encouragement and support during these years.

Dr Dan Cojoc, my tutor for his great assistance during my work.

Prof. Giorgio Stanta for having accepted me as his student and also for taking time to read my manuscript.

Molecular Histopathology and Optical Manipulation labs for such pleasant working atmosphere during these three years.

Prof. Josef Käs for having me accepted as visitor student, and his entire research group for such a lovely staying in Leipzig (expecially Anatol, Pico and Iris, you will be forever in my heart!)

Elisa D'Este and Elisa Migliorini for their help and support.

Last but not least I would like to thanks my parents, my brother and all my family for they unreserved love, Rajko, Anna, Ale, Goran, Jack, Ila, Giulia, Feffe, Sara,Vale, Danae, Marisa, Chiara, Alice and all my friends, with them life is better!